Batteries

DOI: 10.1002/anie.201201429

Challenges Facing Lithium Batteries and Electrical Double-Layer Capacitors

Nam-Soon Choi, Zonghai Chen, Stefan A. Freunberger, , Xiulei Ji, Yang-Kook Sun, Khalil Amine, Gleb Yushin, Linda F. Nazar, Jaephil Cho, and Peter G. Bruce**

Keywords:
battery safety ·
electrical double-layer capacitors ·
energy storage ·
Li–air battery ·
Li–S batteries

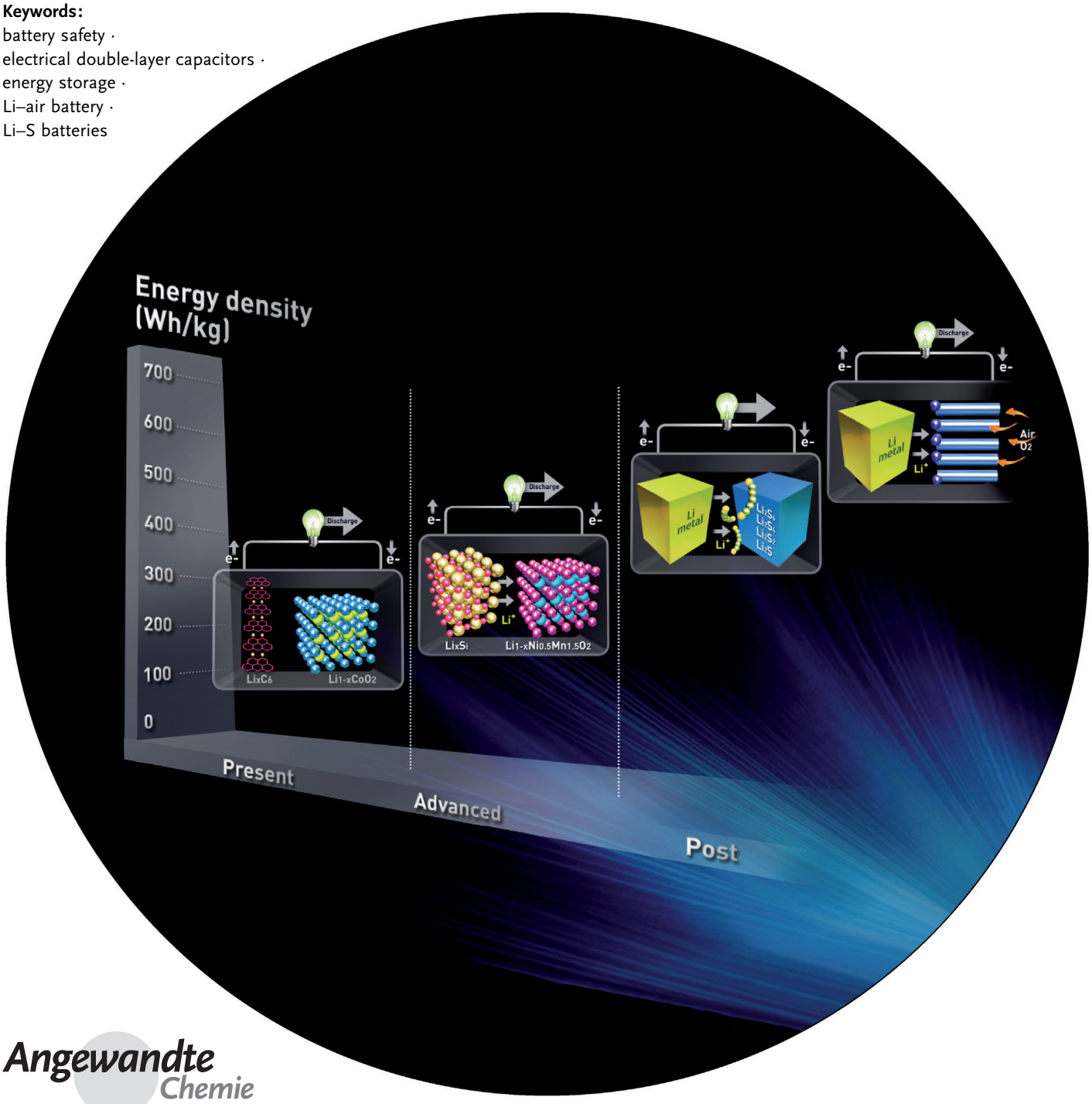

Energy-storage technologies, including electrical double-layer capacitors and rechargeable batteries, have attracted significant attention for applications in portable electronic devices, electric vehicles, bulk electricity storage at power stations, and "load leveling" of renewable sources, such as solar energy and wind power. Transforming lithium batteries and electric double-layer capacitors requires a step change in the science underpinning these devices, including the discovery of new materials, new electrochemistry, and an increased understanding of the processes on which the devices depend. The Review will consider some of the current scientific issues underpinning lithium batteries and electric double-layer capacitors.

From the Contents

1. Introduction

The demand for sustainable and clean energy is becoming more and more critical owing to the emergence of applications such as electric vehicles and the many new types of portable electronic devices currently available. Without energy storage, renewable electricity generation (wind, wave, solar) will be much less viable. Therefore, the search for the next generation of energy-storage materials and devices is extremely important.[1] The high energy density of rechargeable lithium batteries has transformed portable electronics over the past two decades. However, to meet the needs of new markets new generations of lithium batteries are required with increased energy and power density, improved safety, and lower cost. Electric double-layer capacitors (EDLCs) are already used in a variety of applications. The power capability far exceeds that of lithium batteries but their energy density is low. If they are to make maximum impact, new generations are required with higher energy density and lower cost.

Firstly, we shall examine progress on cathode and anode materials, as well as functional electrolytes for highly safe lithium-ion batteries (LIBs). Special attention will be given to the safety characteristics of each class of material. Although LIBs will continue to be a prominent means of storing energy for a number of years, in the longer term new types of batteries will be required. Consideration is given to the challenges and progress on lithium–sulfur (Li–S) and lithium–air (Li–Air) batteries.[2] Finally, recent advances in the expanding field of EDLCs are discussed.

2. Advanced Functional Materials for Safe Lithium-Ion Batteries

The first commercial lithium-ion battery was introduced by the Sony Corporation in the early 1990s. Several technological barriers need to be tackled before the large-scale deployment of the lithium-ion battery for automobile and grid applications can occur. These barriers include high cost, insufficient life, and poor safety characteristics.[3] Massive research and development efforts are underway to address these barriers and thereby enable deployment of this emerging energy-storage technology.

Several well-publicized incidents related to LIBs in use, such as fires and explosions, have raised concerns about their overall safety. Major challenges still remain including the thermal stability of cathodes, anodes, separators, and electrolytes within the battery at high temperatures and the occurrence of internal short circuits that may lead to thermal runaway.

During the charge/discharge process, lithium ions are shuttled between the cathode and the anode through a nonaqueous electrolyte that is sandwiched between the electrodes (Figure 1a).[4] During the charge, lithium ions are removed from the cathode, whose working potential is generally higher than 2.0 V versus Li^+/Li (see Figure 1b), and are inserted into the anode, whose working potential is generally lower than 3.0 V versus Li^+/Li (see Figure 1b),

[*] Prof. N.-S. Choi, Prof. J. Cho
Interdisciplinary School of Green Energy
Ulsan National Institute of Science & Technology (UNIST)
Banyeon-ri, Eonyang-eup, Ulju-gun, Ulsan 689-798 (Republic of Korea)
E-mail: jpcho@unist.ac.kr

Dr. S. A. Freunberger,[+] Prof. P. G. Bruce
School of Chemistry, University of St. Andrews
St. Andrews, Fife, KY16 9ST (UK)
E-mail: p.g.bruce@st-andrews.ac.uk

Prof. G. Yushin
School of Materials Science and Engineering
Georgia Institute of Technology, Atlanta, GA 30332 (USA)

Prof. Y.-K. Sun
Department of Chemical Engineering, Hanyang University
Seongdong-gu, Seoul 133-791 (Republic of Korea)

Dr. Z. Chen, Prof. K. Amine
Chemical Sciences and Engineering Division
Argonne National Laboratory, Argonne, IL 60439 (USA)

Dr. X. Ji, Prof. L. F. Nazar
Department of Chemistry, University of Waterloo (Canada)

[+] Current address: Institute for Chemistry and Technology of Materials, Graz University of Technology (Austria)

Supporting information for this article is available on the WWW under http://dx.doi.org/10.1002/anie.201201429.

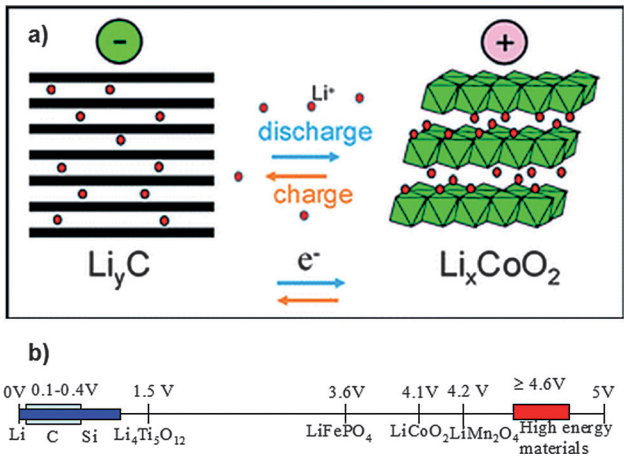

Figure 1. a) The principle of operation of the first commercialized lithium-ion batteries. Lithium ions migrate back and forth between the anode and cathode through the electrolyte upon discharging/charging; electrons doing so similarly through the outer electrical circuit.[4] b) Schematic diagram showing the relative working potential of typical electrode materials for lithium-ion batteries. Copyright Royal Society of Chemistry.

while the electrons are transported from the cathode to the anode through an external circuit. In an ideal lithium-ion cell, lithium ions are reversibly shuttled between the cathode and the anode with 100% efficiency, and no side reactions occur during the charge/discharge process. In reality, the efficiency (technically called "columbic efficiency") is slightly lower than 100%, and several surface side reactions between the electrolyte and electrode occur during normal operation of the cell or under abuse conditions. For instance, when the cell is charged, a highly oxidative transition-metal oxide is formed at the cathode,[5] and highly reductive lithiated graphite is generated at the anode.[6] These side reactions have several negative effects on the cell performance. First of all, they all consume accessible lithium and/or active electrode materials, resulting in a gradual decrease of cell capacity (technically called "capacity fade").[7] In addition, some of the by-products deposit on the surface of the active electrode material and increase the energy barrier for the charge-transfer reaction at the electrode surface, resulting in capacity fade at a high rate.[8] Finally, these side reactions can be kinetically accelerated at elevated temperatures or under abuse conditions and release a large amount of heat in a short period of time. Under this situation, fire or explosion ("thermal runaway") can possibly occur.[9] In a practical lithium-ion cell, these side reactions are kinetically slow at ambient temperature[10] so that a reasonable battery life and thermal stability can be achieved to ensure normal cell operation.

When the first lithium-ion battery was introduced to the market, the practical capacity of an so-called 18650 lithium-ion cell (that is a standard size of 18 mm in diameter and 65 mm in length) was about 0.9 A h. Today, a lithium-ion cell with the same size can easily deliver a much higher practical capacity, 2.6 A h, and prototype cells are capable of more than 3.0 A h. These continuous improvements and others have made lithium-ion batteries ever more useful. Yet, the safety issue remains a major barrier. Battery manufacturers are now able to produce high-quality lithium-ion cells for consumer electronics, with less than one reported safety incident for every one million lithium-ion cells produced. However, this failure rate on the cell level is still too high for applications in plug-in hybrid electric vehicles (PHEVs) and pure electric vehicles (EVs), since several hundred large-format lithium-ion cells will be needed to power a vehicle. The failure of a single cell can generate a large amount of heat and potentially flame, both of which can then trigger thermal runaway of neighboring cells, leading to failure throughout the battery pack. Thus, there is a worldwide effort to tackle the safety issue of lithium batteries. Herein we summarize the latest developments of advanced materials for long-life lithium-ion batteries with high energy density, with special focus on the potential impact of these materials on the safety characteristics of batteries.

2.1. Cathode Materials

For almost two decades, $LiCoO_2$ has been the dominant cathode material for lithium-ion batteries owing to its ease of preparation and stable electrochemical cycling performance, provided the lithium utilization is no more than 50%.[11] Concerns about the high cost of cobalt and the safety characteristics of the batteries have led to the development of alternative cathode materials that offer lower cost, longer life, and improved abuse tolerance. In addition, lithium-ion batteries developed for the transportation sector require higher energy density than the state-of-the-art lithium-ion battery so as to further reduce the weight, size, and cost of battery packs that power automobiles. These requirements

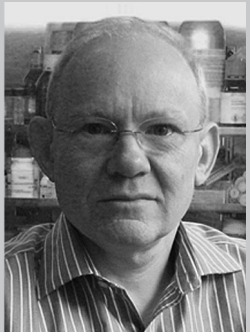

Peter G. Bruce is the Wardlaw Professor of Chemistry at the University of St Andrews. He leads a team focused on the science of energy-storage materials and lithium batteries. Currently his research includes nanostructured intercalation electrodes for lithium ion batteries, crystalline polymer electrolytes, and the Li-O_2 battery.

Jaephil Cho is a Professor and a Dean in the Interdisciplinary School of Green Energy at UNIST (Korea). He is a director of the Converging Research Center for Innovative Battery Technologies and of the IT Research Center. His current research is focused mainly on Li-ion and Zn-air batteries and nanomaterials for energy storage.

have been the major driving force for the development of alternative layered structured materials for full utilization of the lithium in the cathode materials. Other developments in this area have focused on lithium transition-metal phosphates ($LiMPO_4$, M = Fe, Co, Ni, Mn)[12] and lithium transition-metal oxide spinels (LiM_2O_4, M = Mn, Ni, Co).[12f,13]

Before starting discussion, the importance of the cathode materials in terms of the safety needs to be introduced, and although cell design and safety devices are important roles in minimizing the thermal runaway, controlling the heat generation from the cathode electrodes is much more important, and the total generated heat of either cathode or anode is an indicator for evaluating the safety of the materials (Figure 2). The triggering mechanism that induces thermal runaway is directly related to the extent of the cathode thermal instability, and more lithium deintercalation results in increased oxygen generation (amount of oxygen liberated from the lattice) from the cathodes. As a consequence, thermal stability tests need to be carried out for the more-delithiated states. Heat generation from the cathode is three-to-four-times greater than from the graphite anodes at fully charged states because of the substantial amount of oxygen that evolves from the cathode lattice above 200 °C (Figure 2a). Of the various cathode materials (Li_xCoO_2, $Li_xNi_{0.8}Co_{0.15}Al_{0.05}O_2$, $Li_xNi_{1/3}Mn_{1/3}Co_{1/3}O_2$, $Li_xMn_2O_4$, Li_xFePO_4) at the fully charged states, $Li_xMn_2O_4$ and $LixFePO_4$ showed the smallest amounts of oxygen generation (Figure 2b). This is why these two materials are considered as the main cathodes of the Li-ion batteries for PHEVs and EVs.

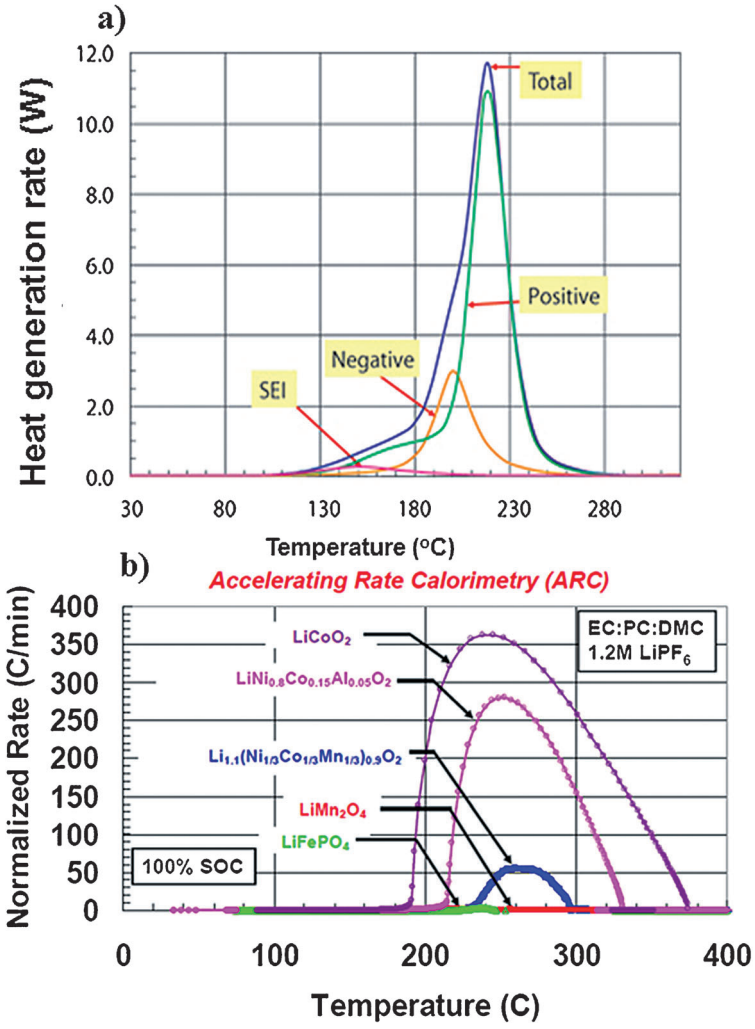

Figure 2. a) DSC scans of anode (negative) graphite and cathode (positive) Li_xCoO_2 after 100% charging[14] and b) accelerating rate calorimetry of various cathodes after 100% charging.[15]

2.1.1. *Layered Lithium Transition Metal Oxides*

In the past decade, major effort has been devoted to searching for high-performance cathode materials in the layered system $LiCoO_2$-$LiMnO_2$-$LiNiO_2$. The driving force of this research effort, at least in part, derives from several advantages associated with low-cobalt-content materials. The price of cobalt has been increasing continuously, and the supply of cobalt can be one of the bottlenecks for the emerging applications of lithium-ion batteries in the transportation sector. Replacing cobalt with relatively abundant Ni/Mn is a cost effective and sustainable strategy for the potentially huge expansion of the market. In addition, the utilization of lithium in $LiCoO_2$ is limited to only 50% for acceptable electrochemical performance, which caps its practical specific capacity at only 140 $mA\,h\,g^{-1}$.[11] Replacing Co with Ni/Mn has been shown to result in high utilization of lithium, approaching capacities of 240 $mA\,h\,g^{-1}$. Finally the introduction of Mn^{4+} to the transition-metal layer can help stabilize the transition-metal oxide framework, since Mn^{4+} doesn't change its valence state during the charge/discharge process.[13f,16] A number of these candidate cathode materials can deliver a reversible capacity above 200 $mA\,h\,g^{-1}$, and some of them even have better thermal stability than $LiCoO_2$. However, these cathodes are still in the process of development to increase their so-called tap density, that is, the amount of material that can be loaded in a specific volume, and to improve their power performance. In addition, this class of materials exhibits an accelerated capacity fade during cycling or storage at elevated temperatures as a result of the chemical reaction between the delithiated cathode and the electrolyte at high operating potential.[17] Such a capacity fade is because Ni and active metal ions dissolve into the electrolytes upon storage above 60 °C, with concurrent formation of NiO on the particle surface. This reaction normally accompanies structural transformation to spinel and NiO-type rock salt structures. To overcome the performance degradation and increase the capacity retention and safety when operated at high potential, several strategies have been proposed and demonstrated.

Research on lithium-rich transition-metal oxides has intensified, with improvements in electrochemical performance and thermal stability. This

class of materials can be described by several formulas, e.g. as $Li[Li_xM_{1-x}]O_2$[18] and $x\,Li_2MnO_3\cdot(1-x)LiMO_2$,[13j,19] in which M stands for a transition-metal such as Mn, Ni, Co, or a mixture of them. If the formula are interpreted structurally, then the first formula implies a model in which extra lithium is randomly doped in the transition-metal site, and the average valence state of the transition-metal element increases with extra lithium content to balance the low valence state of lithium (+1).[18a] Three lithium ions in the cathode have to be pinned down for every lithium ion doped into the transition-metal layer to neutralize the local charge. Therefore, the accessible lithium in the normal potential window is $1-3x$.[20] The second formula is based on a composite structure model proposed by Thackeray and co-workers.[13j] In this case, the extra lithium is accommodated within a new phase Li_2MnO_3, and the whole material is an integrated structure of Li_2MnO_3 sub-domains and $LiMO_2$ sub-domains.[13j,21] The Li_2MnO_3 domain stays inactive when the cathode potential is less than 4.5 V versus Li^+/Li, and the decrease in reversible capacity with the increase of excess lithium can be explained by the reduced content of the layered component $LiMO_2$.[13j] In both models, the extra lithium, either the pinned portion or the Li_2MnO_3, can be electrochemically activated when the working potential is higher than 4.5 V versus Li^+/Li, where oxygen loss from the framework balances the local charge.[13j,17,22] This activation process leads to more accessible lithium at a higher potential and a higher specific capacity, which makes lithium-rich transition-metal oxides promising as high-energy-density cathode materials.[17] In addition to the increased energy density, these materials were also reported to have good thermal stability (onset of thermal decomposition at 250 °C).[23]

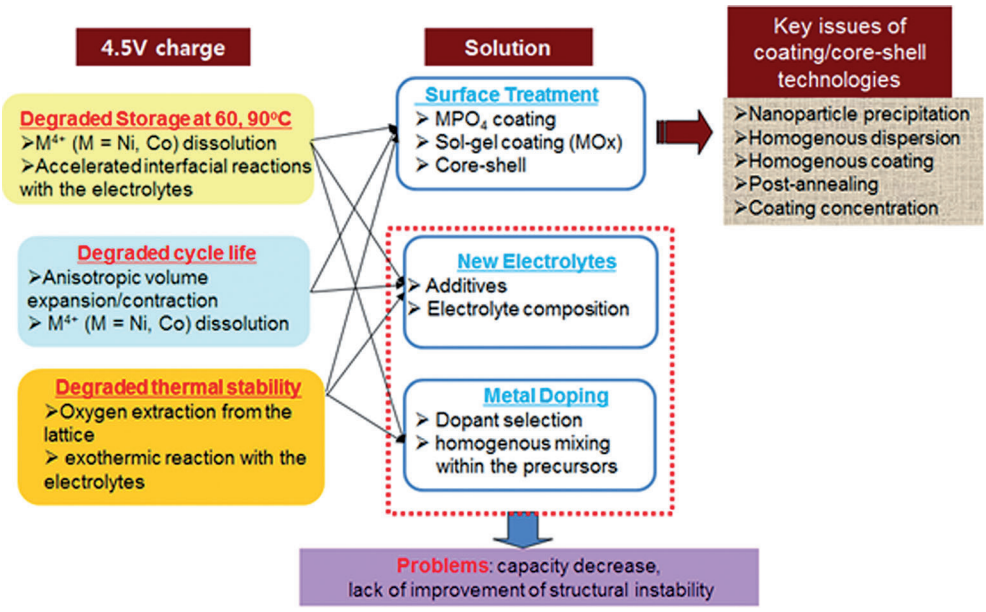

Figure 3. Problems and their solutions for cathode materials under increasing operating voltages and temperatures.

It is well established that a trace amount of HF present in the non-aqueous electrolyte plays an important role in cathode corrosion, which decreases cell life. Reactions with the cathode materials tend to be accelerated by increasing temperature and cut-off voltages. Metal doping and the development of new electrolytes stable under such conditions are opportunities to address this problem. A general approach used to tackle the corrosion has been to apply a surface coating to the cathode materials[24] that functions as an HF scavenger to locally neutralize the non-aqueous electrolyte (Figure 3). Coatings that have been applied, such as AlF_3,[25] Li_3PO_4,[26] $AlPO_4$,[27] act as a physical barrier that prevents direct contact between the cathode material and non-aqueous electrolytes. The surface coating has been consistently reported to improve the cycle life of lithium-ion cells, and even to enable the materials to be cycled to a higher working potential for higher specific capacity with reasonable capacity retention. The surface coating can be applied by several methods: sol–gel coating, chemical vapor deposition, co-precipitation, and other physical deposition techniques. The methods lead to a thin coating layer, but the complete coating necessary for the best protection is difficult. Therefore, these coating techniques have only a limited capability to prevent the oxygen release from lithium-rich materials and the oxidation of electrolytes when nickel-rich cathode materials are charged to a higher potential for higher specific capacity.

Fabrication of core–shell structured materials is the conceptual extension of oxide coating, in which the oxide layer is replaced with a layer of cathode materials having better thermal stability and better compatibility toward non-aqueous electrolyte.[28] In contrast to surface coating, in which the layer is up to 10 nm thick and the coating is non-uniformly distributed across the surface, the shell in the core–shell materials is up to 5 μm thick and covers the core uniformly (Figure 4). Depending on the preparing method, the core and shell can have the same structure, or heterostructures with a different core and shell can be formed. In general, the continuous co-precipitation method leads to the same core and shell structures in different ratios, but the PVP(polyvinyl pyrrolidone)-assisted MnO_x coating results in spinel-layered structures (that is, shell–core) for the nickel-based cathode materials.[35]

The latest advance in this area is the fabrication of a core–shell structure by concentration-gradient coating, in which the concentrations of transition-metal elements are continuously varied to fine tune the material properties while minimizing the mismatch of lattice parameters at the interface between

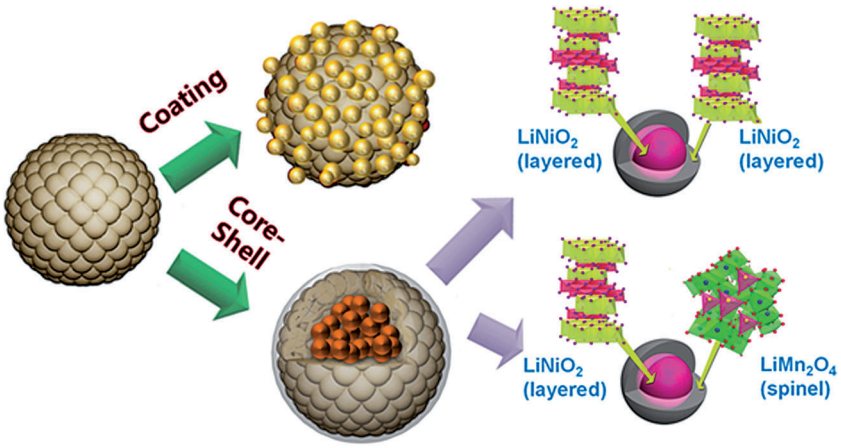

Figure 4. Schematic view of coating and core–shell cathode materials. In the core–shell material, the shell structure consists of either a layered or a spinel structure, depending on the synthetic method.

the core and the shell, thereby ensuring long-term cycling performance.[13h,29]

It should be noted that violent exothermic reactions of the delithiated cathodes with the electrolytes initiate at the cathode surfaces and propagate inwards, therefore, it is very important to introduce a highly stable phase near the surface. With this feature in mind, the heterostructured core–shell cathode provides the core layered phase with improved structural stability when coated by a spinel shell.[35] Pristine $Li_{0.1}[Ni_{0.7}Co_{0.15}Mn_{0.15}]O_2$ shows two diffraction peaks (108) and (110) which merged at 200 °C, indicating that the layered phase ($Li_{1-z}NiO_2$ ($R\bar{3}m$)) decomposed to a cubic spinel phase $Li_zNi_2O_4$ ($Fd\bar{3}m$) at this temperature. However, for the corresponding core–shell cathode, the peaks merged 250 °C, showing that the spinel shell greatly improves the structural stability of the core layered phase.

2.1.2. *Lithium Manganese Oxides Spinels*

Lithium manganese oxide spinels are another class of materials that are of considerable interest because of their low cost, abundant supply, environmental friendliness, good safety characteristics, and high power capability. A disadvantage is that lithium manganese oxides can be severely corroded in acidic electrolyte, especially at elevated temperatures. The corrosion process can lead to some Mn^{2+} ions being dissolved in non-aqueous electrolyte.[30] The dissolved Mn^{2+} ions, whose reduction potential is about 1.8 V versus Li^+/Li, can be easily reduced and form nanosize metal particles on the surface of the graphitic anode, compromising its electrochemical performance.[31] Hence, lithium-ion cells using lithium manganese oxides as the cathode and graphite as the anode generally suffer severe capacity fade at elevated temperatures because of the migration of Mn from the cathode to the anode.[32] A common approach to improve the cathode performance is to heavily dope the lithium manganese oxides with an element having a lower valence state, such as Li[21b,33] or Al.[33a,34] Acoordingly, a higher proportion of Mn^{4+} significantly reduces the reversible capacity.[20] Materials with good electrochemical performance generally have a specific capacity of 80–100 $mA\,h\,g^{-1}$, which is significantly lower than the theoretical value of the undoped counterpart. Application of a surface coating is also widely reported to suppress the corrosion of lithium manganese oxides in non-aqueous electrolyte at high temperature and to reduce the detrimental impact of oxygen release at a high potential.[28c,f,35] In addition, electrolyte additives that can form a robust solid-electrolyte interface are also effective in suppressing the negative impact of Mn migration from the cathode to the anode.[36]

$LiNi_{0.5}Mn_{1.5}O_4$ is another type of material with the spinel structure that delivers a specific capacity close to its theoretical value (148 $mA\,h\,g^{-1}$) and has a high working potential at about 4.8 V versus Li^+/Li.[23,34a,35b,37] Both features make $LiNi_{0.5}Mn_{1.5}O_4$ a promising cathode material for high-energy applications. However, the working potential of $LiNi_{0.5}Mn_{1.5}O_4$ already approaches the thermodynamic stability limit of carbonate solvents; hence, a systematic research is needed to develop technologies that can enhance the compatibility between $LiNi_{0.5}Mn_{1.5}O_4$ and non-aqueous electrolyte to give better cycle life and safety characteristics.

2.1.3. *Lithium Transition-Metal Phosphate*

$LiFePO_4$ was first reported by Goodenough and co-workers as a potential cathode material for lithium-ion batteries in 1997[38] and was considered the safest cathode material for state-of-the-art lithium-ion batteries. This material was originally thought not suitable for high-rate applications because of its low electronic conductivity and Li^+ ion mobility through the $LiFePO_4/FePO_4$ interface.[38a] The rate capability of $LiFePO_4$ was finally unlocked after continuous improvement for almost a decade.[12a,d] The initial approach to tackle the low Li^+ ion mobility through the $LiFePO_4/FePO_4$ interface was to develop nano or nano-structured materials to shorten the Li^+ ion diffusion path.[12c,39] Meanwhile, a conductive carbon coating was also adopted to improve the electronic conductivity of $LiFePO_4$ particles.[12b,40] An extra advantage of the carbon coating is that the carbon can also be used as the reducing agent for Fe^{III}, so that Fe^{III}-based compounds, such as $FePO_4$, can be used as the precursor to replace Fe^{II}-based compounds, such as FeC_2O_4.[41] Ceder and co-workers reported that a super high-rate capability of $LiFePO_4$ could be achieved by a non-stoichiometric synthesis route which generates a special surface coating on the $LiFePO_4$ particles.[12d]

A common initial drawback of lithium-ion cells using $LiFePO_4$-based cathode materials was limited energy density. They exhibited a low working potential, about 0.5 V lower than that of other oxide-based cathode materials. In addition, nanometer-sized particles were needed to ensure high performance of $LiFePO_4$, further reducing the volumetric energy

density of the cell. To partially conquer this shortcoming, Sun and co-workers developed a special synthesis route to prepare nano-structured $LiFePO_4$ with micrometer-sized secondary particles, nanometer-sized primary particles, and percolated electrolyte diffusion channels throughout the secondary particle to facilitate the Li^+ ion diffusion.[42] As an alternative approach to improve the energy density, the Fe in $LiFePO_4$ was replaced with other transition-metals, such as Mn, Co, and Ni, to raise the working potential.[43]

2.2. Anode Materials

The thermal stability of lithiated graphite remains the biggest concern from the perspective of the battery safety, especially for large-format lithium-ion cells and battery packs for automotive and grid applications. For instance, a fully charged lithium-ion cell can undergo thermal runaway when exposed to an external temperature of 160 °C or above.[9] The thermal runaway involves a set of self-accelerating chemical reactions, which, once triggered, can generate an exothermic heat flow that is larger than the heat dissipation rate to the environment. This excess heat increases the cell temperature, resulting in accelerated chemical reactions, exothermic heat flow, and higher temperature. Once triggered without external intervention, the thermal runaway will continue until the reactants are depleted. Chen and co-workers showed that the exothermal reaction in the temperature range between 110 °C and 180 °C observed in lithiated carbon in the presence of electrolyte was caused by the continuous decomposition/formation of a solid electrolyte interphase (SEI).[6d] This exothermic reaction depends mostly on the surface area of carbon. Higher surface area carbon can result in more SEI and therefore more heat generation during thermal decomposition. This initial reaction, which occurs at about 110 °C, can further trigger other exothermal reactions in the cell. Therefore, the latest work on graphitic anodes mainly focuses on the development of a stable artificial solid electrolyte interphase to stabilize the lithiated graphite and improve both safety and cycling performance.

The solid electrolyte interphase is generally formed during the initial charging process of a fresh lithium-ion cell using a graphite anode and an ethylene carbonate/$LiPF_6$-based non-aqueous electrolyte in the potential window 0.6–1.3 V versus Li^+/Li.[44] It is commonly agreed that conventional SEI formed on graphite is generally composed of organic components and some inorganic components, such as LiF, Li_2O, and Li_2CO_3; these inorganic components are insulators to both Li^+ ions and electrons. Therefore, boron-based Lewis acid,[45] or anion receptors, such as tris(pentafluoro phenyl)borane (PTFPB) were proposed as an electrolyte additive to dissolve the inorganic components in the SEI.[46] As a result, both the rate capability and cycling performance were improved when the correct amount of anion receptor was added to the electrolyte.[46] When an excess of anion receptor is added, it tends to promote the formation of SEI,[46] which could be the reason behind the improved thermal stability of lithiated graphite at elevated temperatures.[45g]

The alternative approach is to form an artificial SEI with better thermal stability at a potential higher than 1.3 V versus Li^+/Li during the initial formation process, in which case the lithiated graphite is still protected by the artificial SEI even if the conventional one decomposed under a certain condition. The class of functional materials that can form the artificial SEI generally has one or more unsaturated bond and/or cyclic structure in the molecule, which can be electrochemically activated to initiate the polymerization reaction on the surface of the carbon. Some well described materials for this purpose include 2-vinylpyridine,[47] vinylene carbonate,[48] vinyl ethylene carbonate,[49] lithium bis(oxalato)borate,[50] lithium difluoro(oxalato)borate,[51] lithium tetrafluoro-(oxalato)phosphate[ZC21]. The tradeoff for this type of material is that they generally increase the interfacial impedance of lithium-ion cells; making some of them unsuitable for high-power applications. Two promising additives worth mentioning are lithium difluoro-(oxalato)borate[51a] and lithium tetrafluoro-(oxalato)phosphate,[52] both of which provide excellent protection to improve the cycle life and thermal stability of lithiated graphite and only a very limited increase in the interfacial impedance of cells.

From material perspective, silicon-based anodes are the natural choice for high energy-density batteries. It was demonstrated in the 1970s that some metallic or semi-metallic elements alloy with lithium at room temperature in the presence of a non-aqueous electrolyte. These materials offered the promise of high theoretical capacity, 900 mA h g^{-1} and above (Figure 5),[4] whereas graphite only has a theoretical capacity of 372 mA h g^{-1}. As an example, the alloying reaction between Si and Li can lead to a final product of stoichiometry $Li_{22}Si_5$, delivering a theoretical capacity of 4200 mA h g^{-1}. However, their practical utilization in rechargeable lithium-ion batteries is severely handicapped because of their huge change in volume (up to 250 %)[53] during charge. As a result of such an enormous volume change, for instance, a 40 μm bulk Si anode electrode increases its thickness to over 150 μm, Si cannot be used in the cell alone. If we consider the available empty volume in the cell and that volume expansion of graphite is less than 20 %, then the Si expansion that can be tolerated is less than 40 %. In addition, if nanosized Si powder is used, even with a carbon coating, the resulting electrode density is lower than

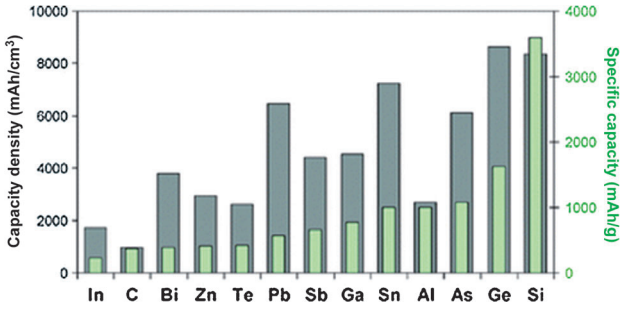

Figure 5. Specific capacities and capacity densities for selected alloying reactions. Values for graphite are given as a reference.[4] Copyright Royal Society of Chemistry.

that of the bulk Si counterpart. As a result of its high surface area, gas generation due to side reactions with the electrolytes is inevitable. In this regard, composites of Si nanoparticles and graphite have been reported.[54] However, although the composite capacity was over 1000 mA h g^{-1}, its capacity retention was not noticeably improved. This is because when carbon is coated on the aggregated Si nanoparticles, the uncoated Si nanoparticles are pulverized and thus lost to its electrical conduction network. Accordingly, composites with carbon and various morphologies on the Si nanostructures, such as nanowires, porous Si, and nanotubes have been published.[55]

Alternatively, SiO anodes have been widely investigated recently as an alternative choice to replace Si. It has been proposed that SiO consists of two phases: amorphous Si domains and amorphous SiO_2 domains (random mixed model).[56] Both of these two domains react electrochemically with lithium. One of the most plausible reaction mechanisms is as follows:[57] Amorphous Si domains: $Si + xLi^+ + xe^- \rightleftarrows Li_xSi$, Amorphous SiO_2 domains: $SiO_2 + yLi^+ + ye^- \rightleftarrows Li_2O$ and Li silicates. The Li_2O and lithium silicates serve as the amorphous matrix phase. Accordingly, the volume-expansion ratio is expected to be reduced, compared with Si.

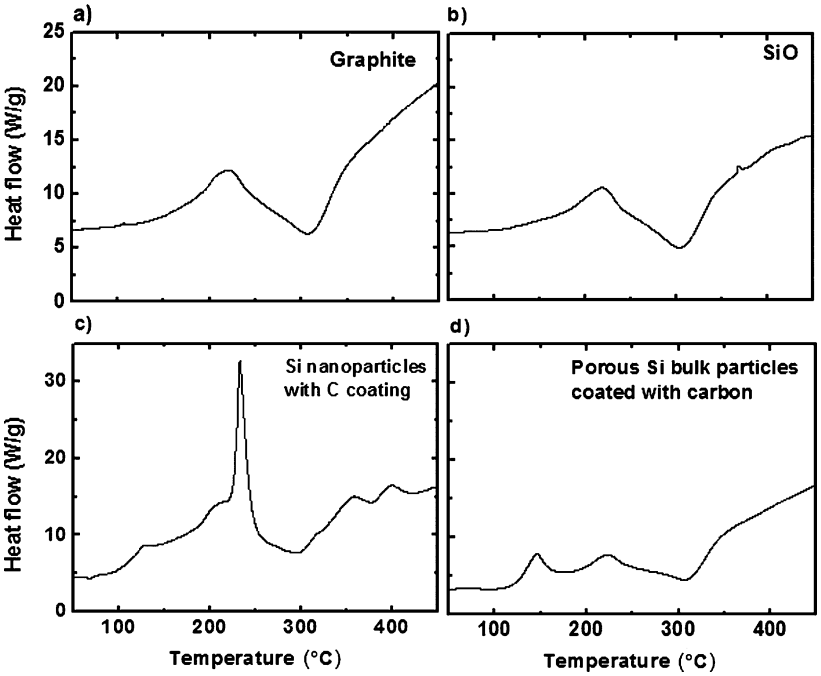

Figure 6. DSC scans of a) graphite (LiC_6), b) SiO, c) Si nanoparticles with carbon coating (carbon was coated after etching), d) porous bulk Si particles with carbon coating. Si-containing samples (b, c, and d) were extracted from the half cells after full lithiation (0 V, 0.1 C) and DSC was measured, after samples were soaked in electrolyte, at a scan rate of 10 °C min^{-1}.

Previously graphite-based anodes have been reported as a source of thermal runaway although the cathode plays a dominant role in such processes. In this regard, it is important to pay attention to the Si anode and whether it is thermally stable in the fully charged states ($Li_{4.1}Si$). Figure 6 shows differential scanning calorimeter (DSC) profiles of graphite, Si, and SiO anodes after full lithiation to 0 V at 0.1 C. Li_6C begins to undergo exothermic decomposition reactions at around 150 °C (onset temperature). In the case of etched Si nanoparticles decomposition starts at approximately 190 °C, followed by a very sharp peak centered at 210 °C. Such a peak height is similar to that observed in the nickel-rich cathodes that underwent in thermal runaway. In the case of SiO, the onset temperature and peak height is similar to graphite, but compared to Si, it shows a much improved thermal stability. In the case of chemically etched bulk Si particles with a carbon coating, the exothermic reaction starts at about 200 °C, followed by continuous further exothermic reactions. However, with the carbon coating, although there is a new peak at about 150 °C which may be due to reactions with an amorphous carbon layer and the electrolyte, the peak height was significantly suppressed. This result clearly indicates that $Li_{4.1}Si$ alloys are thermally unstable, showing violent exothermic reactions.

One striking feature is that after thermal annealing at 400 °C using $Li_{4.1}Si$ soaked in electrolytes, the X-ray diffraction (XRD) patterns are completely different to the pristine samples (Figure 7). First amorphous SiO was converted into the crystalline phases of Li_2O_3 (Li_2CO_3), Li_xSi_y ($Li_{12}Si_7$, Li_7Si_3, Li_7Si_2, Li_2Si), LiOH, Li_2SiO_3, and Li_4SiO_4. Previously, it has been proposed that amorphous SiO changed to amorphous Li_4SiO_4, Li_2SiO_3, and Li_4Si after full lithiation.[56,57b] However, no direct evidence for the formation of such phases has been reported. Thermal annealing induces the nucleation of the amorphous phase to form more-stable crystalline phases. The $Li_{4.1}Si$ completely decomposed to Li_xSi_y phases. It is noticeable that porous bulk Si particles show a much decreased formation of the Li_2O_3 phase compared to Si nanoparticles. This result means that porous bulk Si particles are more thermally stable than Si nanoparticles.

2.3. Safety Inspired Electrolytes

Even though sophisticated internal and external protection mechanisms are used in lithium-ion battery packs, some lithium-ion cells can still undergo thermal runaway in unpredictable situations. It is possible that a failed cell could rupture, and the flame can spread across the battery pack, leading to failure of the whole pack. An electrolyte with low flammability is highly desirable to localize the damage to the individual cell in the event of one cell failing. The approach to tackle this issue is to replace the liquid electrolyte with a solid polymer electrolyte to avoid liquid leakage.[58] However, solid polymer electrolytes have low ionic conductivity at room temperature, and their application is generally limited to high-energy lithium-ion batteries that will be charge/discharged slowly. Gel electrolytes are a compromise approach between the solid polymer and liquid electrolyte; in

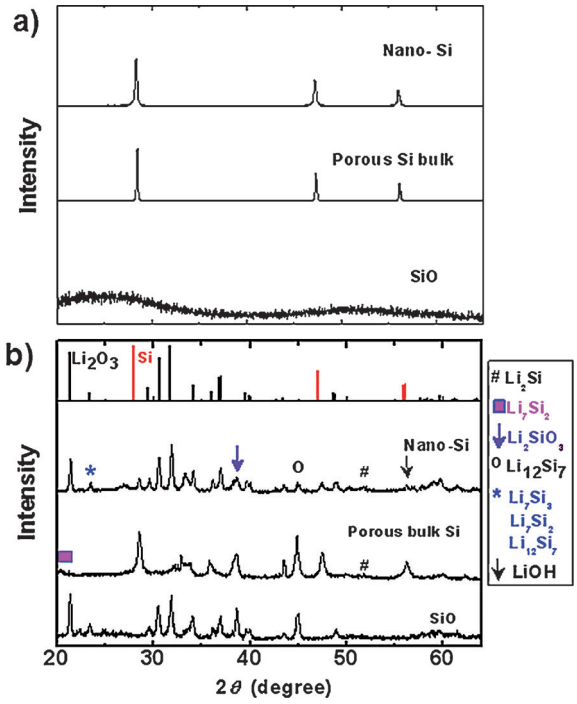

Figure 7. XRD patterns a) before and b) after DSC scans, of etched Si nanoparticles, porous bulk Si particles, and SiO. All the samples were taken from the hermetically sealed DSC pans after DSC runs (Figure 6).

a gel electrolyte a polymer is used as a flexible framework to host a liquid electrolyte to take advantage of the liquid-free properties of the solid polymer and good ionic conductivity of the liquid.[24c,59] Alternatively, a fire retardant can be used as an electrolyte additive to quench the fire or reduce the flammability of solvent vapor in case of the cell venting.[60] In this section, electrolyte technologies related to functional additives, flame-retarding materials,[61] and ionic liquids[62] for safe batteries are presented.

The non-aqueous electrolyte used in lithium-ion batteries generally contains a certain amount of lithium salt, for example, 1.2 M $LiPF_6$, in a solvent mixture of a linear carbonate, such as ethyl methyl carbonate (EMC), and a cyclic carbonate, such as ethylene carbonate (EC). As a rule of thumb, a linear carbonate is selected for its low viscosity for faster lithium-ion diffusion in the electrolyte; a cyclic carbonate is desired for its high dielectric constant to reduce ion pairing or to increase the mobility of ions in the electric field. A non-aqueous electrolyte is an electrical insulator and able to shuttle Li^+ ions between the cathode and the anode. When a lithium-ion cell fails, the electrolyte participates in all the reactions inside the cell, leading to unsafe conditions. Therefore, the electrolyte is a key feature of battery safety. Battery safety is related to the detrimental response of lithium-ion cells at unusual conditions, such as high temperature, short circuits, overcharging, and physical damage, which can lead to self-accelerating reactions, as well as fire and explosion. In the following discussion, we focus on the chemical design that is needed to enhance the safety characteristics of lithium-ion batteries by changing or adding materials that alter the chemistry to the lithium-ion cell.

2.3.1. *Additives for the Solid–Electrolyte Interface*

Current lithium-ion batteries are sensitive to temperature, and they can only work properly in a narrow temperature range. For instance, a fully charged lithium-ion cell will likely undergo thermal runaway when exposed to an external temperature of 160 °C or above.[9] The thermal runaway involves a set of self-accelerating chemical reactions, which, once triggered, can generate an exothermic heat flow that is larger than the heat dissipation rate to the environment. This excess heat increases the cell temperature, resulting in accelerated chemical reactions, further exothermic heat flow, and higher temperature. Once triggered without external intervention, the thermal runaway will continue until the reactants have been depleted. Therefore, improving the thermal stability of the solid–electrolyte interface on graphite is critical for a safe lithium-ion cell. The solid–electrolyte interface is generally formed during the initial charging of a fresh lithium-ion cell containing a graphite anode and ethylene carbonate/$LiPF_6$-based non-aqueous electrolyte in the potential window of 0.6–1.3 V versus Li^+/Li.[63] The conventional solid–electrolyte interface formed on graphite generally consists of organic components and some inorganic components such as LiF, Li_2O, and Li_2CO_3 (Figure 8[65]); these inorganic components are insulators to both Li^+ ions and electrons. Therefore, boron-based Lewis acids[45c,64] or anion receptors, such as tris(pentafluoro phenyl) borane,[64d] were proposed as an electrolyte additive to dissolve the inorganic components at the solid–electrolyte interface.

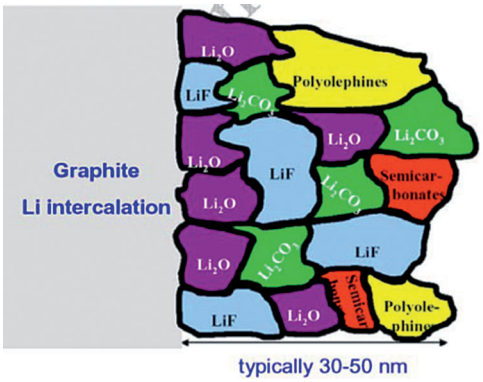

Figure 8. Schematic representation of the chemical composition of the solid–electrolyte interface at the surface of a graphite anode.[65] Copyright Royal Society of Chemistry.

As a result, the rate capability and cycling performance were improved when the correct amount of anion receptor was added to the electrolyte.[64d] The anion receptor tends to promote the formation of the solid–electrolyte interface,[64d] which can improve the thermal stability of lithiated graphite at elevated temperature.[45g] An alternative approach is to develop electrolyte additives that can be electrochemically activated at a potential higher than 1.3 V versus Li^+/Li during the initial process, thereby forming a robust/stable artificial solid–electrolyte interface underneath the conventional one. In this case, the lithiated graphite is still protected by the

artificial solid–electrolyte interface, even if the conventional one were to decompose. This class of electrolyte additive generally has one or more unsaturated bond and/or a cyclic molecular structure, which can be electrochemically activated to initiate the polymerization of the electrode surface. Some additives reported for this purpose include 2-vinylpyridine,[36d] vinylene carbonate,[66] vinyl ethylene carbonate,[49a] lithium bis(oxalato)borate,[50b–d,67] lithium difluoro(oxalato)-borate,[10d,51b,68] and lithium tetrafluoro(oxalato)phosphate.[52] The tradeoff of this type of additive is that they generally increase the interfacial impedance of lithium-ion cells, making them inadequate for high-power applications. Two of these additives are particularly promising, lithium difluoro-(oxalato)borate[68] and lithium tetrafluoro-(oxalato)phosphate,[52] both of which provide excellent protection to improve the cycle life and thermal stability of lithiated graphite with only a very limited increase in the cell interfacial impedance.

2.3.2. Redox Shuttles

Overcharging can dangerously damage lithium-ion cells or batteries. It can lead to chemical and electrochemical reactions between cell components, gas release, and rapid increase of cell temperature, and it can also trigger self-accelerating reactions in batteries that can lead to thermal runaway and possible explosion. A redox shuttle is an electrolyte additive that can be reversibly oxidized/reduced at a characteristic potential and provides intrinsic overcharge protection for lithium-ion batteries. The redox shuttle molecule (S) has a defined redox potential at which it can be oxidized on the cathode and form a radical cation ($S^{\bullet+}$) [Eq. (1)].

$$S \rightarrow S^{\bullet+} + e^- \quad (1)$$

The radical cation then migrates to the anode through the electrolyte and is reduced [Eq. (2)]:

$$S^{\bullet+} + e^- \rightarrow S \quad (2)$$

The redox shuttle molecule then diffuses back to the cathode for the next redox cycle. During normal operation, the redox potential is not reached, and the redox shuttle molecules stay inactive. When the cell is overcharged, the potential of the cathode increases, and the redox cycle of the redox shuttle molecules is then activated. The net reaction of the redox cycle is to shuttle the charge forced by the external circuit through the lithium-ion cell without forcing intercalation/deintercalation of the lithium in the electrodes. The research on redox shuttles for overcharge protection of lithium-ion batteries can be traced back to the 1980s, when Behl et al. reported that I^- has its first oxidation potential at about 3.25 V versus Li^+/Li and, hence, is suitable for overcharge protection of 3 V class lithium-ion batteries.[69] Aromatic compounds were first proposed as promising redox shuttles for overcharge protection of 4 V class lithium-ion batteries in 1999.[70] However, the first stable aromatic redox shuttle, 2,5-di-*tert*-butyl-1,4-dimethoxy, was only reported in 2005 by Chen and co-workers.[71] Its redox potential is about 3.96 V versus Li^+/Li, resulting in unprecedented stability as a redox shuttle for lithium-ion cells. Since then, several promising redox shuttles have been identified to provide overcharge protection of 4 V class cathode materials.[64b,71–72] Although promising data have been obtained for various redox shuttle candidates, their practical utilization in lithium-ion cells hasn't been demonstrated to date. The first issue is the heat generation when the redox shuttle is activated.[73] If the heat generated from the shuttle mechanism cannot be efficiently dispersed, then it can drive the cell into thermal runaway. In addition, the redox shuttle generally has limited solubility in non-aqueous electrolyte, and the maximum overcharge current that can be handled by redox shuttles is generally less than 1 C.[72a,73] Establishment of their structure–property relationships will also be important for designing stable redox shuttles with higher redox potential to accommodate the newly developed high-voltage cathodes.[72d]

2.3.3. Flame-Retarding Solvents

Phosphorous flame retardants have been widely considered as an additive to reduce flammability on the electrolyte because of their self-extinguishing properties; they can scavenge the active hydrogen radicals that contribute to the combustion chain reaction. The basic mechanism of flame retardants can be explained by gas-phase radical quenching and thermal shielding. Phosphorous compounds are transferred into the gas phase at elevated temperature. The evaporated flame retardants undergo homolytic cleavage and lead to the formation of $P^\bullet$ radicals ($[\text{P-based solvent}]_{gas} \rightarrow PO^\bullet$) that can scavenge selectively the active hydrogen and oxygen radicals produced by the combustion of organic solvents. The phosphoric acid formed by the reaction of $P^\bullet$ radicals with organic solvents ($PO^\bullet + OH^\bullet \rightarrow HPO_2^\bullet + 2\,OH^\bullet \rightarrow H_3PO_4$) becomes polyphosphoric acid at elevated temperature and makes a thermal insulation barrier (called char) between burned and non-burned parts by the condensation reaction (Figure 9). The resulting char shields the non-burned parts from heat and oxygen transfer, and effectively impedes the combustion chain reaction of electrolyte decomposition. Trimethyl phosphate (TMP) is an effective flame retardant because of its high phosphorous content and low boiling point of 197 °C, compared to other phosphorous fire-retarding additives.[61d,74]

2.3.4. Ionic Liquids

To improve the safety of batteries, much effort has been devoted to reducing volatility and flammability of organic liquid electrolytes.[75] Mixed electrolytes containing 40 wt % or more of *N*-methyl-*N*-propylpiperidinium bis(trifluoromethane sulfonyl) imide (MPPpTFSI), an ionic liquid (IL), were found to be non-flammable and have good discharge capacities comparable to IL-free electrolytes in Li-ion cells.[76] In this regard, ILs may help to address the safety problem as they are practically non-flammable,[1a,77] and may drastically reduce the risk of thermal runaway. These properties can provide the lithium battery with the level of safety required

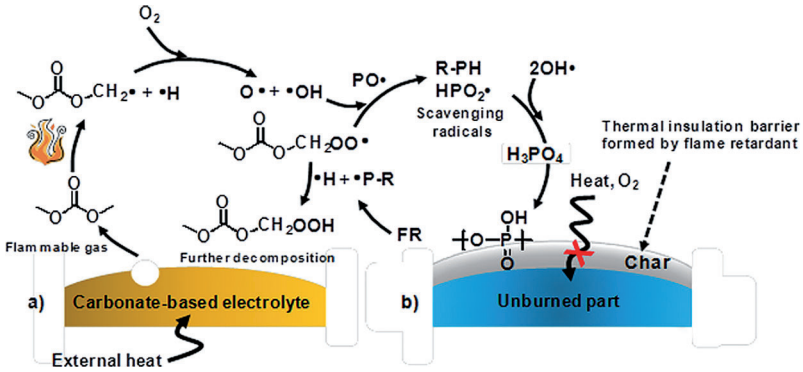

Figure 9. Schematic representation of the non-flammability of electrolytes: a) Thermal decomposition of conventional electrolyte based on carbonate solvents. b) Flame retarding by phosphorous flame retardant (FR) containing electrolyte. c) Suppression of combustion reactions by an ionic liquid-based electrolyte.

for large-scale applications including electric vehicles and smart grids.

The main cause of thermal instability of lithium-ion batteries is a vigorous and exothermic reaction between the electrolyte and the delithiated $Li_{1-x}CoO_2$ cathode.[77g] It has been reported that an exothermic reaction is observed at 250 °C, for $Li_{0.5}CoO_2$ in the absence of an electrolyte, whereas a pronounced exotherm of approximately 800 J g^{-1} cathode with an onset temperature of 175 °C is observed in the presence of the EC/DMC electrolyte.[78] In contrast, ILs with TFSI or tetrafluoroborate (BF_4^-) anions impede the onset of exothermic decomposition of chemically delithiated $Li_{0.49}CoO_2$ and slightly reduce the exothermic heat.[78c] Although ILs containing dicyanamide ($N(CN)_2^-$) or bis(fluorosulfonyl)imide ($[(FSO_2)_2N]^-$, FSI) exhibit considerable exothermic heat of 1500 to 2000 J g^{-1} cathode compared to EC/DMC and other ILs,[79] the onset temperature for the exothermic processes of ethylmethylimidazolium (EMI)-based ILs with the FSI anion was higher than that of EC/DMC in the presence of delithiated $Li_{0.49}CoO_2$.[78c] ILs hardly evaporate and hence delithiated $Li_{0.49}CoO_2$ is covered with IL of the liquid phase at elevated temperatures. The addition of ILs into the electrolyte solution can retard the heat evolution from the exothermic reaction between IL and delithiated $Li_{1-x}CoO_2$ cathode.[80] As a co-solvent in EC/EMC with 1.3 M $LiPF_6$, ILs, such as EMITFSI and MPPpTFSI, were reported to decrease the flammability of electrolytes and to reduce the exothermic heat evolution of lithiated graphite anodes at elevated temperatures.[81]

The limiting reactions of ILs in the cathode and the anode sides of their electrochemical stability windows were previously explored.[82] A key issue that should be overcome is the cathodic stability of ILs in connection with the anode side in LIBs. In principle, ionic liquids are very unstable at the potential of lithium reduction; the cations are very sensitive to electron injection.[1a] For instance, the typical ionic-liquid cation, EMI, is stable up to a cathodic potential of around 1.0 V versus Li/Li$^+$ when a graphitized carbon anode is charged.[62] The reductive decomposition of ILs on an anode surface, which restricts their applications, is closely linked to the structure of the cations and anions (Figure 10). All the IL-containing electrolytes have a lower anodic stability than DMC with 1 M LiTFSI. (Note, DMC does not form an effective solid electrolyte interphase (SEI) layer and hence does not hinder reductive decomposition of ILs.) It is clearly seen that the use of piperidinium cations instead of pyrrolidinium and quaternary ammonium cations results in superior anodic stability. Moreover, BF_4^- ion containing ILs undergo electrochemical reduction readily compared to non-nucleophilic anions, such as TFSI and tris(pentafluoroethyl)trifluorophosphate (FAP). This situation indicates that the BF_4^- ion is prone to consume the electrons that should be utilized for Li intercalation into a graphite anode. To suppress the reductive decomposition of ILs upon charging, SEI forming additives, such as vinylene carbonate[83] or fluoroethylene carbonate[84] have been used.

The drawbacks of ILs, which include high viscosity leading to poor wettability of the composite electrodes used in LIBs, poor low-temperature performances, and very high prices, extremely restricts their application in LIBs.[82a] Despite these problems, the electrolytes based on ILs are promising contenders in the design of safe batteries. Recently, lithium batteries using oxygen from air at the cathode, have attracted world-wide attention. In this open system, the use of electrolytes with low volatility is strictly required. With this in mind, ILs have been investigated as a nonvolatile electrolyte solvent for Li–Air batteries.[85]

3. Lithium–Sulfur and Lithium–Air Batteries

3.1. From Intercalation to Integration

Intercalation-based lithium-ion batteries will eventually reach their energy storage limits. Although superior to any other commercial rechargeable battery in terms of energy

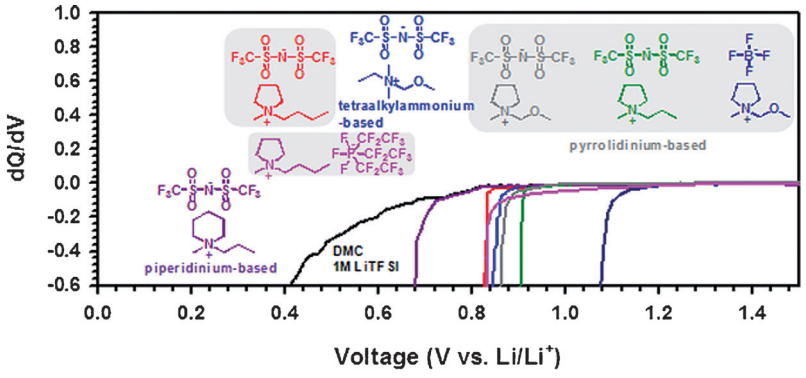

Figure 10. Differential capacity (dQ/dV) versus cell potential for half cells of graphite/Li with DMC/IL (3/7, v/v)/1 M LiTFSI during the first Li intercalation.

storage, it will be difficult to achieve long driving ranges, such as 500 km, required for transport applications, with these batteries. New systems are being sought for the next-generation batteries to provide much higher energy storage, and reduced cost, which move beyond intercalation chemistry into the realms of "integration" chemistry. Conventional lithium-ion batteries (LIBs) are based on intercalation electrodes which exhibit dual electronic–ionic conductivity, and an interstitial filled crystalline structure that reversibly (de)inserts Li ions with minimal structural change. These characteristics were once believed indispensible qualities for electrode materials to function for LIBs. To significantly increase the energy storage requires a decrease in the number of, and/or atomic weight of, atoms per Li exchanged, Figure 11 a. This requirement cannot be fulfilled with a crystal

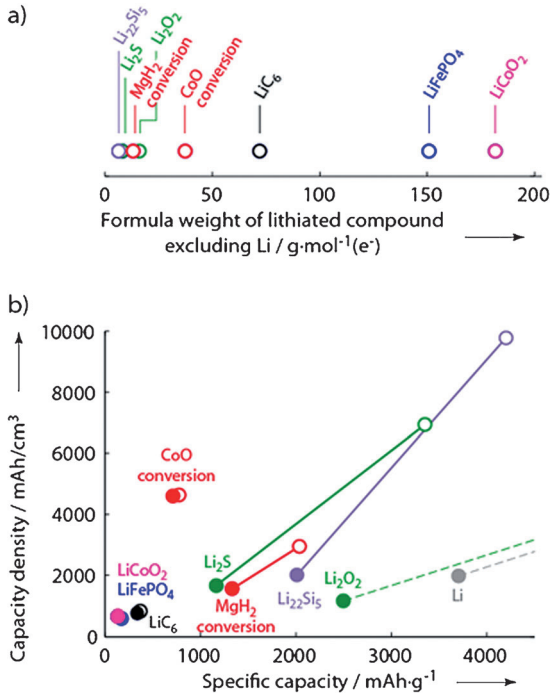

Figure 11. a) Formula weight of the non-lithium components of active electrode materials per mole of electrons passed. b) Capacity per weight and volume of lithiated (filled symbols) and delithiated (open symbols) active material. For $LiCoO_2$, 0.5 Li per formula unit is assumed to be cycled on charge/discharge. The delithiated state for Li and Li_2O_2 is taken as zero mass and volume.

structure that remains stable. Examples are the alloying or conversion reactions in which repeated discharge/charge cycles involve major structural changes often necessitating the use of nanostructured materials.[86] Major structural changes also occur during the electrochemical reactions in Li–Air[87] and Li–S[88] batteries, in which new compounds are formed. The volume changes in going from the charged to discharged states are illustrated in Figure 11 b. It must be recognized that as one electrode expands the other contracts. Therefore, if a cell can be designed in which the volume change at one electrode can off-set, in part, the volume change at the other electrode, then the overall cell volume may remain constant.

The high theoretical specific energy (energy stored per unit mass) of the Li–Air and Li–S cells, compared with Li-ion cells, Table 1, arises because Li metal is used instead of a graphite anode and Li_2O_2/LiOH/Li_2S store more charge per unit mass than intercalation cathodes, such as $LiCoO_2$ or

Table 1: Data for several electrochemical reactions that form the basis of energy-storage devices.

Battery	Cell Voltage [V]	Theoretical specific energy [Wh kg^{-1}]	Theoretical energy density [Wh L^{-1}]
Li ion: $^1/_2\,C_6Li + Li_{0.5}CoO_2 \rightleftarrows 3\,C + LiCoO_2$	3.8	387	1015
Li–S: $2\,Li + S \rightleftarrows Li_2S$	2.2	2567	2199[b] (Li + Li_2S)
Li–O_2 (non-aqueous): $2\,Li + O_2 \rightleftarrows Li_2O_2$	3.0	3505	3436[c] (Li + Li_2O_2)
Li–O_2 (aqueous): $2\,Li + {}^1/_2\,O_2 + H_2O \rightleftarrows 2\,LiOH$[d]	3.2	3582	2234[e] (Li + H_2O + LiOH)

[a] Based on volume of ZnO at the end of discharge. [b] Based on the sum of the volumes of Li at the beginning and Li_2S at the end of discharge. [c] Based on the sum of the volumes of Li at the beginning and Li_2O_2 at the end of discharge. [d] Assuming the product is anhydrous LiOH and alkaline conditions. [e] Based on the sum of the volumes of Li + H_2O consumed and the LiOH at the end of discharge.

$LiFePO_4$ (Figure 11 a). However, practical energy storage will be lower than the theoretical values in Table 1. The cathode cannot consist only of Li_2O_2, LiOH, or Li_2S but must include a conductive matrix within which the active discharged products form, thus adding mass and volume to the cathode. Although Li metal is an attractive anode because of its high theoretical specific energy, in practice it reacts with the electrolyte forming a solid electrolyte interface (SEI) layer composed of lithium salts. Such passivation is essential for the functioning of the Li anode but continuous reformation of the SEI layer on each charge/discharge cycle inevitably consumes lithium, resulting in the need to include excess lithium to obtain a reasonable number of cycles. Of course, as for all cells, further reduction in energy storage arises from the inclusion of current collectors and packaging.

In the case of air-based cathodes the need for gas diffusion channels transporting the air to the cathode surface must also be taken into account. One potential advantage is that such gas channels also provide cooling, avoiding the need for additional cooling vents in large batteries. The practical specific energies anticipated for a Li–air cell are shown in Figure 12 where they are compared with several other battery technologies. Since few, if any, realistic prototypes for Li–air cells have yet been constructed, the values presented should only be regarded as very rough estimates based on scaling down from the theoretical specific energy by the factor used

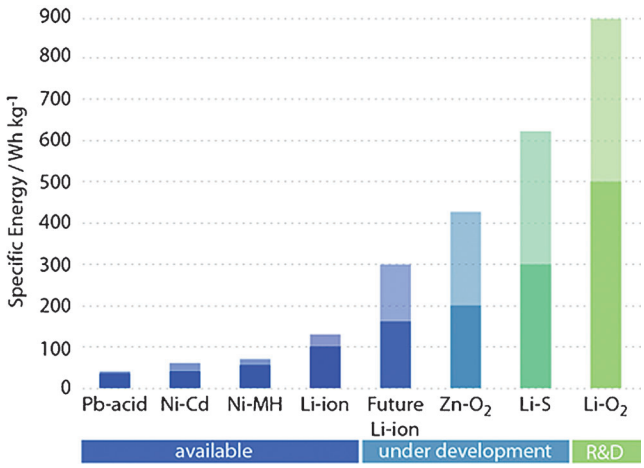

Figure 12. Estimated practical specific energies for future rechargeable batteries in comparison to established systems. For future technologies, a range of anticipated specific energies is given.

for Li–S cells, for which realistic prototypes do exist.[2,88] They show a considerable reduction in specific energy from theory to practice but also that the estimated practical specific energies are significantly higher than those for alternative battery technologies. It should also be noted that the greatest improvement of the Li–air battery over the Li–ion battery is seen in the specific energy, the energy densities (volumetric) may be similar or only marginally higher (Table 1 and Figure 12).

3.2. Lithium–Sulfur Battery

The sulfur molecule (S_8)—eight sulfur atoms arranged in a puckered ring—represents the most stable configuration of sulfur at standard temperature and pressure (STP). The α-sulfur phase has a "crankshaft" structure with the space group of *Fddd-D*$_{2h}$, as shown in Figure 13.[89] One unit cell contains 16 molecules, and the density of α-sulfur is 2.07 g cm^{-3}. On increasing the temperature, molten sulfur exhibits a sudden increase of viscosity near 159 °C, often termed as the "λ temperature", where the S_8 rings start to be cleaved and polymerize into long chains.[89] The lowest viscosity of molten sulfur is thus obtained around 155 °C before the polymerization begins.

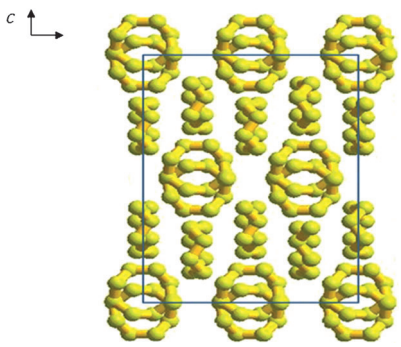

Figure 13. The "crankshaft" structure of orthorhombic α-sulfur. The section in the outlined square corresponds to one unit cell.

The lost cost of elemental sulfur has (about $150 per ton) has made it attractive for many uses in the past thousand years. Its first critical application was for war: as an ingredient in "feu grégeois" (Greek Fire), whose secret composition (sulfur + carbon) was critical for the survival of the Byzantine Empire, and in gun powder. Herbet et al. first conceived elemental sulfur as a positive electrode in 1962.[90] A sulfur electrode has many valuable characteristics, such as low equivalent weight, high capacity, low cost, and nontoxicity. Considerable efforts have been devoted to alkali-metal–sulfur energy-storage systems, such as Na–S batteries,[91] which operate at 300–350 °C and Li–S batteries operating at room temperature. In a Li–S cell, the overall redox couple, described by the reaction $S_8 + 16\,Li \leftrightarrow 8\,Li_2S$ lies at an average voltage of approximately 2.15 V with respect to Li^+/Li, a potential about 2/3 of that exhibited by intercalation positive electrodes. However, this is offset by the theoretical specific capacity afforded by the non-topotactic integration process, of 1672 mA h g^{-1}, the highest value for any known solid cathode materials. Theoretical values can approach 2500 Wh kg^{-1} or 2800 Wh L^{-1} on a weight or volume basis, respectively,[92] assuming complete reaction to Li_2S. The energy density (Wh L^{-1}) and specific energy (Wh kg^{-1}) is the product of the cell voltage (V) and the specific and volumetric capacity (mA h g^{-1} or mA h cm^{-3}) based on the total mass of cathode and anode (S + 2 Li). Thus, compared to conventional LIB, Li–S batteries have the opportunity to provide an energy density at least five-times higher at a much lower cost.

3.2.1. Challenges of Li–S Batteries

Despite the considerable advantages of the Li–S battery, it is plagued with problems that have prevented its practical realization until recently. The first challenge is low conductivity. It is well-known that both sulfur and its insoluble discharge products are excellent electronic insulators and sulfur is not ionically conductive either.[93] This necessitates the connection of the active mass with substantial amounts of electronic conductors, such as carbon or metals, and a fluid electrolyte or efficient ionic conductors. A high ratio (A m^{-1}) of contact area over the sulfur mass is required to achieve good conductivity, and the particle size of the sulfur active mass needs to be minimized to reduce the diffusion paths.

Various challenges arise from the solubility of the polysulfide ions (S_n^{2-}) formed on reduction of S_8 or upon oxidation of insoluble sulfides.[94] Polysulfide ions can diffuse through the electrolyte onto the lithium anode and directly react with lithium in a parasitic reaction, which can result in the formation of dendrites and cause depletion of the lithium electrode.[95] Secondly, dissolution leads to a polysulfide shuttle phenomenon. Polysulfide (S_n) ions of longer chains diffuse to the lithium negative electrode where lower order polysulfides (S_{n-x}) form. S_{n-x} ions diffuse back to the positive electrode and are re-oxidized back into S_n. The above process takes place repeatedly, thus creating an internal "shuttle" phenomenon which markedly reduces the coulombic efficiency (discharge capacity/charge capacity). This also can

cause an internal current and consequently self discharge, evidenced by shelf voltage degradation.[96] On the other hand, such "redox" shuttles provide intrinsic overcharge tolerance for Li–S batteries.[97] Mathematical modeling has yielded a good quantitative understanding of the shuttle phenomenon in Li–S batteries.[98] The modeling encompasses theoretical models of the charge process, charge and discharge capacity, thermal effects, self-discharge, and a comparison of simulated and experimental data. The study provides evidence that self-discharge, charge–discharge efficiency, and overcharge protection are all facets of the same phenomenon. Thirdly, on the completion of each cycle, polysulfides in solution are reduced to insoluble Li_2S_2 and/or Li_2S and can be deposited back onto the electronic conductors in the cathode. These sulfides gradually form agglomerates over prolonged cycling,[99] which become electrochemically inaccessible and cause active mass loss, capacity fading, and build-up of impedance layers. The sulfur electrode—where most of the problems originate—is believed to be the key to improving Li–S batteries. Innovations of electrolytes and Li anode are also necessary to make the Li–S battery a secure, reliable, and efficient technology.

3.2.2. *Carbon–Sulfur Positive Electrodes*

Carbonaceous materials are extensively employed as conductors in the battery industry, and they play a crucial role in the sulfur electrode. In the earliest Li–S cell configuration, bulk carbon and sulfur powder was simply mixed together to form an electrode. These cells suffered low capacity, and poor discharge/cycle efficiency. To obtain good conductivity, additional carbon was added, which decreased the energy density of the cells. Peled et al. first described the concept of loading sulfur into the porous structure of carbon materials to form more efficient electronic contact.[100] Much more recently, carbon coatings (18 nm thick), sputtered onto a sulfur cathode,[101] have been used to similar effect. These cathodes exhibit a very high capacity of 1178 $mA\,h\,g^{-1}$ on first discharge but considerable fading. Impedance measurements showed that the interfacial resistance of the non-coated sulfur cathode increased substantially after 50 cycles while the carbon-coated sulfur cathode exhibited somewhat less interfacial resistance. However, it was not revealed if the carbon layer simply functions as a physical barrier to prevent polysulfide ions from diffusion.

Qiu et al. studied sulfur/multiwalled carbon nanotube (MWCNT) composites, but they focused on MWCNT-core/sulfur-shell structures instead of pore filling.[102] These systems have limitations. The surface area and pore volume of CNTs are typically less than 350 $m^2\,g^{-1}$ and 0.5 $cm^3\,g^{-1}$ respectively,[103] which restricts the capacity for the active mass that can be accommodated. Second, the 1D structure of CNTs is generally less favorable for Li-ion diffusion, compared to a 3D case. Moreover, the tubes are normally several microns long, which may induce discontinuous sulfur loading. Third, the diameter of CNTs—typically several tens of nanometers—is larger than ideal. A departure from typical MWCNT–S composites is provided by the recent work of Wang et al., who reported on sulfur-impregnated "disordered" carbon nanotubes (DCNTs) prepared by a template wetting method utilizing anodic aluminum oxide membranes.[104] To bind the sulfur to the semi-graphitized DCNTs, a heating step (up to 500 °C) was employed, with the aim of chemically trapping sulfur as "S_2" molecules within the graphitic clusters of the DCNTs. Heat treatment at 500 °C (compared to 160 °C), was beneficial for capacity stabilization; electrodes showed retention up to 73 % over 100 cycles at intermediate rates. However, these high-temperature composites contain only 40 wt % sulfur, and a very significant drop was noted on the first cycle owing to excess sulfur on the surface on the DCNTs.

Carbon nanofibers have also been used as conducting wires;[105] although recent improvements in nanofiber technologies, through electrospinning, and in methods for sulfur deposition have greatly increased the electrochemical performance. Capacities are reported up to 1100 $mA\,h\,g^{-1}$ at a rate of C/10 in porous carbon/sulfur nanofibers.[106] If sulfur is loaded into hollow carbon nanofiber tubes, an S-C-S core–shell structure will form. This was nicely demonstrated by Cui et al., for hollow carbon nanofiber arrays fabricated using anodized aluminum oxide templates, they reported a capacity of 750 $mA\,h\,g^{-1}$ at C/5 after 150 cycles. Such porous and/or hollow carbon nanofiber materials offer inexpensive processing and low-cost materials if thin-film deposition methods can be avoided.

The popularity of graphene has resulted in promising new approaches for the encapsulation of sulfur particles within graphene oxide and graphene-based carbon materials.[107] These have employed different "rational design syntheses" to prepare a variety of composites. They include functionalized graphene sheets that sandwich sulfur particles incorporated by melt-treatment to create a 3D architecture with 70 wt % sulfur;[107a] and graphene-oxide sheets that envelope sulfur nanoparticles prepared by the deposition of sulfur by reduction of precursors from solution.[107b–d] In the latter materials, sulfur contents vary from 66–70 wt %[107b,c] to up to 87 wt %[107d] and particularly robust cycling stability was observed in ionic liquid/polyethyleneglycol dimethyl ether (PEGDME) electrolytes over 50 cycles at a C/10 rate, at a capacity of 950 $mA\,h\,g^{-1}$.[107c] The "oxo" functional groups on the graphene oxides appear to play a significant role in binding polysulfide ions and providing a barrier to dissolution. The wide range of graphene/graphene oxide compositions allowed by this route, and the ability to tune the functional chemistry and also incorporate high sulfur/carbon content make this an appealing and flexible platform for future work.

Most recently, mesoporous carbons have found great applications in Li–S batteries. A carbon with a pore size less than 3 nm was employed in a sulfur electrode described by Gao et al.[108] Upon sulfur loading, the surface area dramatically decreased from 1473 $m^2\,g^{-1}$ carbon to 24 $m^2\,g^{-1}$ composite (57 wt % sulfur), which suggests not only a successful sulfur loading but also that the pores are nearly completely filled. The composite exhibits an initial discharge capacity of 740 $mA\,h\,g^{-1}$ (down to a potential of 1.5 V versus Li^+/Li). Surprisingly, the electrode with 75 wt % sulfur could not be recharged.

Much attention has been focused on improving the electronic contact in carbon–sulfur composite electrodes.

Recently, ionic transportation has been taken into account as well. Liang et al. reported a carbon–sulfur nanocomposite based on a hierarchically structured micro-mesoporous carbon.[109] A mesoporous carbon was treated by a post activation method to generate micropores in the carbon walls. Sulfur was loaded, but only into the micropores, by a wet-impregnation method (Figure 14). The empty mesopores accommodate the soluble polysulfide ions formed during cycling.

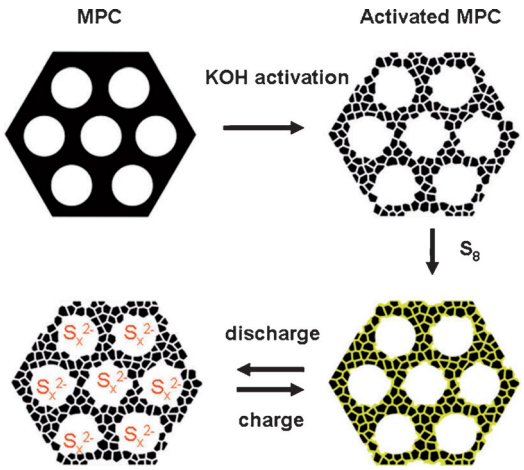

Figure 14. Illustration of the S/C composite cathode material with bimodal porous carbon as the support. MPC = mesoporous carbon.[102] Copyright Royal Society of Chemistry.

Utilization of sulfur is strongly affected by the percentage of active mass in the electrode. The composite containing 51.5 wt% sulfur exhibits a first discharge capacity of 818 mA h g^{-1} (obtained at a potential of 1.2 V versus Li^+/Li). At a sulfur loading of 11.7 wt%, a capacity of 1584 mA h g^{-1} (95% sulfur utilization) is achieved in the first cycle at a very high current rate of 2500 mA g^{-1}. Rapid capacity fading is observed for this composite. Importantly, the carbon–sulfur composite based on microporous carbon exhibits inferior performance compared to its mesoporous carbon counterpart: its first discharge capacity is only 388 mA h g^{-1}. This might suggest that sulfur-stuffed micropores would not provide good ionic conductivity, although this has been contradicted by later reports (see below).

Some of the best electrochemical properties reported for carbon–sulfur composites are exhibited by ordered, interwoven carbon–sulfur composites that are composed of high pore-volume carbons with bicontinuous nanostructures. These studies began with investigations of a carbon known as CMK-3.[110] Sulfur is readily incorporated from the melt by capillary forces. The impregnation temperature is optimal at 155 °C where the viscosity of molten sulfur is the lowest. With this impregnation method, the percentage of active mass can be precisely controlled. Excess pore volume in the nanocomposite can be precisely tuned to provide pathways for electrolyte/Li^+ ingress and to accommodate the active mass volume expansion during cycling. The conductive carbon framework constrains the sulfur within its channels and generates the essential electrical contact (Figure 15). Kinetic inhibition to diffusion within the framework and the sorption properties of the carbon aid in trapping the polysulfides formed during redox. Thus immobilized, full reduction to Li_2S_2/Li_2S (or oxidation to S_8 on charging) is achieved within the carbon framework.

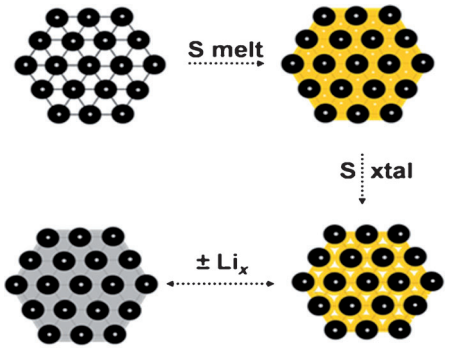

Figure 15. Schematic representation of sulfur (yellow) confined in the interconnected pore structure of the mesoporous carbon, CMK-3, formed from carbon tubes that are held apart by carbon nanofibers to form channels. The view is down the channels. Lower panels represent subsequent discharging–charging of sulfur with Li, illustrating the strategy of pore filling to tune for volume-expansion/contraction.[110] Copyright Nature Publishing Group.

Remarkably stable and excellent electrochemical behavior has been reported, for example, by two groups that have generated small-pore carbon spheres impregnated with sulfur by sublimation. In the one study, the carbon spheres had a 3 nm pore outer shell that housed a hollow interior;[111] whereas in the other, the carbon pore size was less than 1.5 nm, and permeated the entire carbon sphere.[112] In this system, a stable capacity of 800 mA h g^{-1} over 100 cycles was reported at current densities as high as 400 mA h g^{-1}, although the sulfur content was only 42 wt%. Much higher sulfur content was achievable in the mesoporous-shell carbon spheres with the hollow interior, presumably because of their ability to absorb sulfur within the interior (up to 70 wt%), with reported capacities of 970 mA h g^{-1} at a C/2 rate with 91% capacity retention over 100 cycles. This promising approach is only limited by the apparent difficulty of imbibing the sulfur vapor through the porous shell into the interior, a process which required three "passes" to complete; nonetheless it suggests that polysulfide diffusion can be retained with such tailored design concepts.

3.2.3. *Catholyte Cells*

Another configuration for Li–S batteries is the "all liquid" system, first reported by Rauh et al.,[113] that relies on the high solubility of polysulfide ions which function as the initial positive electrode, and are dissolved in an organic electrolyte. To increase the energy density of the cell, a high concentration of polysulfide ions is preferred. THF can dissolve polysulfide ions at an equivalent concentration of 20 M sulfur. However, the high viscosity of the concentrated polysulfide

solution may lead to much decreased ionic conductivity. Co-solvents (e.g. toluene) can be added to the electrolyte to decrease the viscosity and thus increase the conductivity. Electrolyte additives are also used to maintain solubility and increase the fraction of active species in solution.[114]

On the anode side, self-discharge of 0.5 % per day at 25 °C and 4.4 % per day at 71 °C, which is caused by the polysulfide shuttle mechanism, is observed. This represents more rapid self-discharge compared to other cell configurations. Self-discharge is closely related to the Li anode corrosion caused by the soluble polysulfide ions that forms a Li_2S/Li_2S_2 solid electrolyte interface (SEI) film on the Li anode surface, as shown by many impedance studies.[115] However, the SEI cannot prevent further Li anode corrosion because the polysulfide ions can react with Li_2S/Li_2S_2 in the SEI to form polysulfide ions of shorter chains which diffuse into the electrolyte, resulting in a "cleaned" Li surface. The partially clean Li anode can react with polysulfide ions to again form the Li_2S/Li_2S_2 SEI. The SEI is thus in a dynamic equilibrium state. This process occurs repetitively, which causes continuous corrosion of the Li anode. These reactions lead to a high concentration of short polysulfide ions on the anode side, which promotes the shuttle phenomenon. The corrosion rate can be reduced by employing polysulfide ions of low order. This approach is effective because of the lower electromotive force that describes the reactions between shorter polysulfide ions and Li_2S/Li_2S_2 in the SEI.[95a] For example, the corrosion rate in a solution of $Li_2S_{6.6}$ decreases by five orders compared to elemental sulfur. If the polysulfide positive electrode is in excess compared to the Li electrode, the Li anode may be depleted by the corrosion. On the cathode side, although the positive electrode is in solution at the initial stage, insoluble sulfides are deposited extensively onto the current collector in the last stage of the discharge process, forming thick sulfide agglomerates.[116] This leads to the loss of active mass on the positive electrode.

An "all liquid" system cannot solve the problems of Li–S cells—neither at the cathode side nor at the anode side—and falls short of the mark for stable long-term electrochemical performance.

3.2.4. Lithium Anode Protection

The Li negative electrode is problematic for any Li (metal) battery system owing to the possibility of dendrite formation during the charge process (Li deposition), which can cause short-circuits. Problems of anode corrosion and polysulfide shuttling further necessitate Li anode protection for Li–S batteries. A protective layer should be able to protect the Li metal from reacting with the other battery components while providing high ionic conductivity to facilitate high performance of the battery. A solid electrolyte interface (SEI) as a protection layer can be formed simply by reacting lithium in situ with the electrolyte or an oxidative species in a controlled reaction.[117] Polymer protection layers can be formed by a ultra-violet curing method.[118] Very recently, Mikhaylik, Aurbach et al. discovered that the positive effect of a $LiNO_3$ additive in the electrolyte mainly lies in the protective film of Li_xNO_y and/or Li_xSO_y on the Li anode.[119] Detailed surface-science studies show these films are formed by the reactions of NO_3^- ions directly with the Li anode or with other species which are formed on the Li anode by reactions with the electrolyte solvent or the salt (i.e., TFSI).[120] The layers formed by these controlled reactions are typically porous structures that contain defects which allow polysulfide ions to diffuse to the Li metal surface. The SEI structure may deteriorate as a result of self-discharge reactions. Pre-formed impervious protection layers have also been intensively sought. Lithium phosphorus oxynitride (LiPON) is one such material that has been investigated as a potential Li-electrolyte for solid-state lithium microbatteries. The sputtering of a protective LiPON layer on a Li anode was first described by Bates in 1994.[121] Later, Visco and Chu described a plasma approach to form a glass protection layer on alkali metals.[122] However, the lithium anode must have a very clean and smooth surface, which is very challenging for commercial Li foils. To solve this problem, Visco and Tsang reversed the procedure sequence to form LiPON protected Li. Instead of sputtering LiPON onto the Li anode, Li is sputtered onto a LiPON protection layer which is pre-formed on a smooth silicon substrate to obtain a high quality film.[123] Protection membranes with multiple layers have been described as well.[124]

3.2.5. New Electrolytes for the Sulfur Battery

Ionic liquids as alternative electrolytes exhibit many desirable characteristics, such as non-flammability, low vapor pressure, good thermal stability, and high Li-salt solubility. However, ionic liquids based on imidazolium cations, such as ethylmethylimidazolium (EMI), typically have very poor stability at voltages below 1.1 V versus Li^+/Li, owing to their propensity for reduction.[125] This is problematic for applications in Li–S batteries. Cairns et al. reported that the compatibility of ionic-liquid electrolytes towards the Li anode can be improved by the addition of PEGDME or tetraethyleneglycol dimethyl ether (TEGDME) into the electrolyte.[126] Ai et al. reported that the methylbutyl piperidinium cation based ionic liquid (PP14-TFSI), which has a wide potential window from −0.15 to 5.2 V versus Li^+/Li, is quite stable with respect to the lithium anode.[127] Cyclic voltammograms of sulfur/carbon electrodes in this ionic liquid electrolyte show unique reduction behavior which is different from that in organic electrolytes. The difference is possibly caused by the low solubility of polysulfide ions in ionic liquids, although this has not been proved directly. As mentioned above, rather stable cycling behavior has been observed in such systems.[107c]

Sulfide glasses such as $Li_2S–SiS_2$ and $Li_2S–P_2S_5$ are good room-temperature lithium-ion conductors.[128] By using 80 mol % Li_2S·20 mol % P_2S_5 glass as an electrolyte, Hayashi et al. prepared an all-solid sulfur cell in which the cathode (sulfur and copper) exhibits a stabilized discharge capacity of 650 mA h g^{-1} for 20 cycles.[129] A thio-LISICON electrolyte has also been employed in an all-solid sulfur cell.[130] Most recently, the glass ceramic 80 Li_2S·20 P_2S_5 electrolyte compositions (which rely on $Li_7P_3S_{11}$ as the active ion conductor) have been employed very successfully in solid-state Li–S cells

with a sulfur–carbon positive electrode, and a Li–In alloy negative electrode. These cells retained a remarkable reversible capacity of over 850 mA h g^{-1} with stable cycling over 200 cycles at moderate current densities of 333 mA g^{-1}.[131]

Arabinda et al. described the use of ion-selective membranes as a functional separator between the anode and cathode in 1974.[132] The separator is designed to be only a Li-ion conductor which effectively blocks polysulfide-ion diffusion. These membranes are made of synthetic polyelectrolytes which typically contain a large number of sulfonated groups, such as SO_3^-. Loosely bound Li^+ ions function as the counterions. In the battery, Li ions readily diffuse into electrolyte because of the concentration gradient, which renders the separator net negatively charged. Thus, negatively charged polysulfide ions are electrostatically repelled by the separator. Polymers containing fluorine were also investigated as separator materials, which showed some improved results (probably related to their hydrophobic nature) compared to non-fluorinated polymers.[133]

3.3. Lithium–Air (O_2) Battery

3.3.1. Operation and Energy Storage

Non-aqueous and aqueous Li–air cells were first described by Abraham[134] and Visco,[135] respectively (Figure 16). On discharge, the lithium-metal anode is oxidized releasing Li^+ ions into the electrolyte and O_2 from the air is reduced in the pores of the cathode, which are flooded with electrolyte. When a suitable non-aqueous electrolyte is used, O_2^{2-} is formed and combines with Li^+ to precipitate Li_2O_2 as the final product in the pores of the cathode. Charging involves oxidation of the Li_2O_2 to reform Li^+ and O_2.[136] The overall cell reaction is $2Li^+ + O_2 + 2e^- \rightleftarrows Li_2O_2$ and corresponds to a theoretical open circuit voltage of 2.96 V versus Li^+/Li.[137] In the case of an aqueous electrolyte, OH^- and then LiOH form on discharge, the LiOH being oxidized on charging.[138] The overall cell reaction is in this case $2Li^+ + {}^1/_2\,O_2 + H_2O + 2e^- \rightleftarrows 2LiOH$, corresponding to a theoretical open circuit voltage of 3.35 V.[139] It should be noted that the electrolyte solvent, H_2O, is involved in the cell reaction and this is sometimes referred to as a Li–water battery. The aqueous Li–air battery can also operate in acidic media, where the overall cell reaction is $2Li + {}^1/_2\,O_2 + 2AH \rightleftarrows 2ALi + H_2O$ and with an open circuit potential of 4.07 V in the case of AH being acetic acid.[140] However, many other organic and inorganic acids have been considered.[141] The aqueous Li battery concept has recently been extended to the use of redox couples, such as $Fe(NO_3)_3/Fe(NO_3)_2$ instead of O_2, by Goodenough et al.[142] To date, most of the effort on aqueous Li–air batteries has focused on alkaline electrolytes, and this is reflected in this Review.

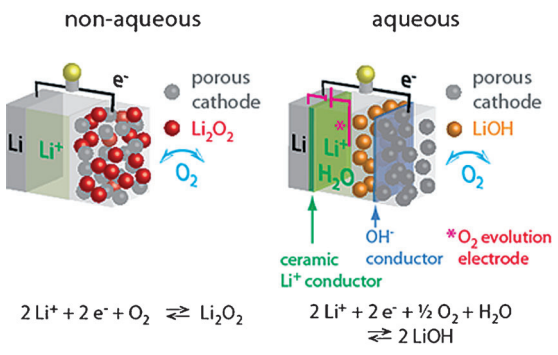

Figure 16. Schematic representation of aqueous and non-aqueous Li–air cells.

3.3.2. The Non-Aqueous Li–Air Cell

Transforming the Li–air battery from theory to practice presents a number of scientific and technological challenges; several of the most significant are shown in Figure 17. To operate the cell in air, H_2O and CO_2 must not be allowed to enter the porous cathode, thus preventing formation of LiOH and Li_2CO_3. Zhang and co-workers have examined protecting the cathode with hydrophobic membranes, such as polymethylsiloxane and silicalite[143] or Melinex (DuPont), a polyester–polyethylene glycol co-polymer, or high-density polyethylene films.[112] Using such an approach, it was possible to discharge a cell in ambient air with 20% relative humidity for one month.[112] These results indicate progress is possible but more work is required to optimize membranes that will block

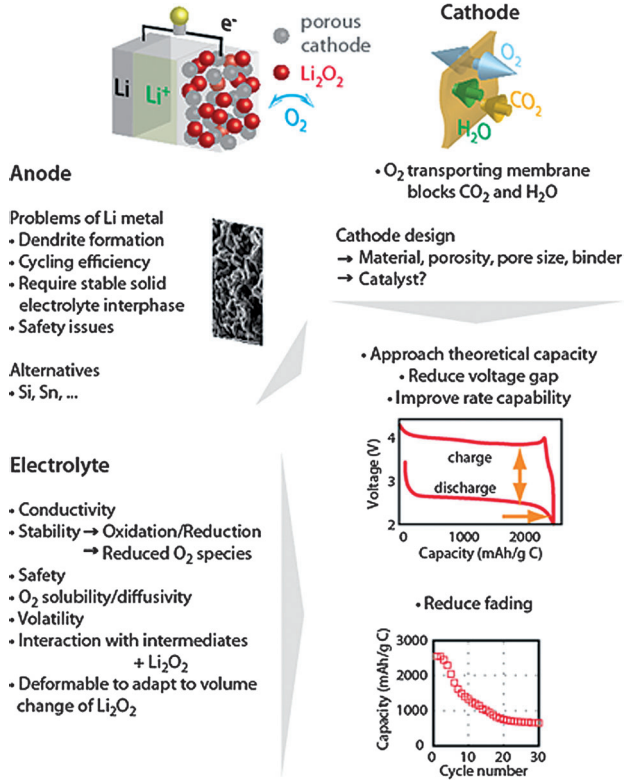

Figure 17. Challenges facing the non-aqueous Li–air battery. Key performance properties: capacity, polarization, rate capability, and capacity fading. Data taken from a cell with an organic carbonate electrolyte, Li/1 M $LiPF_6$ in propylene carbonate/(Super P/Kynar/α-MnO_2 nanowires).[149] Use of more stable ether electrolytes, for example, glymes reduces, although does not eliminate, capacity fading.[145b,150] Image of Li dendrites taken from Ref. [151]. Copyright: Royal Society of Chemistry, American Chemical Society, Elsevier, and The Electrochemical Society.

CO_2 and H_2O while allowing facile O_2 transport. Carbon has been the material of choice from which to form porous electrodes for fuel cells and metal–air batteries because it is of low cost, high conductivity, and is ease of processing. Aside from the nature of the substrate, the design of the porous electrode presents multiple challenges.[144] If Li_2O_2 forms as a film on the electrode, being an insulator, it may slow the rate of reaction, even at a film thickness of only a few tens of nm.[144b] However, studies to date suggest that the formed Li_2O_2 has a morphology of micron-sized toroidal particles made up of smaller primary particles, so such limitations may not occur in practice.[145] If the pores are large then much of the volume of the electrode may be inactive, if they are too small, Li_2O_2 may block the entrances to the pores. It is anticipated that a narrow pore size distribution within the range 10–100 nm will be optimal.[144a,146] However, it is also important to avoid electrolyte evaporation at the gas interface, thus tapered pores that narrow towards the gas interface may offer an advantage. To ensure facile transport of O_2 to the electrode surface, a gas-diffusion electrode is desirable within which O_2 is transported as far as possible in the gas phase before it enters the electrolyte near the site of reduction on the electrode surface. In aqueous systems this is achieved by a porous electrode which has hydrophilic and hydrophobic channels, the former filled with electrolyte and the latter acting as gas diffusion channels. This is more difficult to arrange in a non-aqueous system and emphasizes the important issue of the electrolyte wetting the electrode surface. If a catalyst is also to be used, then consideration must be given to its particle size and distribution (loading) on the surfaces of the porous electrode.[147] "Catalysts" have been employed extensively in porous cathodes for non-aqueous Li–air cells.[139,148]

However, early studies were carried out in electrolytes that are now known to be unstable, for example, organic carbonates, and it is now recognized in these cases that catalytic electrolyte decomposition is the dominant process. Although the absence of Li_2O_2 formation in organic carbonates on discharge precludes studying the effect of a "catalyst" on Li_2O_2 formation using such solvents, this may not be the case for Li_2O_2 oxidation.[136a,148f] Differential electrochemical mass spectrometry (DEMS) has shown that oxidation of an electrode containing Li_2O_2 in a propylene carbonate based electrolyte evolves only O_2.[136a] The study included several first-row transition-metal oxides and concluded that the lowest charging voltage was obtained with α-MnO_2 nanowires loaded onto carbon.[147a,148d] Comparison with the kinetics of H_2O_2 decomposition in an aqueous environment using the same series of compounds, demonstrated similar trends.[148f] However, recent studied by McCloskey et al. suggest that there is no catalytic effect on Li_2O_2 oxidation.[152] More work is required to better understand the kinetics of Li_2O_2 formation and decomposition and the possible role of a catalyst.

Currently, the electrolyte is a major focus of research.[2] The Li–air battery imposes more requirements on the electrolyte than Li–ion cells (see Figure 17). These are a) high Li^+-ion conductivity, b) stability to oxidation and reduction within the voltage range of the cell, c) safety, d) sufficient O_2 solubility and diffusivity to enable high rates, e) low volatility to avoid evaporation at the interface with the gas phase, f) chemical stability towards reduced O_2 species, g) favorable interaction with intermediates and Li_2O_2 to allow for fast formation and decomposition of Li_2O_2 at high packing density, h) a deformable electrode to adapt to the shape changes during formation/disappearance of Li_2O_2. The five requirements (d) to (h) are in combination unique to Li–air chemistry and impose conflicting requirements on the materials. The challenge is formidable. Early studies of the non-aqueous Li–air batteries employed organic carbonate electrolytes because of their low volatility, compatibility with Li metal, and high oxidation stability (greater than 4.5 V versus Li^+/Li, which was necessary to charge the cells). However, previous investigation of O_2 as a contaminant in organic carbonate electrolytes in Li-ion batteries has shown evidence of electrolyte instability and this has since been confirmed by several research groups in the context of the Li–O_2 battery.[149,153] Using a combination of techniques including FTIR, surface-enhanced Raman spectroscopy (SERS), DEMS, and NMR spectroscopy it has been shown that in electrolytes, such as $LiPF_6$ in propylene carbonate, on discharge, O_2 is first reduced to O_2^- which, being a strong nucleophile, attacks the organic carbonate molecule leading ultimately to the formation of compounds such as $C_3H_6(OCO_2Li)_2$, Li_2CO_3, HCO_2Li, CH_3CO_2Li, CO_2, and H_2O; the exact species formed and their relative ratios depending on the specific organic carbonate. O_2 attack on organic carbonates was not unexpected but the ability of Li–air cells to cycle encouraged the belief that, in addition to electrolyte degradation, reversible Li_2O_2 formation/decomposition was occurring. However, recent SERS and DEMS studies also show that there is little or no evidence of Li_2O_2 formation.[149] Instead, the ability to charge the cell depends on the decomposition of the solid products that accumulate in the electrode on discharge. Cycling involves the repeated decomposition of the electrolyte on discharge and then oxidation of the decomposition products on charging, that is, back-to-back irreversible reactions.[149] This situation explains the observation that Li–air cells with such electrolytes can sustain several tens of cycles. A variety of ether-based electrolytes both linear (e.g. $CH_3O(CH_2CH_2O)_4CH_3$) and cyclic (e.g. 1,3-dioxolane; $C_4O_2H_8$) have been studied and, as expected, exhibit greater stability towards reduced oxygen species than the organic carbonates.[145,150,153a,e,154] Li_2O_2 is formed on the first discharge but is accompanied by side reactions.[153e,155] The formation of Li_2O_2 is not reversible, with up to 40 % loss on the first cycle in dimethoxyethane (DME) being reported.[153e] Li_2O_2 formation is no longer evident after a few cycles.[155] Amide-based electrolytes, such as dimethylformamide, show greater stability than ethers, nevertheless a degree of decomposition impedes prolonged cyclability.[156] Identifying electrolytes that are stable towards reduced oxygen species and that permit reversible Li_2O_2 formation, which can be sustained on cycling without significant side reactions, is one of the major challenges in this field at present. Increasingly, computational methods are used to gain insight into solvent stability and to identify promising directions.[154,157] Electrolytes other than the conventional non-aqueous liquids discussed above have

been explored. Ionic-liquid electrolytes based on 1-ethyl-3-methyl imidizolium bis(trifluoromethane sulfonyl) imide, owing to its hydrophobicity, permitted discharge of a Li–air cell for 56 days in air.[85,158] Work on liquid ethers has been extended to siloxane-modified ethers[154] and higher molecular weight solid polyethers, for example, poly(ethylene oxide) ($[CH_2CH_2O]_n$).[159] For the solid polyethers, charging between 3.1 and 3.2 V versus Li^+/Li was reported.

Li^+-ion conducting ceramic electrolytes, specifically $18.5\,Li_2O{:}6.07\,Al_2O_3{:}37.05\,GeO_2{:}37.05\,P_2O_5$ (LAGP) have been used in a Li–O_2 cell and demonstrated operation for up to 40 cycles at elevated temperatures (30–105 °C).[160] More work is needed on all these less-conventional electrolytes to give stable cycling and demonstrate whether or not Li_2O_2 is forming with high purity and decomposes reversibly on cycling. Particularly in the case of a solid electrolyte, the question of how solid Li_2O_2 forms in significant quantities remains to be clarified.

Although not a practical electrolyte, $LiClO_4$ in CH_3CN has been used to carry out SERS and DEMS studies of the fundamental reactions involved in O_2 reduction to Li_2O_2 and its oxidation on Au, Figure 18.[136a] Such studies are in accord with electrochemical measurements. The mechanistic steps on reduction are given by Equations (3a–c):

$$O_2 + e^- \rightarrow O_2^- \quad (3a)$$

$$O_2^- + Li^+ \rightarrow LiO_2 \quad (3b)$$

$$2\,LiO_2 \rightarrow Li_2O_2 + O_2 \quad (3c)$$

Several studies suggest also the direct reductions [Eq. (3d,e) can occur.[136b,159,161]

$$LiO_2 + Li^+ + e^- \rightarrow Li_2O_2 \quad (3d)$$

$$Li_2O_2 + Li^+ + e^- \rightarrow 2\,Li_2O \quad (3e)$$

The reaction in Equation (3d) occurs at lower voltages than that in (3a)[136a] and there has, to date, been only speculation for the formation of Li_2O. Oxidation of Li_2O_2 follows Equation (4).

$$Li_2O_2 \rightarrow 2\,Li^+ + 2\,e^- + O_2 \quad (4)$$

It is noteworthy that oxidation does not proceed by the reverse pathway to reduction, this relates to the separation of the charge and discharge voltages, even when the electrolyte itself is stable.[136a]

There is no doubt that the lithium-metal anode presents a formidable challenge. In addition to the cycling inefficiency necessitating excess Li, O_2 can transfer from cathode to anode and react with the lithium metal. A solid electrolyte capable of conducting Li^+ ions can be placed between the Li and the liquid electrolyte in an attempt to address these problems.[135,140,162] Such a protected lithium anode is essential for aqueous Li–air systems, it has been a major focus of attention in that field, and will be discussed in more detail below. An alternative approach is to replace the Li metal with Si or Sn.[163] However, these materials would have to be alloyed with Li prior to cell assembly or the cells fabricated in the discharged state (with Li_2O_2 already in the cathode). Of course, Si and Sn have their own challenges in terms of stability and cycling efficiency. Clearly the anode will be a major focus of investigation in the future and indeed interest in the Li–O_2 cells is prompting a renaissance of interest in lithium-metal anodes.

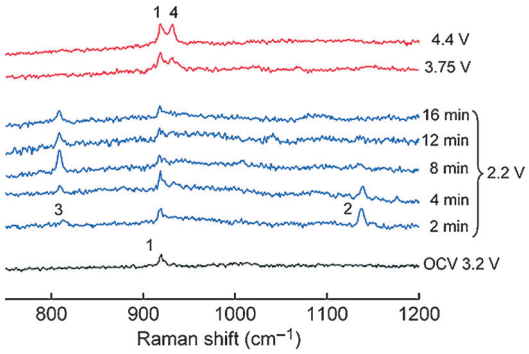

Figure 18. In situ surface-enhanced Raman spectroscopy during O_2 reduction and re-oxidation on Au in O_2-saturated 0.1 M $LiClO_4$ in CH_3CN. Spectra collected at a series of times and at the reducing potential of 2.2 V versus Li/Li^+ followed by another spectrum after subsequent oxidation at 4.4 V. The signals are assigned as follows: 1) C–C symmetric stretch of CH_3CN at 918 cm^{-1}, 2) O–O stretch of LiO_2 at 1137 cm^{-1}, 3) O–O stretch of Li_2O_2 at 808 cm^{-1}; 4) Cl–O stretch of ClO_4^- at 931 cm^{-1}.[136a]

The current focus is largely on rechargeable, rather than primary, Li–air cells, driven by the future needs for energy storage. Much of the above discussion, especially regarding electrolyte and electrode stability, relates to rechargeable Li—air batteries. For a primary battery, it may not matter if the electrolyte decomposes on discharge. For a rechargeable Li–air battery, the lesson we must learn from the experience with organic carbonate electrolytes is that observing electrochemical rechargeability alone is not proof of reversibility. A truly rechargeable battery must be based on highly reversible reactions at the electrodes. No reaction leads to products that are 100% pure or is 100% reversible, however if the electrode reactions are accompanied by significant side reactions (electrolyte decomposition) and even if the decomposition products can themselves be decomposed on charging, eventually the electrolyte will be consumed and the battery will fail. As a result, for a rechargeable Li–air battery, it is important to demonstrate that Li_2O_2 is formed in high purity on discharge, can be oxidized on charging, and that this is can be sustained on cycling. A combination of electrical measurements and spectroscopic methods is essential to demonstrate a truly rechargeable Li–air battery.

3.3.3. The Aqueous Li–Air cell

The challenges facing the aqueous cell are shown in Figure 19. Although it is not necessary to protect the cathode from ingress of H_2O, (although of course it is important not to lose/gain H_2O from the cell to ensure water balance) CO_2 must still be avoided, therefore a membrane covering the

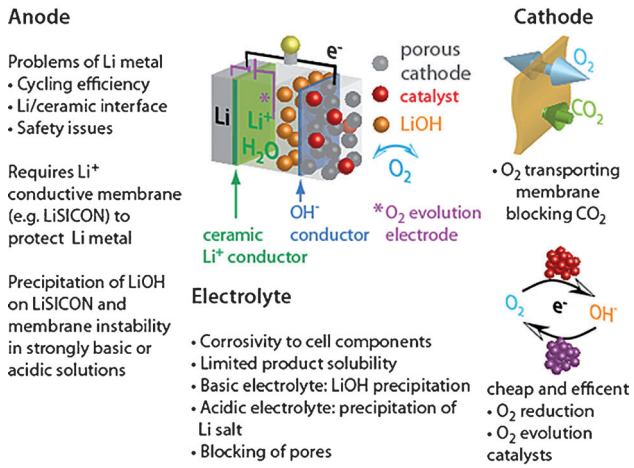

Figure 19. Challenges facing the aqueous Li–air battery.

cathode and blocking CO_2 while allowing facile transport of O_2 is important.

The most widely used aqueous electrolytes are alkaline solutions, in which the discharge product at the cathode is LiOH. Saturation of LiOH is reached at 5.3 mol L^{-1}, corresponding to a specific capacity of only around 170 mA h g^{-1} (based on electrolyte alone) that is, barely more than a lithium-ion cell. To access higher capacities, a flow-cell design, in which the electrolyte is constantly replenished with a fresh solution, has been proposed; the same authors have also proposed recharging by collecting the LiOH, extracting lithium metal, then mechanically replacing the anode.[138a,164] Otherwise, to obtain high capacities, it is necessary to allow the LiOH to precipitate. To avoid solid LiOH blocking the pores of the cathode, an anionic exchange membrane is employed to separate the cathode from the electrolyte (Figure 19).[135b] Such a membrane permits OH^- ions generated in the porous cathode on discharge to be transported out into the bulk electrolyte, while preventing the Li^+ ions from entering the cathode, hence LiOH precipitates outside the porous cathode. Without the need to accommodate a solid discharge product, as in the case of non-aqueous Li–air battery, the porous cathode design can be somewhat simplified and is much closer to the gas-diffusion electrode familiar in aqueous-based fuel cells and other aqueous metal–air batteries.[135b] The key design principles of the porous electrode are efficient O_2 transport in the gas-diffusion channels and exchange of O_2 between these channels and the electrolyte near the sites of the O_2 reduction catalyst on the electrode surface, good dispersion of the catalyst, and a high active surface area. To charge the cell, a third (O_2 evolution) electrode is located in the bulk electrolyte outside the cathode.[135b] Cheap and efficient O_2 reduction and evolution catalysts are required. Separation of the oxygen reduction and evolution electrodes permits the use of different catalysts for each electrode. Moreover, basic conditions allow for non-precious metal catalysts.[165] It is interesting to note that recent progress with grapheme-based electrode materials has led to metal-free and therefore cheap electrodes for acidic Li–air cells.[166] This development permits access to higher energy densities, as a result of the increased thermodynamic voltage in acidic media and higher solubility of the products.

A major focus of attention has been the lithium-metal anode protected by a lithium-ion conducting ceramic electrolyte. The most commonly used ceramic membrane is LISICON with the composition $Li_{(1+x+y)}Al_xTi_{2-x}Si_yP_{(3-y)}O_{12}$ (marketed by Ohara Incorporated, Japan).[167] Although it is of course essential to protect the lithium-metal anode in an aqueous cell, such a ceramic membrane is not without its challenges. LISICON is reduced in contact with Li^0 and the Li/ceramic interface is difficult to cycle. Efforts to address these issues involve introducing an interlayer of LIPON[135b] or a thin film of a non-aqueous liquid or gel electrolyte.[140] However, such liquid or gel electrolytes introduce the Li cycling problems mentioned above. Furthermore, the alkaline electrolyte can attack the ceramic membrane resulting in an increase in the interfacial impedance and therefore the overall impedance of the cell. The membrane can become clogged with precipitated LiOH. Both protection of the membrane from strongly basic conditions and the avoidance of LiOH deposition can be achieved using a Li^+-conducting polymer on the electrolyte side of the ceramic.[135b] The necessity for these numerous layers introduces considerable complexity. There remains much scope for new protective membranes that can address the challenges just described. Nevertheless the aqueous lithium–air cell is a potentially promising approach and small prototypes have shown the ability to sustain several hundred cycles, albeit at relatively modest capacities. Such cycling has indicated that the charge–discharge voltage separation can be as low as 0.3 V at current density of 0.1 mA cm^{-2} or 0.9 V at 0.5 mA cm^{-2}.

4. Electric Double-Layer Capacitors

4.1. General Principles and Cell Construction

In the simplest configuration an electric double-layer capacitor (EDLC) consists of two electrodes immersed into electrolyte and separated by an ion-conducting but electron-insulating membrane. Upon the application of a potential to one of the electrodes the ions of the opposite sign accumulate on its surface in a quantity proportional to the applied voltage, forming a so-called electrical double layer. This double layer consists of an electrical space charge from the electrode side and an ion space charge from the electrolyte side.[168] The charge storage mechanism in pure EDLC is non-Faradaic, which means that during charging and discharging of this device no charge transfer takes place across the electrode/electrolyte interface and the energy storage is electrostatic in nature.

Apart from electrostatic ion adsorption, carbon materials with functional groups on their surfaces may additionally exhibit chemical interactions with selected electrolytes, which involve fast and often reversible charge-transfer reactions between the carbon surface and the electrolyte ions. Such processes are called Faradaic. The adsorption of ions under the application of an electric field could be described by an adsorption isotherm, which describes the surface coverage of

the adsorbed species at constant temperature as a function of their concentration, controlled by the applied voltage.[169] At a constant temperature and voltage, the coverage of the surface by ions is controlled by the balance between the changes in entropy and enthalpy of a system. If the enthalpy of ion–carbon electrode interactions deviates weakly from its average value, the accumulated surface charge will strongly depend on the applied voltage and the pseudocapacitance will exhibit a sharp peak at certain voltage values as typically observed in batteries.[170] Many pseudocapacitive materials (including transition-metal oxides, conductive polymers, and functionalized or doped carbons) may show a very broad capacitance peak or demonstrate almost no dependence of the pseudocapacitance on the applied voltage.[170–171] This situation may indicate that the pseudocapacitive ion-adsorption sites have a very broad distribution of enthalpies. Some authors employ the "pseudocapacitance" designation only when the charge accumulated during Faradaic processes is a continuous and, ideally, a linear function of the applied voltage. In this case, experimental differentiation between non-Faradaic electrostatic ion adsorption and a fast Faradaic electrochemical ion adsorption becomes particularly difficult.

The energy density of an EDLC is determined by the capacitance of positive and negative electrodes and the maximum voltage, at which the device can be operated [Eq. (5)].

$$E^{\mathrm{EDLC}} = \left(\frac{C_- C_+}{C_- + C_+}\right)\left(V_{\max}^{\mathrm{EDLC}}\right)^2 \tag{5}$$

To maximize the energy of an EDLC the capacitance of both electrodes should be the same. In this case [Eq. (6)]:

$$E^{\mathrm{EDLC}} = \frac{1}{2} C \left(V_{\max}^{\mathrm{EDLC}}\right)^2 \tag{6}$$

The maximum voltage is generally determined by the stability window (from the lowest stable potential $V_{\mathrm{low}}{}^{\mathrm{stable}}$ to the highest stable potential $V_{\mathrm{high}}{}^{\mathrm{stable}}$) of the selected electrolyte. Impurities and functional groups on carbon, however, may catalyze electrolyte decomposition and increase $V_{\mathrm{low}}{}^{\mathrm{stable}}$ or decrease $V_{\mathrm{high}}{}^{\mathrm{stable}}$, thus lowering EDLC maximum voltage and energy density. The Supporting Information provides a brief discussion of routes to maximize the EDLC voltage (Supporting Information, Figure S1).

4.2. Electrolyte–Electrode Interactions

Traditionally, a Helmholtz electric double layer consisting of solvated ions was used to understand the energy-storage mechanism. Solvated ions were often believed not to enter the pores if their size exceeded the pore dimensions. However, by studying over 30 different porous carbons in KOH electrolyte it was found that the specific surface area (SSA) of the carbon does not have a clear correlation with the specific capacitance.[172] Furthermore, increasing SSA with a simultaneous increase in the average pore size was shown not to increase the specific capacitance either.[172] Another study investigated the correlation of the pore size and SSA accessible to N_2 gas with that accessible by positive and negative ions in both aqueous and organic electrolytes.[173] The study concluded that a distortion of solvation shells is dependent on both the ion and the solvent. In 2006 two research groups[174] observed significant enhancement of the specific capacitance in small micropores, in which the ion solvation shell becomes highly distorted and partially removed.[174a] The resulting smaller charge-separation distance between the ion centers and the pore walls leads to greatly increased capacitance.[174,175] Yet, when the pore size becomes smaller than the critical (often unsolvated) ion size, the access of the ions into the pores becomes limited[174a,176] and, additionally, the transport of ions inside such pores becomes slow.

A recent study revealed the significant effect of pore tortuosity on slowing down the transport of ions within carbon nanopores.[177] Electrochemical impedance spectroscopy measurements and cyclic voltammetry studies showed up to three orders of magnitude enhancements in the ion transport and frequency response accompanying the micropore alignment and a decrease in the concentration of obstacles for ion diffusion. The positive effect of electrolyte wetting on the carbon surface has been discussed in many publications.[178] Improved electrolyte wetting behavior commonly improves the charge–discharge rate and allows higher specific capacitance values to be achieved. Furthermore, defects on the surface of the carbon were proposed to interact with the solvation shells of the ions, decreasing the average carbon-surface–ion separation distance, and thereby increasing specific capacitance[179]

4.3. Electrode Materials

To clearly distinguish capacitor-type electrochemical energy storage from battery-type systems described in other sections of this Review, we focus only on devices containing pure-carbon electrodes exhibiting primarily a non-Faradaic double-layer energy-storage mechanism. Various types of carbon materials with high surface area, high electrical conductivity, as well as a range of shapes, sizes, and pore size distributions could be synthesized on a large commercial scale. Some common examples of such carbons include: activated carbon, carbide derived carbon (CDC), zeolite-templated carbon (ZTC), graphene, carbon nanotubes, carbon onions, and carbon aerogels (Figure 20, and 21 and Table 2). However, in this Section, we focus on recent progresses on carbon nanotubes and graphene.

4.3.1. Carbon Nanotubes

Carbon nanotubes (CNTs; Figure 19e) have relatively low BET SSA, low density (which may thus lead to a low volumetric capacitance), and are typically difficult to process into thick electrodes using conventional electrode preparation methods. However, they offer very high electrical conductivity and open porosity, which may allow fast ion transport and thus high power characteristics of EDLCs. One

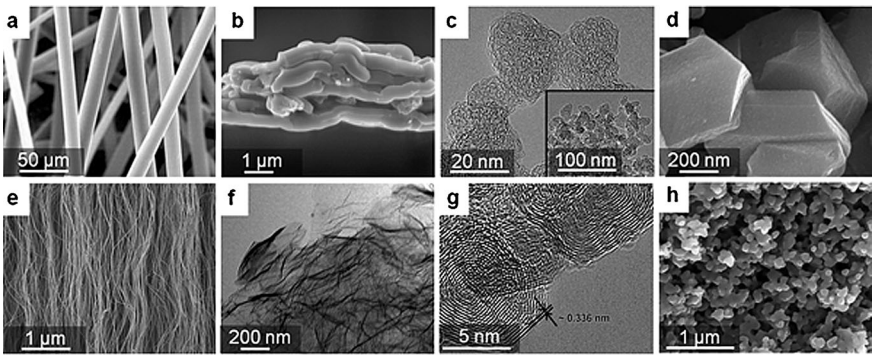

Figure 20. Electron microscopy images of high surface area carbon materials: a) SEM of active carbon fibers.[180] b) SEM of templated carbide-derived carbon.[181] c) TEM of carbide-derived carbon nanoparticles.[182] d) SEM of zeolite-templated carbon.[177] e) SEM of vertically aligned MWCNTs.[183] f) TEM of multi-layer graphene flakes.[184] g) TEM of carbon onions.[179b] h) SEM of carbon aerogel particles.[185] Copyright: American Chemical Society, Elsevier, The Electrochemical Society, and John Wiley & Sons, Inc.

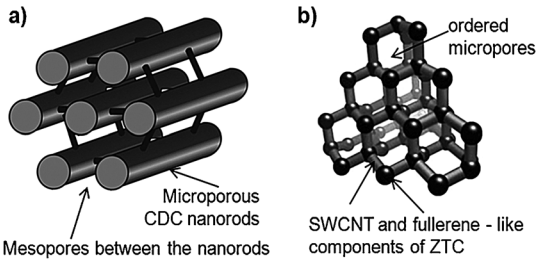

Figure 21. Schematic representation of the pore structure for two classes of structured porous carbons: a) template carbide-derived carbon[181,186] and b) zeolite-templated carbon.[187] Copyright: American Chemical Society, Elsevier, and John Wiley & Sons, Inc.

Table 2: Selected properties of some of the nanostructured carbon materials used in EDLCs.

Carbon electrode material	SBET [$m^2 g^{-1}$]	Capacitance in organic and IL electrolytes [$F g^{-1}$]	Capacitance in aqueous electrolytes [$F g^{-1}$]
Activated carbon (AC)	800–3500	50–300	50–300
Carbide-derived carbon (CDC)	600–2800	70–180	60–220
Zeolite-templated carbon (ZTC)	1000–3600	80–190	150–340
Carbon nanotube (CNT)	400–1200	15–100	15–210
Graphene	300–3100	100–240	40–220
Onion-like carbon (OLC)	400-650	20-60	15-50
Carbon aerogel	100–1000	7–80	20–190

of the earliest studies describing the abilities of thin CNT-based EDLC electrodes to provide high power and high rate performance was reported in 1997.[188] In this study multi-walled CNTs (MWCNTs) with an average diameter of 8 nm were treated in nitric acid and processed into thin (25 μm) electrodes. When tested in concentrated (38 wt.%) H_2SO_4 electrolyte the CNTs showed moderately high specific capacitance of 102 $F g^{-1}$ but offered a high operating frequency of up to 100 Hz.[188]

SWCNTs offer higher SSA than MWCNTs, but tend to bundle and may contain semiconducting tubes, which is undesirable for EDLC applications. A first electrochemical study on single-walled CNT (SWCNT) bundles having individual tubes of 1.2–1.4 nm diameter and 10 nm bundle diameter was reported in 2000.[189] The SWCNT bundles were processed into a paper with a density of 0.3–0.4 $g cm^{-3}$ and thickness of 25-40 μm, in which tubes hold together purely by van der Waals interactions. BET SSA of the samples was not provided. In three-electrode cells with aqueous electrolytes (1M NaCl, 7M H_2SO_4, and 5M KOH) most SWCNT paper samples showed capacitance ranging from 19 to 26 $F g^{-1}$ for scan rates up to 500 $mV s^{-1}$, with several samples exhibiting capacitance as high as 30–41 $F g^{-1}$ in 1M NaCl.[189] A small capacitance decrease (less than 15%) was observed when the sweep rate was increased from 5 to 500 $mV s^{-1}$,[189] which is characteristic of high-power devices. Broad redox/pseudocapacitive peaks observed in most SWCNT electrodes because of the presence of oxygen-containing functional groups could be eliminated by annealing the material at 900°C in Ar.[189]

A follow-up study by the same research group investigated the electrochemical performance of SWCNT papers in aqueous (0.1M) solutions of NaCl, CsCl, benzyltriethylammonium chloride (BTEAC), $LiNO_3$, $NaNO_3$, $Ca(NO_3)_2$, and trimethylammonium nitrate (TMAN), as well as in organic electrolytes, such as $LiClO_4$ and TBATFB in acetonitrile (AN) solvent.[190] Interestingly, while no well-defined Faradaic signals were observed with TBATFB-based electrolyte, a $LiClO_4$-based electrolyte demonstrated clear reduction/oxidation responses.[190] Capacitance values similar to that of Ref. [189] were achieved. This study was also one of the first that utilized electrochemical quartz-crystal microbalance (EQCM) instrumentation, and which detected electrode mass changes of up to around 1% in aqueous electrolytes and in a TEATFB-based organic electrolyte, and up to about 4% in a 1M $LiClO_4$-based organic electrolyte upon charging.[190] When used in IL electrolytes with different anions (such as bis(trifluoromethanesulfonyl) amide (BFSA), dicyanamide (DCA), hexafluorophosphate (HFP), and *p*-tolunesulfonate (PTS)) and cations (such as R,R0-Imidazolium and R,R0-Pyrrolidinium) SWCNT paper demonstrated capacitance ranging from 14 to 24 $F g^{-1}$, but offered a very-high voltage stability window of up to 5.5 V.[191]

The first study of MWCNTs grown directly on conductive graphite-foil substrates was reported in 2002. Misaligned MWCNTs with a diameter of 50 nm showed an unusually high specific capacitance of 116–153 $F g^{-1}$ in 1M aqueous solution of H_2SO_4, and up to 13–79 $F g^{-1}$ in 0.1M $LiClO_4$-based organic electrolyte, for sweep rates from 100 to 2 $mV s^{-1}$.[192] The study

assumed invariance in the capacitance and mass of graphitic foil substrates after the CNT growth, which may or may not be correct.[192] Development of methods to grow CNTs on bulk metal substrates (such as an Inconel alloy) improved the current collector/CNT contact resistance and rate capability.[193] In this study, however, a capacitance of only 18 $F g^{-1}$ was achieved in 6 M KOH electrolyte.[193] In another study, however, vertically aligned MWCNTs grown to 0.15 mm on Inconel foils showed specific capacitance as high as 83 $F g^{-1}$ at 1 $mV s^{-1}$ and 47 $F g^{-1}$ at 1000 $mV s^{-1}$ in organic electrolyte based on 1 M TEATFB salt solution.[194] Various MWCNT electrodes (including those grown directly on Al foil) with BET SSA ranging from 47 to 1064 $m^2 g^{-1}$ and a density ranging from 0.1 to 0.9 $g cm^{-3}$, were also investigated in 1 M TEATFB organic electrolyte.[195] As their capacitance values were quite modest (8–16 $F cm^{-3}$, over three-times smaller than that of commercial activated carbons) it was concluded that this technology would unlikely be acceptable for mainstream EDLC applications.[195]

Aligned CNT forests (Figure 19e) provide higher rate capability than misaligned ones having the same thickness, this is due to the straight shape of the pores and thus their lower ionic resistance. However, the as-grown (either aligned or misaligned) CNT forests generally have very high porosity (up to 98% pore volume/empty space) and thus exhibit very low volumetric capacitance. A simple method to produce electrodes with greatly enhanced density was proposed in 2006.[196] This method described the introduction of liquid into 0.1–1.5 mm long aligned SWCNT forest (2.8 nm average tube diameter), followed by the evaporation of the liquid, which causes an electrode densification of over 20 times (to an average tube separation distance of 0.9 nm) and preserves the very high degree of tube alignment and high BET SSA of 1000 $m^2 g^{-1}$.[196] The specific capacitance of densified SWCNT electrode reached 80 $F g^{-1}$ in TEATFB-based organic electrolyte.[196]

Significant enhancement of the vertically aligned MWCNTs' capacitance was observed after plasma activation.[197] Aligned MWCNT electrodes with approximately 50 nm diameter were synthesized on Ni substrates and investigated in 6 M KOH electrolyte. The ammonia plasma etching increased the BET SSA from 9.6 to 86.5 $m^2 g^{-1}$ and specific capacitance from 37 to 207 $F g^{-1}$.[197] These values are unusually high for the modest surface area of these samples (up to 239 $\mu F cm^{-2}$) and thus very promising, but the origin of such high area-normalized capacitance remains unclear. Yet, similarly unusually high values of specific capacitance of plasma-activated MWCNTs were reported in the studies by another research group.[198] The use of oxygen plasma on 0.1–0.2 mm tall, vertically aligned MWCNT electrodes (5–10 nm in diameter) resulted in opening of the CNT tips, increasing the SSA to 400 $m^2 g^{-1}$, and increasing the number of defects and functional groups on the tubes' outer walls, which, in turn, lead to outstanding specific capacitance (over 400 $F g^{-1}$) in IL electrolytes.[198] This value is significantly higher than that of similar vertically aligned MWCNTs that were not exposed to plasma etching/activation (27 $F g^{-1}$ in ILs,[199] and 11–22 $F g^{-1}$ in 6 M KOH[200]). Unfortunately, plasma-activated samples decorated with functional groups may potentially have issues with low cycle stability and high leakage current, but such studies were not presented in either of the reports.[197,198]

The CNT-based layer-by-layer (LBL) assembly consists of the repeated, sequential immersion of a substrate into different aqueous solutions of functionalized CNTs, some having only a positive charge (such as amine functional groups, CNT-NH_2) and others having only a negative charge (such as carboxylic functional groups, CNT-COOH) on their surface.[201] Ultra-thin (less than 1 micron) but self-supporting films could be prepared by cross-linking CNT bi-layers at temperatures as low as 150 °C.[201b] The specific capacitance of LBL CNT films was found to approach 160 $F g^{-1}$ in 1 M H_2SO_4,[201b] which could be a result of the pseudocapacitive effect of the functional groups on their surface. Indeed, heat-treatment of LBL CNTs in an H_2 atmosphere at 300 °C for 3 h reduced both the amount of functional groups and the estimated specific capacitance (to 60 $F g^{-1}$).[201b]

The binder-free LBL CNT films (up to 3 μm in thickness) were investigated as a positive electrode in Li-ion battery/supercapacitor hybrid devices.[201a] After heat-treatment in vacuum at 150 °C and in H_2 at 300 °C, the LBL CNT films produced showed significant improvements in electrical conductivity and mechanical stability. They also demonstrated unusually high density of 0.8 $g cm^{-3}$ (their porosity of 30% was significantly smaller than the theoretically possible value for misaligned CNTs) and contained nearly 11 atom% oxygen and 4 atom% nitrogen.[201a] Owing to the pseudocapacitance induced by the functional groups, the LBL CNT electrodes demonstrated ultra-high capacitance of 250 $F g^{-1}$ in organic electrolyte based on a 1 M $LiPF_6$ salt dissolved in a mixture of carbonates when tested in the voltage range from 1.5 to 4.5 versus Li/Li^+.[201a] When LBL CNT films were heat-treated at 500 °C to reduce the number of functional groups, they showed a reduced specific capacitance of 150 $F g^{-1}$, although this is significant when compared to that of CNT-COOH and CNT-NH_2 (both less than 100 $F g^{-1}$), and of pristine CNTs (below 50 $F g^{-1}$) bonded together using 20 wt.% PVDF binder. The small capacitance of the functionalized CNTs was explained by the presence of a binder that blocks access of the Li ions to the functional groups.[201a] The LBL CNT film was found to store Li ions up to a gravimetric capacity of 200 $mA h g^{-1}$ and demonstrated ultra-high power (100 $kW kg_{CNT}^{-1}$) and good cycle life (several thousand cycles) in a full cell (LBL CNT vs. $Li_4Ti_5O_{12}$ (LTO)) configuration.[201a]

In contrast to LBL assembling, electrophoretic (EP) deposition is a significantly faster thin-film fabrication technique. It involves formation of a good suspension of (e.g. negatively) charged CNTs and application of an opposite (e.g. positive) potential (commonly 10–50 V) to a metal current collector to attract CNTs.[202] The EP CNT films with moderate capacitance (20 $F g^{-1}$ in 6 M KOH) demonstrated an operating frequency in excess of 1000 Hz (the "knee" frequency in the impedance plot was about 7500 Hz) and a power density in excess of 20 $kW kg^{-1}$.[202a]

Formation of a highly concentrated (such as 27 mg per mL) colloidal suspension of MWCNT in dimethylformamide (DMF) was shown to produce thin, locally aligned MWCNT sheets if the suspension is deposited on Ni foil and dried.[203]

While the specific capacitance of the produced sub-μm electrodes was modest (20 $F g^{-1}$ in 6 M KOH electrolyte), the sheet resistance of the electrodes was low and their power characteristics were very high (30 $kW kg^{-1}$).[203]

4.3.2. Graphene

One of the first studies of graphene structures (Figure 20 f) in different electrolytes was reported in 2008.[204] Graphene was prepared by thermal exfoliation of graphitic oxide (GO) at 1050 °C, which resulted in a material with BET SSA of 925 $m^2 g^{-1}$. The specific capacitance of graphene electrode in 1 M H_2SO_4 (100–117 $F g^{-1}$ for sweep rates ranging from 1 to 0.01 $V s^{-1}$ for exfoliated GO) compared favorably with that of onion like carbon (OLC; 35 $F g^{-1}$), MWCNT (8–14 $F g^{-1}$), and SWCNT (50–70 $F g^{-1}$). In ionic liquid (*N*-butyl-*N*-methylpyrrolidinium bis(trifluoromethanesulfonyl)imide or $PYR_{14}TFSI$), exfoliated and reduced GO exhibited specific capacitance approaching 75 $F g^{-1}$.[204] Soon after that, an alternative method for graphene synthesis involving suspending GO sheets in water and then reducing them by using hydrazine hydrate resulted in graphene structures agglomerated into 15–20 μm size particles exhibiting moderately high BET SSA of 705 $m^2 g^{-1}$.[205] Surprisingly, graphene particles showed a high specific capacitance of 100–135 $F g^{-1}$ in 5.5 M KOH electrolyte and up to 99 $F g^{-1}$ in organic electrolyte based on 1 M $TEABF_4$ salt.[205] While both the specific and more importantly volumetric capacitance of graphene was significantly smaller than that of activated carbons, these two publications generated significant interest and multiple follow-up publications in 2009–2011. To minimize the agglomeration of individual graphene layers, a reduction of GO by hydrazine in the gaseous phase was proposed.[206] This process modification allowed researchers to further improve the specific capacitance of graphene to a very high initial value of 205 $F g^{-1}$ in 30 % KOH solution (reduced to 170 $F g^{-1}$ after 1200 cycles), in spite of the low measured BET SSA of 320 $m^2 g^{-1}$.[206] An alternative process of avoiding graphene agglomeration and the preparation of stable graphene colloids involved reducing exfoliated GO with *p*-phenylene diamine (PPD), which causes positive surface charge on graphene fragments induced by adsorbing the oxidation product of PPD.[207] By using EP deposition of graphene on Ni, thin EDLC electrodes with the desired thickness and specific capacitance up to 164 $F g^{-1}$ in 6 M KOH could be prepared.[207] A stable aqueous suspension of graphene was also prepared by a noncovalent functionalization of graphene with 1-pyrenecarboxylic acid (PCA) by a nondestructive π–π stacking (aromatic interaction) mechanism.[208] The -COOH group of PCA facilitates the graphene stability in water and allows formation of EDLC electrodes with capacitance approaching 120 $F g^{-1}$ in non-specified electrolytes.[208] Reduction of the size of graphene platelets may also minimize their tendency to agglomerate. Exfoliation of oxidized carbon nanofibers and subsequent reduction in hydrazine showed specific capacitance of 82–132 $F g^{-1}$ in 2 M H_2SO_4, depending on the size of the graphene segments, with the highest capacitance observed in the smallest graphene platelets (which had the lateral dimensions of 170 nm and an average thickness of 1 nm).[209]

In situ electrochemical reduction of GO was proposed in 2009, and involved gradual in situ transformation of GO electrodes into graphene electrodes during CV cycling in the potential range from −1 to + 1 V versus a reversible hydrogen electrode (RHE) in 0.1 M Na_2SO_4 solution.[210] After 2000 cycles the electrode exhibited impressive specific capacitance of 165 $F g^{-1}$.[210] The electrochemical performance of graphene electrodes, prepared using thermal exfoliation of GO at low temperature (250–400 °C) in air and with subsequent optional carbonization at higher temperature (700–900 °C) in N_2, was evaluated in 2 M KOH electrolyte. The produced functionalized graphene had an average pore size of 17–20 nm, BET SSA ranging from 329 to 737 $m^2 g^{-1}$, and showed specific capacitance of 221–233 $F g^{-1}$ for samples produced without annealing in N_2, and 95–114 $F g^{-1}$ for sample after such an annealing.[211] In spite of lowering the specific capacitance, the high-temperature annealing significantly improved the electrode rate capability, showing up to 79 % capacitance retention when the sweep rate was increased from 5 to 100 $mV s^{-1}$.[211]

Partial reduction of a GO suspension by hydrobromic acid resulted in the formation of functionalized graphene, which exhibited specific capacitance of up to 129 $F g^{-1}$ at 10 $mV s^{-1}$ in 1 M H_2SO_4 and up to half of that in 1-butyl-3-methylimidazolium hexafluorophosphate (BMIHFP) ionic liquid in a symmetrical two-electrode EDLC.[212] When evaluated in a three-electrode configuration the electrodes exhibited capacitance of up to 198 $F g^{-1}$ when evaluated using CV tests and up to 348 $F g^{-1}$ when evaluated using galvanostatic charge–discharge tests in 1 M H_2SO_4.[212] The origin of the large difference in the performance results depending on the testing technique was not discussed.[212] Partial mild reduction of a GO suspension in dimethylformamide (DMF) was also performed by simply heating the suspension to 150 °C in an oil bath for different durations.[213] Electrodes with small electrode density (under 0.2 $mg cm^{-2}$) showed a specific capacitance of approximately 180 $F g^{-1}$ when evaluated from CV tests, and up to 276 $F g^{-1}$ when evaluated using galvanostatic charge–discharge tests in 1 M H_2SO_4 (both tests performed in three electrode configuration).[213]

Vertically aligned graphene sheets grown by plasma-enhanced CVD on carbon cloth were proposed for ultra-high power and ultra-high frequency performance.[206] This idea was further developed in 2010, when sub-μm long graphene nanosheets were synthesized on Ni substrates using plasma-enhanced CVD and exhibited a BET SSA of 1100 $m^2 g^{-1}$.[214] The capacitance of the nanosheet-based EDLC decreased from 375 to 140 μF when the frequency was increased from 0.01 to 10 000 Hz, which allowed the produced EDLC to be efficiently used for AC filtering at a characteristic frequency of 120 Hz.[214] In an organic electrolyte the capacitance was 50 % higher than in aqueous one but the frequency response was inferior.[214] The produced material showed a frequency response comparable to that of Al electrolytic capacitors, while offering higher volumetric capacitance and maximum operating voltage.[214]

Thermal reduction of GO (having initial interlayer spacing of 0.6 nm) in Ar at 200–1000 °C produced a graphitic material with a very small BET SSA of 5 m^2g^{-1} and interlayer spacing of 0.33–0.46 nm.[215] This partially reduced GO material, having negligibly small initial capacitance was electrochemically activated in a traditional TEATFB electrolyte in the potential window of −2.1 to + 1.6 versus the carbon quasi-reference electrode. The activation caused the subsequent intercalation of anions and cations in between graphene layers and a dramatic increase in the specific capacitance up to an impressive 220 $F g^{-1}$.[215] While neither the pore size nor the density of the activated sample were reported, its volumetric capacitance is expected to be very high, owing to the small pore size, which is just large enough for ion insertion. It is still arguable if such a material should be called "activated graphite" or "multi-layered graphene", but it is clearly one of the most promising materials for EDLC reported to date.

Limitations of most mesoporous graphene samples decorated with multiple functional groups and having high pseudo-capacitance include low electrode density and thus low volumetric capacitance, as well as the expected high leakage current and limited cycle life. Such issues, however, have historically been ignored and rarely presented or discussed. Most specific capacitance values reported in the literature for graphene do not come from symmetric two-electrode tests and thus over-estimate the real performance. Similarly to the CNTs and OLC, mesoporous graphene electrodes are unlikely to replace traditional activated carbon-based EDLC electrodes with the rare exception of devices operating at ultra-high frequency and competing with electrolytic capacitors.

5. Summary and Outlook

There has been a global trend to develop a safe lithium-ion battery with high energy density that meets the emerging applications in the transportation sector. The research effort on the cathode has been centered on high-Ni-content and lithium-rich transition-metal oxides, which can deliver a reversible capacity of more than 200 mA h g^{-1}. However, naturally unstable Ni^{3+} ions are apt to reduce to Ni^{2+} on the cathode surface in the form of NiO, and this reaction accelerates with increasing temperatures. Further structural instability from the higher oxidation state of Ni^{4+} with increasing cut-off voltages leads to substantial oxygen generation from the lattice at elevated temperatures. Recently, larger amounts of Ni were substituted by electrochemical inactive Mn ions to counteract such inherent problems, but increasing the Mn content increased the charge transfer resistance, resulting in decreased electrochemical performance (rate capability). On the other hand, increasing Mn content preserves the initial structural integrity during the high-temperature heating as well as electrochemical cycling. In this regard, applying a coating or core–shell methods to the cathode material may solving both the problem of rate capability and the thermal instability of the delithiated states. Nano-structured Si-based composite materials showed promise for providing significantly higher specific capacity than the conventional graphite anode, but larger amounts of heat generation from the nanosized Si, in spite of carbon coating, is still a great concern. As far as we are concerned, porous bulk Si coated with the carbon is the best solution to minimize the exothermic reaction with the electrolytes.

The development of a robust and thermally stable solid–electrolyte interface is critical to enhance the safety of the anode materials. Flame retarding solvents and low-volatile ionic liquids have been considered as promising materials for the suppression of flammability of electrolytes and enhanced thermal stability of batteries. Research is also underway to develop high-voltage electrolytes and novel electrolyte additives to protect cathode, carbon, and Si-based anode materials.

The progress achieved to date shows that the Li–S battery is a very promising energy-storage system, although the theoretical full capacity over extended cycling has not been realized to date. However, exciting reports of optimized systems have appeared over the last few years with 800 mA h g^{-1} capacities over 100 cycles, at good rates (over C/5) and with good capacity retention and coulombic efficiencies that approach > 96 %.

By loading sulfur into a nanoporous carbon in a controlled manner, nanocomposite electrodes can exhibit high electronic and ionic conductivity and a high adsorption capacity for polysulfides. However, because of the dissolution of polysulfides—even at a very slow rate—the morphology of the active mass will change, resulting in degraded charge transfer and accessibility. This requires additives, and porous carbons in particular, to execute a multi-functional task. Nanocomposites based on functionalized mesoporous carbons and graphenes represent the most promising candidates as positive electrodes in Li–S cells, and polymer coatings provide more even more scope.

The functionality of various nanostructured carbons, in particular, allows for substantial potential in improving the overall performance of Li–S batteries. Together with advances in the Li anode and electrolytes, nanocomposite electrodes will hopefully enable the Li–S battery to be a highly efficient and reliable energy-storage system in the very near future. We note that initial steps have also been taken to extend the chemistry using porous carbon/sulfur cathodes to Mg–S batteries that utilize a Mg anode[216] and tailor-designed electrolytes. Although cycling was not demonstrated because of capacity fade due to polysulfide dissolution, this marks an interesting and important new direction.

The combination of the highest theoretical specific energy of any rechargeable battery and the need for a step-change in energy storage in the long-term will ensure intense interest in aqueous and non-aqueous Li–O_2 batteries now and for some time to come. Aqueous Li–O_2 batteries present particular challenges centered on the lithium anode, its protection, cyclability, stability, and safety. New Li^+ conductive protective membranes that are thinner/better conductors, more stable, and enable reversible and facile Li plating and stripping are required to optimize performance.

The non-aqueous Li–O_2 battery is the newest energy-storage device discussed in this Review. Significant progress

has been made recently in understanding the fundamental processes occurring in the cell. It is now known that organic carbonate electrolytes are too unstable and that ethers, although more stable, may not be sufficiently stable on cycling for use in such cells. As a result, suitable stable, non-volatile non-aqueous electrolytes have yet to be identified. Progress in understanding the mechanisms of O_2 reduction and Li_2O_2 oxidation will pave the way to achieving better control of the kinetics and hence reduce the gap between the charge and discharge voltage, important in improving the round-trip energy efficiency and rate capability. As well as new electrolytes, further work will examine cathode stability and optimization of porous electrode architecture. Future work must also address the lithium anode in terms of safety and cycling stability, perhaps with similar strategies to those for aqueous systems.

The significant progress in material science and electrochemistry of nanostructured carbon materials has made it possible to produce advanced electrochemical capacitors with greatly improved performance characteristics suitable for a continuously increasing number of applications. The novel design of electrochemical capacitors cover almost the entire performance range (in terms of power and energy density) existing between conventional capacitors and electrochemical batteries. Their rapid charging rate (from 20 down to 0.01 s), the long cycle life (up to 1 000 00 cycles) and the broad operational temperature window (from −70 to above +100 °C) are yet unmatched by high-power batteries. The overall prospects and the associated advantages of using EDLC devices in new applications will power further efforts in research, development and production of materials for future electrical double-layer capacitors.

This research was supported by the MKE (The Ministry of Knowledge Economy), Korea, under the ITRC (Information Technology Research Center) support program supervised by the NIPA (National IT Industry Promotion Agency) (NIPA-2011-C1090-1100-0002) and by the Converging Research Center Program through the Ministry of Education, Science and Technology (2012K001251). P.G.B. and S.A.F. are indebted to the EPSRC and SUPERGEN for financial support. Part of this research was funded by U.S. Department of Energy, FreedomCAR and Vehicle Technologies Office. Argonne National Laboratory is operated for the U.S. Department of Energy by UChicago Argonne, LLC, under contract DE-AC02-06CH11357. Part of this research was supported by the Energy Efficiency & Resources program of the Korea Institute of Energy Technology Evaluation and Planning (KETEP) grant funded by the Korea government Ministry of Knowledge Economy (20118510010030).

Received: February 21, 2012
Revised: May 18, 2012
Published online: September 10, 2012

[1] a) V. Etacheri, R. Marom, R. Elazari, G. Salitra, D. Aurbach, *Energy Environ. Sci.* **2011**, *4*, 3243 – 3262; b) G. Jeong, Y. U. Kim, H. Kim, Y. J. Kim, H. J. Sohn, *Energy Environ. Sci.* **2011**, *4*, 1986 – 2002; c) B. Dunn, H. Kamath, J.-M. Tarascon, *Science* **2011**, *334*, 928 – 935.

[2] P. G. Bruce, S. A. Freunberger, L. J. Hardwick, J.-M. Tarascon, *Nat. Mater.* **2012**, *11*, 19 – 29.

[3] J. B. Goodenough, H. D. Abruña, M. V. Buchanan, Basic Research Needs for Electric Energy Storage: Report of the Basic Energy Sciences Workshop on Electrical Energy Storage, U.S. Department of Energy, Office of Basic Energy Sciences, Washington, DC, **2007**.

[4] M. R. Palacín, *Chem. Soc. Rev.* **2009**, *38*, 2565 – 2575.

[5] a) D. D. MacNeil, J. R. Dahn, *J. Electrochem. Soc.* **2002**, *149*, A912 – A919; b) D. D. MacNeil, T. D. Hatchard, J. R. Dahn, *J. Electrochem. Soc.* **2001**, *148*, A663 – A667; c) D. D. MacNeil, Z. H. Lu, Z. H. Chen, J. R. Dahn, *J. Power Sources* **2002**, *108*, 8 – 14.

[6] a) M. N. Richard, J. R. Dahn, *J. Electrochem. Soc.* **1999**, *146*, 2068 – 2077; b) D. D. MacNeil, J. R. Dahn, *J. Electrochem. Soc.* **2003**, *150*, A21 – A28; c) Z. H. Chen, Y. Qin, J. Liu, K. Amine, *Electrochem. Solid-State Lett.* **2009**, *12*, A69 – A72; d) Z. Chen, Y. Qini, Y. Ren, W. Lu, C. Orendorff, E. P. Roth, K. Amine, *Energy Environ. Sci.* **2011**, *4*, 4023 – 4030.

[7] M. D. M. Dubarry, B. Y. Liaw, M. S. Chen, S. S. Chyan, K. C. Han, W. T. Sie, S. H. Wu, *J. Power Sources* **2011**, *196*, 3420 – 3425.

[8] a) D. P. Abraham, J. L. Knuth, D. W. Dees, I. Bloom, J. P. Christophersen, *J. Power Sources* **2007**, *170*, 465 – 475; b) D. P. Abraham, E. M. Reynolds, P. L. Schultz, A. N. Jansen, D. W. Dees, *J. Electrochem. Soc.* **2006**, *153*, A1610 – A1616.

[9] J. W. Jiang, H. Fortier, J. N. Reimers, J. R. Dahn, *J. Electrochem. Soc.* **2004**, *151*, A609 – A613.

[10] a) R. Yazami, Y. F. Reynier, *Electrochim. Acta* **2002**, *47*, 1217 – 1223; b) M. D. Levi, C. Wang, D. Aurbach, *J. Electrochem. Soc.* **2004**, *151*, A781 – A790; c) Ref. [6c, 7].

[11] a) K.-T. Lee, S. Jeong, J. Cho, *Acc. Chem. Res.* **2012**, DOI: 10.1021/ar200224h; b) S. Jeong, S. Park, J. Cho, *Adv. Energy Mater.* **2011**, *1*, 821 – 828.

[12] a) S. Y. Chung, J. T. Bloking, Y. M. Chiang, *Nat. Mater.* **2002**, *1*, 123 – 128; b) Z. H. Chen, J. R. Dahn, *J. Electrochem. Soc.* **2002**, *149*, A1184 – A1189; c) P. S. Herle, B. Ellis, N. Coombs, L. F. Nazar, *Nat. Mater.* **2004**, *3*, 147 – 152; d) B. Kang, G. Ceder, *Nature* **2009**, *458*, 190 – 193; e) H. H. Yi, C. L. Hu, H. S. Fang, B. Yang, Y. C. Yao, W. H. Ma, Y. N. Dai, *Electrochim. Acta* **2011**, *56*, 4052 – 4057; f) M. S. Whittingham, *Chem. Rev.* **2004**, *104*, 4271 – 4301.

[13] a) K. Ariyoshi, Y. Maeda, T. Kawai, T. Ohzuku, *J. Electrochem. Soc.* **2011**, *158*, A281 – A284; b) T. Ohzuku, M. Nagayama, K. Tsuji, K. Ariyoshi, *J. Mater. Chem.* **2011**, *21*, 10179 – 10188; c) N. Yabuuchi, Y. Makimura, T. Ohzuku, *J. Electrochem. Soc.* **2007**, *154*, A314 – A321; d) W. B. Luo, X. H. Li, J. R. Dahn, *Chem. Mater.* **2010**, *22*, 5065 – 5073; e) J. Jiang, J. R. Dahn, *Electrochim. Acta* **2006**, *51*, 3413 – 3416; f) D. D. MacNeil, Z. Lu, J. R. Dahn, *J. Electrochem. Soc.* **2002**, *149*, A1332 – A1336; g) Y. K. Sun, S. T. Myung, M. H. Kim, J. Prakash, K. Amine, *J. Am. Chem. Soc.* **2005**, *127*, 13411 – 13418; h) Y. K. Sun, S. T. Myung, B. C. Park, J. Prakash, I. Belharouak, K. Amine, *Nat. Mater.* **2009**, *8*, 320 – 324; i) C. S. Johnson, N. C. Li, C. Lefief, J. T. Vaughey, M. M. Thackeray, *Chem. Mater.* **2008**, *20*, 6095 – 6106; j) M. M. Thackeray, S. H. Kang, C. S. Johnson, J. T. Vaughey, R. Benedek, S. A. Hackney, *J. Mater. Chem.* **2007**, *17*, 3112 – 3125.

[14] http://www.comsol.com/stories/kobelco_lithium_ion_batteries/full/.

[15] http://www.transportation.anl.gov/batteries/.

[16] a) B. J. Hwang, Y. W. Tsai, D. Carlier, G. Ceder, *Chem. Mater.* **2003**, *15*, 3676 – 3682; b) M. G. Kim, H. J. Shin, J. H. Kim, S. H. Park, Y. K. Sun, *J. Electrochem. Soc.* **2005**, *152*, A1320 – A1328.

[17] Z. H. Chen, Y. K. Sun, K. Amine, *J. Electrochem. Soc.* **2006**, *153*, A1818 – A1822.

[18] a) Z. H. Lu, D. D. MacNeil, J. R. Dahn, *Electrochem. Solid-State Lett.* **2001**, *4*, A191 – A194; b) E. Shinova, T. Mandzhukova, E. Grigorova, M. Hristov, R. Stoyanova, D. Nihtianova, E. Zhecheva, *Solid State Ionics* **2011**, *187*, 43 – 49.

[19] N. Yabuuchi, K. Yoshii, S. T. Myung, I. Nakai, S. Komaba, *J. Am. Chem. Soc.* **2011**, *133*, 4404 – 4419.

[20] Y. Gao, J. N. Reimers, J. R. Dahn, *Phys. Rev. B* **1996**, *54*, 3878 – 3883.

[21] a) J. Bareño, C. H. Lei, J. G. Wen, S. H. Kang, I. Petrov, D. P. Abraham, *Adv. Mater.* **2010**, *22*, 1122 – 1127; b) J. Bareño, M. Balasubramanian, S. H. Kang, J. G. Wen, C. H. Lei, S. V. Pol, I. Petrov, D. P. Abraham, *Chem. Mater.* **2011**, *23*, 2039 – 2050.

[22] Z. H. Lu, J. R. Dahn, *J. Electrochem. Soc.* **2002**, *149*, A815 – A822.

[23] H. X. Deng, I. Belharouak, Y. K. Sun, K. Amine, *J. Mater. Chem.* **2009**, *19*, 4510 – 4516.

[24] a) Z. H. Chen, J. R. Dahn, *Electrochem. Solid-State Lett.* **2002**, *5*, A213 – A216; b) Y. K. Sun, K. J. Hong, J. Prakash, K. Amine, *Electrochem. Commun.* **2002**, *4*, 344 – 348; c) Y. K. Sun, Y. S. Lee, M. Yoshio, K. Amine, *Electrochem. Solid-State Lett.* **2002**, *5*, A99 – A102; d) Z. H. Chen, J. R. Dahn, *Electrochem. Solid-State Lett.* **2003**, *6*, A221 – A224; e) Z. H. Chen, Y. Qin, K. Amine, Y. K. Sun, *J. Mater. Chem.* **2010**, *20*, 7606 – 7612; f) J. Cho, T. Kim, Y. Kim, B. Park, *Electrochem. Solid-State Lett.* **2001**, *4*, A159 – A161.

[25] a) K. S. Lee, S. T. Myung, D. W. Kim, Y. K. Sun, *J. Power Sources* **2011**, *196*, 6974 – 6977; b) H. B. Kim, B. C. Park, S. T. Myung, K. Amine, J. Prakash, Y. K. Sun, *J. Power Sources* **2008**, *179*, 347 – 350.

[26] a) H. G. Song, J. Y. Kim, K. T. Kim, Y. J. Park, *J. Power Sources* **2011**, *196*, 6847 – 6855; b) Y. Jin, N. Li, C. H. Chen, S. Q. Wei, *Electrochem. Solid-State Lett.* **2006**, *9*, A273 – A276; c) H. Miyashiro, S. Seki, Y. Kobayashi, Y. Ohno, Y. Mita, A. Usami, *Electrochem. Commun.* **2005**, *7*, 1083 – 1086; d) Y. Kobayashi, H. Miyashiro, K. Takei, H. Shigemura, M. Tabuchi, H. Kageyama, T. Iwahori, *J. Electrochem. Soc.* **2003**, *150*, A1577 – A1582.

[27] a) J. Kim, M. Noh, J. Cho, H. Kim, K. B. Kim, *J. Electrochem. Soc.* **2005**, *152*, A1142 – A1148; b) G. R. Hu, X. R. Deng, Z. D. Peng, K. Du, *Electrochim. Acta* **2008**, *53*, 2567 – 2573; c) B. Kim, C. Kim, T. G. Kim, D. Ahn, B. Park, *J. Electrochem. Soc.* **2006**, *153*, A1773 – A1777; d) S. E. Lee, E. Kim, J. Cho, *Electrochem. Solid-State Lett.* **2007**, *10*, A1 – A4; e) X. L. Ma, C. W. Wang, X. Y. Han, J. T. Sun, *J. Alloys Compd.* **2008**, *453*, 352 – 355; f) S. Verdier, L. El Ouatani, R. Dedryvere, F. Bonhomme, P. Biensan, D. Gonbeau, *J. Electrochem. Soc.* **2007**, *154*, A1088 – A1099; g) Y. Wu, A. V. Murugan, A. Manthiram, *J. Electrochem. Soc.* **2008**, *155*, A635 – A641; h) J. Cho, *Electrochim. Acta* **2003**, *48*, 2807 – 2811; i) J. Cho, *Electrochem. Commun.* **2003**, *5*, 146 – 148; j) J. Cho, T. J. Kim, J. Kim, M. Noh, B. Park, *J. Electrochem. Soc.* **2004**, *151*, A1899 – A1904; k) J. Cho, J. G. Lee, B. Kim, T. G. Kim, J. Kim, B. Park, *Electrochim. Acta* **2005**, *50*, 4182 – 4187.

[28] a) Y. K. Sun, S. T. Myung, M. H. Kim, J. H. Kim, *Electrochem. Solid-State Lett.* **2006**, *9*, A171 – A174; b) Ref. [13g]; c) H. W. Chan, J. G. Duh, H. S. Sheu, *J. Electrochem. Soc.* **2006**, *153*, A1533 – A1538; d) Y. K. Sun, S. T. Myung, B. C. Park, K. Amine, *Chem. Mater.* **2006**, *18*, 5159 – 5163; e) B. C. Parka, H. J. Bang, K. Amine, E. Jung, Y. K. Sun, *J. Power Sources* **2007**, *174*, 658 – 662; f) K. Vediappan, C. W. Lee, *Phys. Scr.* **2010**, *T139*, 014040; g) Z. L. Yang, C. Cao, F. F. Liu, D. R. Chen, X. L. Jiao, *Solid State Ionics* **2010**, *181*, 678 – 683; h) M. Jo, Y. K. Lee, K. M. Kim, J. Cho, *J. Electrochem. Soc.* **2010**, *157*, A841 – A845.

[29] a) Y. K. Sun, D. H. Kim, H. G. Jung, S. T. Myung, K. Amine, *Electrochim. Acta* **2010**, *55*, 8621 – 8627; b) Y. K. Sun, D. H. Kim, C. S. Yoon, S. T. Myung, J. Prakash, K. Amine, *Adv. Funct. Mater.* **2010**, *20*, 485 – 491; c) Y. K. Sun, B. R. Lee, H. J. Noh, H. M. Wu, S. T. Myung, K. Amine, *J. Mater. Chem.* **2011**, *21*, 10108 – 10112.

[30] a) K. Amine, J. Liu, S. Kang, I. Belharouak, Y. Hyung, D. Vissers, G. Henriksen, *J. Power Sources* **2004**, *129*, 14 – 19; b) S. Lim, J. Cho, *Electrochem. Commun.* **2008**, *10*, 1478 – 1481; c) J. Choa, M. M. Thackeray, *J. Electrochem. Soc.* **1999**, *146*, 3577 – 3582.

[31] a) N. Kumagai, S. Komaba, Y. Kataoka, M. Koyanagi, *Chem. Lett.* **2000**, 1154 – 1155; b) J. Cho, *J. Mater. Chem.* **2008**, *18*, 2257 – 2261.

[32] H. Tsunekawa, S. Tanimoto, R. Marubayashi, M. Fujita, K. Kifune, M. Sano, *J. Electrochem. Soc.* **2002**, *149*, A1326 – A1331.

[33] a) J. W. Song, C. C. Nguyen, H. Choi, K. H. Lee, K. H. Han, Y. J. Kim, S. Choy, S. W. Song, *J. Electrochem. Soc.* **2011**, *158*, A458 – A464; b) Z. H. Chen, K. Amine, *J. Electrochem. Soc.* **2006**, *153*, A1279 – A1283; c) Z. H. Chen, K. Amine, *J. Electrochem. Soc.* **2006**, *153*, A316 – A320.

[34] a) G. B. Zhong, Y. Y. Wang, Z. C. Zhang, C. H. Chen, *Electrochim. Acta* **2011**, *56*, 6554 – 6561; b) Y. L. Ding, J. Xie, G. S. Cao, T. J. Zhu, H. M. Yu, X. B. Zhao, *J. Phys. Chem. C* **2011**, *115*, 9821 – 9825.

[35] a) Y. Bai, C. Wu, F. Wu, *Trans. Nonferrous Met. Soc. China* **2007**, *17*, S892 – S896; b) H. B. Kang, S. T. Myung, K. Amine, S. M. Lee, Y. K. Sun, *J. Power Sources* **2010**, *195*, 2023 – 2028; c) Ref [30b]; d) H. Sahan, H. Goktepe, S. Patat, A. Ulgen, *Solid State Ionics* **2010**, *181*, 1437 – 1444; e) T. F. Yi, J. Shu, Y. R. Zhu, A. N. Zhou, R. S. Zhu, *Electrochem. Commun.* **2009**, *11*, 91 – 94.

[36] a) K. Amine, J. Liu, I. Belharouak, S. H. Kang, I. Bloom, D. Vissers, G. Henriksen, *J. Power Sources* **2005**, *146*, 111 – 115; b) Y. X. Guo, Z. G. Yin, Z. Y. Tao, X. H. Li, Z. X. Wang, *J. Power Sources* **2008**, *184*, 513 – 516; c) I. B. Stojković, N. D. Cvjeticanin, S. V. Mentus, *Electrochem. Commun.* **2010**, *12*, 371 – 373; d) S. Komaba, T. Itabashi, T. Ohtsuka, H. Groult, N. Kumagai, B. Kaplan, H. Yashiro, *J. Electrochem. Soc.* **2005**, *152*, A937 – A946; e) S. Komaba, T. Ohtsuka, B. Kaplan, T. Itabashi, N. Kumagai, H. Groult, *Chem. Lett.* **2002**, 1236 – 1237.

[37] a) Y. Y. Sun, Y. F. Yang, X. C. Zhao, H. X. Shao, *Electrochim. Acta* **2011**, *56*, 5934 – 5939; b) H. M. Wu, I. Belharouak, A. Abouimrane, Y. K. Sun, K. Amine, *J. Power Sources* **2010**, *195*, 2909 – 2913; c) Ref. [28h].

[38] a) A. K. Padhi, K. S. Nanjundaswamy, J. B. Goodenough, *J. Electrochem. Soc.* **1997**, *144*, 1188 – 1194; b) A. K. Padhi, K. S. Nanjundaswamy, C. Masquelier, S. Okada, J. B. Goodenough, *J. Electrochem. Soc.* **1997**, *144*, 1609 – 1613; c) L. X. Yuan, Z. H. Wang, W. X. Zhang, X. L. Hu, J. T. Chen, Y. H. Huang, J. B. Goodenough, *Energy Environ. Sci.* **2011**, *4*, 269 – 284.

[39] a) K. F. Hsu, S. Y. Tsay, B. J. Hwang, *J. Mater. Chem.* **2004**, *14*, 2690 – 2695; b) P. P. Prosini, M. Carewska, S. Scaccia, P. Wisniewski, M. Pasquali, *Electrochim. Acta* **2003**, *48*, 4205 – 4211.

[40] C. M. Julien, K. Zaghib, A. Mauger, M. Massot, A. Ait-Salah, M. Selmane, F. Gendron, *J. Appl. Phys.* **2006**, *100*, 063511.

[41] N. Ravet, M. Gauthier, K. Zaghib, J. B. Goodenough, A. Mauger, F. Gendron, Julien, *Chem. Mater.* **2007**, *19*, 2595 – 2602.

[42] Y. S. Park, H. J. Bang, S. M. Oh, Y. K. Sun, S. M. Lee, *J. Power Sources* **2009**, *190*, 553 – 557.

[43] a) D. Morgan, A. Van der Ven, G. Ceder, *Electrochem. Solid-State Lett.* **2004**, *7*, A30 – A32; b) H. Yoo, M. Jo, B. Kim, H. Kim, J. Cho, *Adv. Energy Mater.* **2011**, *1*, 347 – 351; c) S. P. Ong, A. Jain, G. Hautier, B. Kang, G. Ceder, *Electrochem. Commun.* **2010**, *12*, 427 – 430; d) M. M. Doeff, J. J. Chen, T. E. Conry, R. G. Wang, J. Wilcox, A. Aumentado, *J. Mater. Res.* **2010**, *25*, 1460 – 1468; e) A. S. Zimmermann, B. B. Van Aken, H. Schmid, J. P. Rivera, J. Li, D. Vaknin, M. Fiebig, *Eur. Phys. J. B* **2009**, *71*, 355 – 360; f) W. Tian, J. Y. Li, J. W. Lynn, J. L. Zarestky, D. Vaknin, *Phys. Rev. B* **2008**, *78*, 184429; g) J. Y. Li, W. Tian, Y.

Chen, J. L. Zarestky, J. W. Lynn, D. Vaknin, *Phys. Rev. B* **2009**, *79*, 144410; h) W. Kim, C. H. Rhee, H. J. Kim, S. J. Moon, C. S. Kim, *Appl. Phys. Lett.* **2010**, *96*, 242505.

[44] a) R. Imhof, P. Novak, *J. Electrochem. Soc.* **1998**, *145*, 1081 – 1087; b) K. Xu, *Chem. Rev.* **2004**, *104*, 4303 – 4417.

[45] a) Y. Qin, Z. H. Chen, H. S. Lee, X. Q. Yang, K. Amine, *J. Phys. Chem. C* **2010**, *114*, 15202 – 15206; b) Z. H. Chen, K. Amine, *Electrochem. Commun.* **2007**, *9*, 703 – 707; c) Z. H. Chen, K. Amine, *J. Electrochem. Soc.* **2009**, *156*, A672 – A676; d) Z. H. Chen, J. Liu, K. Arnine, *Electrochim. Acta* **2008**, *53*, 3267 – 3270; e) Z. H. Chen, K. Amine, *J. Electrochem. Soc.* **2006**, *153*, A1221 – A1225; f) L. F. Li, H. S. Lee, H. Li, X. Q. Yang, X. J. Huang, *Electrochem. Commun.* **2009**, *11*, 2296 – 2299; g) M. Herstedt, M. Stjerndahl, T. Gustafsson, K. Edstrom, *Electrochem. Commun.* **2003**, *5*, 467 – 472.

[46] H. S. Lee, Z. F. Ma, X. Q. Yang, X. Sun, J. McBreen, *J. Electrochem. Soc.* **2004**, *151*, A1429 – A1435.

[47] Ref. [36d].

[48] L. El Ouatani, R. Dedryvere, C. Siret, P. Biensan, D. Gonbeau, *J. Electrochem. Soc.* **2009**, *156*, A468 – A477.

[49] a) Y. B. Fu, C. Chen, C. C. Qiu, X. H. Ma, *J. Appl. Electrochem.* **2009**, *39*, 2597 – 2603; b) J. Li, W. H. Yao, Y. S. Meng, Y. Yang, *J. Phys. Chem. C* **2008**, *112*, 12550 – 12556.

[50] a) C. Täubert, M. Fleischhammer, M. Wohlfahrt-Mehrens, U. Wietelmann, T. Buhrmester, *J. Electrochem. Soc.* **2010**, *157*, A721 – A728; b) W. Q. Lu, Z. H. Chen, H. Joachin, J. Prakash, J. Liu, K. Amine, *J. Power Sources* **2007**, *163*, 1074 – 1079; c) K. Xu, S. S. Zhang, T. R. Jow, *Electrochem. Solid-State Lett.* **2005**, *8*, A365 – A368; d) Z. H. Chen, W. Q. Lu, J. Liu, K. Amine, *Electrochim. Acta* **2006**, *51*, 3322 – 3326.

[51] a) J. Liu, Z. H. Chen, S. Busking, K. Amine, *Electrochem. Commun.* **2007**, *9*, 475 – 479; b) Z. H. Chen, J. Liu, K. Amine, *Electrochem. Solid-State Lett.* **2007**, *10*, A45 – A47.

[52] Y. Qin, Z. H. Chen, J. Liu, K. Amine, *Electrochem. Solid-State Lett.* **2010**, *13*, A11 – A14.

[53] a) L. Y. Beaulieu, T. D. Hatchard, A. Bonakdarpour, M. D. Fleischauer, J. R. Dahn, *J. Electrochem. Soc.* **2003**, *150*, A1457 – A1464; b) L. Y. Beaulieu, A. D. Rutenberg, J. R. Dahn, *Microsc. Microanal.* **2002**, *8*, 422 – 428; c) M. Park, Y. Cho, K. Kim, J. Kim, M. Liu, J. Cho, *Angew. Chem.* **2011**, *123*, 9821 – 9824; *Angew. Chem. Int. Ed.* **2011**, *50*, 9647 – 9650.

[54] a) K. T. Lee, J. Cho, *Nano Today* **2011**, *6*, 28 – 41; b) N.-S. Choi, Y. Yao, Y. Cui, J. Cho, *J. Mater. Chem.* **2011**, *21*, 9825 – 9840; c) M. K. Song, S. Park, F. M. Alamgir, J. Cho, M. Liu, *Mater. Sci. Eng. R* **2011**, *72*, 203 – 252; d) C.-M. Park, J.-H. Kim, H. Kim, H.-J. Sohn, *Chem. Soc. Rev.* **2010**, *39*, 3115 – 3141; e) B. M. Bang, H. Kim, H. K. Song, J. Cho, S. Park, *Energy Environ. Sci.* **2011**, *4*, 5013 – 5019; f) J. Cho, *J. Mater. Chem.* **2010**, *20*, 4009 – 4014; g) J.-I. L. H. Yoo, H. Kim, J.-P. Lee, J. Cho, S. Park, *Nano Lett.* **2011**, *11*, 4324 – 4328.

[55] a) H. Kim, M. Seo, M.-H. Park, J. Cho, *Angew. Chem.* **2010**, *122*, 2192 – 2195; *Angew. Chem. Int. Ed.* **2010**, *49*, 2146 – 2149; b) H. Jia, P. Gao, J. Yang, J. Wang, Y. Nuli, Z. Yang, *Adv. Energy Mater.* **2011**, *1*, 1036 – 1039; c) U. Kasavajjula, C. Wang, A. J. Appleby, *J. Power Sources* **2007**, *163*, 1003 – 1039; d) M. G. Kim, J. Cho, *Adv. Funct. Mater.* **2009**, *19*, 14971514; e) A. Magasinski, P. Dixon, B. Hertzberg, A. Kvit, J. Ayala, G. Yushin, *Nat. Mater.* **2010**, *9*, 353 – 358; f) J. R. Szczech, S. Jin, *Energy Environ. Sci.* **2011**, *4*, 56 – 72.

[56] R. Nagai, F. Kita, M. Yamada, H. Katayama, *Hitachi Rev.* **2011**, *60*, 28 – 32.

[57] a) M. Miyachi, H. Yamamoto, H. Kawai, T. Ohta, M. Shirakata, *J. Electrochem. Soc.* **2005**, *152*, A2089 – A2091; b) Y. Yamada, Y. Iriyama, T. Abe, Z. Ogumi, *J. Electrochem. Soc.* **2010**, *157*, A26 – A30; c) H. Nakai, T. Kubota, A. Kita, A. Kawashima, *J. Electrochem. Soc.* **2011**, *158*, A798 – A801; d) N. S. Choi, K. H. Yew, K. Y. Lee, M. Sung, H. Kim, S. S. Kim, *J. Power Sources* **2006**, *161*, 1254 – 1259.

[58] a) H. M. Xiong, Z. D. Wang, D. P. Xie, L. Cheng, Y. Y. Xia, *J. Mater. Chem.* **2006**, *16*, 1345 – 1349; b) R. Ulrich, J. W. Zwanziger, S. M. De Paul, A. Reiche, H. Leuninger, H. W. Spiess, U. Wiesner, *Adv. Mater.* **2002**, *14*, 1134 – 1137; c) F. Kaneko, S. Wada, M. Nakayama, M. Wakihara, J. Koki, S. Kuroki, *Adv. Funct. Mater.* **2009**, *19*, 918 – 925.

[59] a) Z. H. Chen, L. Z. Zhang, R. West, K. Amine, *Electrochim. Acta* **2008**, *53*, 3262 – 3266; b) Y. F. Zhou, S. Xie, X. W. Ge, C. H. Chen, K. Amine, *J. Appl. Electrochem.* **2004**, *34*, 1119 – 1125.

[60] a) Y. E. Hyung, D. R. Vissers, K. Amine, *J. Power Sources* **2003**, *119*, 383 – 387; b) T. Achiha, T. Nakajima, Y. Ohzawa, M. Koh, A. Yamauchi, M. Kagawa, H. Aoyama, *J. Electrochem. Soc.* **2010**, *157*, A707 – A712; c) S. Dalavi, M. Q. Xu, B. Ravdel, L. Zhou, B. L. Lucht, *J. Electrochem. Soc.* **2010**, *157*, A1113 – A1120; d) D. H. Doughty, E. P. Roth, C. C. Crafts, G. Nagasubramanian, G. Henriksen, K. Amine, *J. Power Sources* **2005**, *146*, 116 – 120.

[61] a) M. S. Ding, K. Xu, T. R. Jow, *J. Electrochem. Soc.* **2002**, *149*, A1489 – A1498; b) K. Xu, M. S. Ding, S. S. Zhang, J. L. Allen, T. R. Jow, *J. Electrochem. Soc.* **2002**, *149*, A622 – A626; c) X. M. Wang, E. Yasukawa, S. Kasuya, *J. Electrochem. Soc.* **2001**, *148*, A1058 – A1065; d) X. M. Wang, E. Yasukawa, S. Kasuya, *J. Electrochem. Soc.* **2001**, *148*, A1066 – A1071.

[62] I. A. Profatilova, N. S. Choi, S. W. Roh, S. S. Kim, *J. Power Sources* **2009**, *192*, 636 – 643.

[63] Ref. [44a].

[64] a) Y. Qin, Z. H. Chen, H. S. Lee, X. Q. Yang, K. Amine, *J. Phys. Chem. C* **2010**, *114*, 15202 – 15206; b) Ref. [45b]; c) Ref. [45d]; d) Ref. [45e]; e) Ref. [46]; f) Ref. [45f].

[65] E. Peled, D. Golodnitsky, G. Ardel, *J. Electrochem. Soc.* **1997**, *144*, L208 – L210.

[66] Ref. [48].

[67] C. Täubert, M. Fleischhammer, M. Wohlfahrt-Mehrens, U. Wietelmann, T. Buhrmester, *J. Electrochem. Soc.* **2011**, *157*, A721 – A728.

[68] Ref. [51].

[69] a) W. K. Behl, *J. Electrochem. Soc.* **1989**, *136*, 2305 – 2310; b) W. K. Behl, D. T. Chin, *J. Electrochem. Soc.* **1988**, *135*, 16 – 21; c) W. K. Behl, D. T. Chin, *J. Electrochem. Soc.* **1988**, *135*, 21 – 25.

[70] M. Adachi, K. Tanaka, K. Sekai, *J. Electrochem. Soc.* **1999**, *146*, 1256 – 1261.

[71] J. Chen, C. Buhrmester, J. R. Dahn, *Electrochem. Solid-State Lett.* **2005**, *8*, A59 – A62.

[72] a) Z. Chen, J. Liu, A. N. Jansen, G. GirishKumar, B. Casteel, K. Amine, *Electrochem. Solid-State Lett.* **2010**, *13*, A39 – A42; b) W. Weng, Z. C. Zhang, P. C. Redfern, L. A. Curtiss, K. Amine, *J. Power Sources* **2011**, *196*, 1530 – 1536; c) Z. C. Zhang, L. Zhang, J. A. Schlueter, P. C. Redfern, L. Curtiss, K. Amine, *J. Power Sources* **2010**, *195*, 4957 – 4962; d) L. Zhang, Z. C. Zhang, H. M. Wu, K. Amine, *Energy Environ. Sci.* **2011**, *4*, 2858 – 2862; e) C. Buhrmester, L. Moshurchak, R. C. L. Wang, J. R. Dahn, *J. Electrochem. Soc.* **2006**, *153*, A288 – A294; f) C. Buhrmester, L. M. Moshurchak, R. L. Wang, J. R. Dahn, *J. Electrochem. Soc.* **2006**, *153*, A1800 – A1804; g) L. M. Moshurchak, C. Buhrmester, J. R. Dahn, *J. Electrochem. Soc.* **2008**, *155*, A129 – A131; h) L. M. Moshurchak, W. M. Lamanna, M. Bulinski, R. L. Wang, R. R. Garsuch, J. W. Jiang, D. Magnuson, M. Triemert, J. R. Dahn, *J. Electrochem. Soc.* **2009**, *156*, A309 – A312.

[73] J. R. Dahn, J. W. Jiang, L. M. Moshurchak, M. D. Fleischauer, C. Buhrmester, L. J. Krause, *J. Electrochem. Soc.* **2005**, *152*, A1283 – A1289.

[74] J. W. Hastie, *J. Res. Natl. Bur. Stand. Sect. A* **1973**, *77*, 733 – 754.

[75] a) E. Markevich, V. Baranchugov, D. Aurbach, *Electrochem. Commun.* **2006**, *8*, 1331 – 1334; b) V. Baranchugov, E. Markevich, E. Pollak, G. Salitra, D. Aurbach, *Electrochem. Commun.* **2007**, *9*, 796 – 800.

[76] H. Nakagawa, Y. Fujino, S. Kozono, Y. Katayama, T. Nukuda, H. Sakaebe, H. Matsumoto, K. Tatsumi, *J. Power Sources* **2007**, *174*, 1021 – 1026.

[77] a) M. Galiński, A. Lewandowski, I. Stepniak, *Electrochim. Acta* **2006**, *51*, 5567 – 5580; b) H. Ohno, K. Fukumoto, *Electrochemistry* **2008**, *76*, 16 – 23; c) M. Armand, F. Endres, D. R. MacFarlane, H. Ohno, B. Scrosati, *Nat. Mater.* **2009**, *8*, 621 – 629; d) Y. Y. Lu, S. S. Moganty, J. L. Schaefer, L. A. Archer, *J. Mater. Chem.* **2012**, *22*, 4066 – 4072; e) S. S. Moganty, N. Jayaprakash, J. L. Nugent, J. Shen, L. A. Archer, *Angew. Chem.* **2010**, *122*, 9344 – 9347; *Angew. Chem. Int. Ed.* **2010**, *49*, 9158 – 9161; f) Ref. [77d]; g) A. Lewandowski, A. Swiderska-Mocek, *J. Power Sources* **2009**, *194*, 601 – 609.

[78] a) D. D. MacNeil, J. R. Dahn, *J. Electrochem. Soc.* **2001**, *148*, A1205 – A1210; b) Y. Baba, S. Okada, J. Yamaki, *Solid State Ionics* **2002**, *148*, 311 – 316; c) Y. A. Mariko Hori, Manyi Jin, Seiji Maeda, Seiichirou Hayakawa, *The 49th Battery Symposium in Japan* **2008**.

[79] a) R. Vijayaraghavan, M. Surianarayanan, V. Armel, D. R. MacFarlane, V. P. Sridhar, *Chem. Commun.* **2009**, 6297 – 6299; b) J. H. Huang, A. F. Hollenkamp, *J. Phys. Chem. C* **2010**, *114*, 21840 – 21847.

[80] L. Larush, V. Borgel, E. Markevich, O. Haik, E. Zinigrad, D. Aurbach, G. Semrau, M. Schmidt, *J. Power Sources* **2009**, *189*, 217 – 223.

[81] Ref. [62].

[82] a) E. Markevich, V. Baranchugov, G. Salitra, D. Aurbach, M. A. Schmidt, *J. Electrochem. Soc.* **2008**, *155*, A132 – A137; b) E. Markevich, R. Sharabi, V. Borgel, H. Gottlieb, G. Salitra, D. Aurbach, G. Semrau, M. A. Schmidt, *Electrochim. Acta* **2010**, *55*, 2687 – 2696.

[83] M. Holzapfel, C. Jost, A. Prodi-Schwab, F. Krumeich, A. Wursig, H. Buqa, P. Novak, *Carbon* **2005**, *43*, 1488 – 1498.

[84] N. S. Choi, Y. Lee, S. S. Kim, S. C. Shin, Y. M. Kang, *J. Power Sources* **2010**, *195*, 2368 – 2371.

[85] T. Kuboki, T. Okuyama, T. Ohsaki, N. Takami, *J. Power Sources* **2005**, *146*, 766 – 769.

[86] a) T. Ogasawara, A. Debart, M. Holzapfel, P. Novak, P. G. Bruce, *J. Am. Chem. Soc.* **2006**, *128*, 1390 – 1393; b) P. Poizot, S. Laruelle, S. Grugeon, L. Dupont, J. M. Tarascon, *Nature* **2000**, *407*, 496 – 499.

[87] S. Seki, Y. Kobayashi, H. Miyashiro, Y. Ohno, Y. Mita, A. Usami, N. Terada, M. Watanabe, *Electrochem. Solid-State Lett.* **2005**, *8*, A577 – A578.

[88] X. Ji, L. F. Nazar, *J. Mater. Chem.* **2010**, *20*, 9821 – 9826.

[89] A. M. Kellas, *J. Chem. Soc. Trans.* **1918**, *113*, 903 – 922.

[90] J. U. D. Herbert, US Patent 3043896, **1962**.

[91] K. M. Abraham, R. D. Rauh, S. B. Brummer, *Electrochim. Acta* **1978**, *23*, 501 – 507.

[92] D. Peramunage, S. Licht, *Science* **1993**, *261*, 1029 – 1032.

[93] J. A. Dean, *Lange's Handbook of Chemistry*, McGraw-Hill, New York, **1985**, pp. 3 – 5.

[94] R. D. Rauh, F. S. Shuker, J. M. Marston, S. B. Brummer, *J. Inorg. Nucl. Chem.* **1977**, *39*, 1761 – 1766.

[95] a) H. Yamin, E. Peled, *J. Power Sources* **1983**, *9*, 281 – 287; b) J. I. Yamaki, S. I. Tobishima, Y. Sakurai, K. I. Saito, K. Hayashi, *J. Appl. Electrochem.* **1998**, *28*, 135 – 140.

[96] a) B. M. L. Rao, J. A. Shropshire, *J. Electrochem. Soc.* **1981**, *128*, 942 – 945; b) Y. V. Mikhaylik, J. R. Akridge, *J. Electrochem. Soc.* **2003**, *150*, A306 – A311.

[97] M.-Y. Chu, US Patent 5686201, **1997**.

[98] Y. V. Mikhaylik, J. R. Akridge, *J. Electrochem. Soc.* **2004**, *151*, A1969 – A1976.

[99] a) S. E. Cheon, K. S. Ko, J. H. Cho, S. W. Kim, E. Y. Chin, H. T. Kim, *J. Electrochem. Soc.* **2003**, *150*, A800 – A805; b) B. H. Jeon, J. H. Yeon, K. M. Kim, I. J. Chung, *J. Power Sources* **2002**, *109*, 89 – 97.

[100] E. Peled, A. Gorenshtein, M. Segal, Y. Sternberg, *J. Power Sources* **1989**, *26*, 269 – 271.

[101] Y. J. Choi, Y. D. Chung, C. Y. Baek, K. W. Kim, H. J. Ahn, J. H. Ahn, *J. Power Sources* **2008**, *184*, 548 – 552.

[102] L. Ji, M. Rao, S. Aloni, L. Wang, E. J. Cairns, Y. Zhang, *Energy Environ. Sci.* **2011**, *4*, 5053 – 5059.

[103] J. J. Niu, J. N. Wang, Y. Jiang, L. F. Su, J. Ma, *Microporous Mesoporous Mater.* **2007**, *100*, 1 – 5.

[104] J. C. Guo, Y. H. Xu, C. S. Wang, *Nano Lett.* **2011**, *11*, 4288 – 4294.

[105] P. G. Bruce, S. A. Freunberger, L. J. Hardwick, J.-M. Tarascon, *Nat. Mater.* **2012**, *11*, 19 – 29.

[106] Ref. [102].

[107] a) Y. L. Cao, X. L. Li, I. A. Aksay, J. Lemmon, Z. M. Nie, Z. G. Yang, J. Liu, *Phys. Chem. Chem. Phys.* **2011**, *13*, 7660 – 7665; b) H. L. Wang, Y. Yang, Y. Y. Liang, J. T. Robinson, Y. G. Li, A. Jackson, Y. Cui, H. J. Dai, *Nano Lett.* **2011**, *11*, 2644 – 2647; c) L. W. Ji, M. M. Rao, H. M. Zheng, L. Zhang, Y. C. Li, W. H. Duan, J. H. Guo, E. J. Cairns, Y. G. Zhang, *J. Am. Chem. Soc.* **2011**, *133*, 18522 – 18525; d) S. Evers, L. F. Nazar, *Chem. Commun.* **2012**, *48*, 1233 – 1235.

[108] C. Lai, X. P. Gao, B. Zhang, T. Y. Yan, Z. Zhou, *J. Phys. Chem. C* **2009**, *113*, 4712 – 4716.

[109] C. Liang, N. J. Dudney, J. Y. Howe, *Chem. Mater.* **2009**, *21*, 4724 – 4730.

[110] X. Ji, K. T. Lee, L. F. Nazar, *Nat. Mater.* **2009**, *8*, 500 – 506.

[111] N. Jayaprakash, J. Shen, S. S. Moganty, A. Corona, L. A. Archer, *Angew. Chem.* **2011**, *123*, 6026 – 6030; *Angew. Chem. Int. Ed.* **2011**, *50*, 5904 – 5908.

[112] B. Zhang, X. Qin, G. R. Li, X. P. Gao, *Energy Environ. Sci.* **2010**, *3*, 1531 – 1537.

[113] R. D. Rauh, K. M. Abraham, G. F. Pearson, J. K. Surprenant, S. B. Brummer, *J. Electrochem. Soc.* **1979**, *126*, 523 – 527.

[114] Y. V. Mikhaylik, US Patent 7354680, **2008**.

[115] V. S. Kolosnitsyn, E. V. Kuzmina, E. V. Karaseva, S. E. Mochalov, *J. Power Sources* **2011**, *196*, 1478 – 1482.

[116] C. Barchasz, J. C. Lepretre, F. Alloin, S. Patoux, *J. Power Sources* **2012**, *199*, 322 – 330.

[117] L. C. De Jonghe, S. J. Visco, US Patent 4917974, **1990**.

[118] Y. M. Lee, N.-S. Choi, J. H. Park, J.-K. Park, *J. Power Sources* **2003**, *119 – 121*, 964 – 972.

[119] Y. V. Mikhaylic, US Patent 5314765, **2008**.

[120] D. Aurbach, E. Pollak, R. Elazari, G. Salitra, C. S. Kelley, J. Affinito, *J. Electrochem. Soc.* **2009**, *156*, A694 – A702.

[121] J. B. Bates, US Patent 5314765, **1994**.

[122] S. J. Visco, M.-Y. Chu, US Patent 6025094, **2000**.

[123] S. J. Visco, F.-Y. Tsang, US Patent 6214061, **2001**.

[124] a) S. J. Visco, Y. S. Nimon, B. D. Katz, US Patent 7282302, **2007**; b) Y. S. Nimon, M.-Y. Chu, S. J. Visco, US Patent 6955866 B6955862, **2005**.

[125] J. Fuller, R. T. Carlin, R. A. Osteryoung, *J. Electrochem. Soc.* **1997**, *144*, 3881 – 3886.

[126] a) J. H. Shin, E. J. Cairns, *J. Power Sources* **2008**, *177*, 537 – 545; b) E. J. C. J. H. Shin, *J. Electrochem. Soc.* **2008**, *155*, A368 – A373.

[127] L. X. Yuan, J. K. Feng, X. P. Ai, Y. L. Cao, S. L. Chen, H. X. Yang, *Electrochem. Commun.* **2006**, *8*, 610 – 614.

[128] a) J.-P. M. R. Mercier, B. Fahys, G. Robert, *Solid State Ionics* **1981**, *5*, 663; b) M. R. A. Pradel, *Solid State Ionics* **1986**, *18 – 19*, 351.

[129] A. Hayashi, T. Ohtomo, F. Mizuno, K. Tadanaga, M. Tatsumisago, *Electrochem. Commun.* **2003**, *5*, 701 – 705.

[130] T. Kobayashi, Y. Imade, D. Shishihara, K. Homma, M. Nagao, R. Watanabe, T. Yokoi, A. Yamada, R. Kanno, T. Tatsumi, *J. Power Sources* **2008**, *182*, 621 – 625.

[131] a) M. Nagao, A. Hayashi, M. Tatsumisago, *Electrochim. Acta* **2011**, *56*, 6055 – 6059; b) A. Hayashi, K. Minami, S. Ujiie, M. Tatsumisago, *J. Non-Cryst. Solids* **2010**, *356*, 2670 – 2673.

[132] N. D. Arabinda, Needham, B. Per, M. Andover, US Patent 3806369, **1974**.

[133] Y.-G. Ryu, J. Y. Kim, S. M. Lee, 204th Meeting of The Electrochemical Society, Abs. 398. Florida, USA, **2003**.

[134] K. M. Abraham, Z. Jiang, *J. Electrochem. Soc.* **1996**, *143*, 1 – 5.

[135] a) S. J. Visco, B. D. Katz, Y. S. Nimon, L. C. De Jonghe, PolyPlus Battery Company (Berkeley, CA, US), United States Patent, US20070117007, **2007**; b) P. Stevens, G. Toussaint, G. Caillon, P. Viaud, P. Vinatier, C. Cantau, O. Fichet, C. Sarrazin, M. Mallouki, *ECS Trans.* **2010**, *28*, 1 – 12.

[136] a) Z. Peng, S. A. Freunberger, L. J. Hardwick, Y. Chen, V. Giordani, F. Bardé, P. Novák, D. Graham, J.-M. Tarascon, P. G. Bruce, *Angew. Chem.* **2011**, *123*, 6475 – 6479; *Angew. Chem. Int. Ed.* **2011**, *50*, 6351 – 6355; b) C. O. Laoire, S. Mukerjee, K. M. Abraham, E. J. Plichta, M. A. Hendrickson, *J. Phys. Chem. C* **2009**, *113*, 20127 – 20134; c) C. O. Laoire, S. Mukerjee, K. M. Abraham, E. J. Plichta, M. A. Hendrickson, *J. Phys. Chem. C* **2010**, *114*, 9178 – 9186.

[137] M. W. Chase, *J. Phys. Chem. Ref. Data Monogr. 9, 4th ed.* **1998**, 1510.

[138] a) Y. Wang, H. Zhou, *J. Power Sources* **2010**, *195*, 358 – 361; b) T. Zhang, N. Imanishi, Y. Shimonishi, A. Hirano, Y. Takeda, O. Yamamoto, N. Sammes, *Chem. Commun.* **2010**, *46*, 1661 – 1663.

[139] D. Linden, T. B. Reddy, *Handbook of Batteries*, 3rd ed., McGraw-Hill, New York, **2002**.

[140] T. Zhang, N. Imanishi, Y. Shimonishi, A. Hirano, J. Xie, Y. Takeda, O. Yamamoto, N. Sammes, *J. Electrochem. Soc.* **2010**, *157*, A214 – A218.

[141] J. P. Zheng, P. Andrei, M. Hendrickson, E. J. Plichta, *J. Electrochem. Soc.* **2011**, *158*, A43 – A46.

[142] a) A. Nytén, A. Abouimrane, M. Armand, T. Gustafsson, J. O. Thomas, *Electrochem. Commun.* **2005**, *7*, 156 – 160; b) J. B. Goodenough, Y. Kim, *J. Power Sources* **2011**, *196*, 6688 – 6694.

[143] a) D. Wang, J. Xiao, W. Xu, J.-G. Zhang, *J. Electrochem. Soc.* **2010**, *157*, A760 – A764; b) J. Zhang, W. Xu, W. Liu, *J. Power Sources* **2010**, *195*, 7438 – 7444.

[144] a) P. Andrei, J. P. Zheng, M. Hendrickson, E. J. Plichta, *J. Electrochem. Soc.* **2010**, *157*, A1287 – A1295; b) P. Albertus, G. Girishkumar, B. McCloskey, R. S. Sanchez-Carrera, B. Kozinsky, J. Christensen, A. C. Luntz, *J. Electrochem. Soc.* **2011**, *158*, A343 – A351.

[145] a) Y.-C. Lu, D. G. Kwabi, K. P. C. Yao, J. R. Harding, J. Zhou, L. Zuin, Y. Shao-Horn, *Energy Environ. Sci.* **2011**, *4*, 2999 – 3007; b) R. R. Mitchell, B. M. Gallant, C. V. Thompson, Y. Shao-Horn, *Energy Environ. Sci.* **2011**, *4*, 2952 – 2958.

[146] a) M. Mirzaeian, P. J. Hall, *Electrochim. Acta* **2009**, *54*, 7444 – 7451; b) J. Xiao, D. Wang, W. Xu, D. Wang, R. E. Williford, J. Liu, J.-G. Zhang, *J. Electrochem. Soc.* **2010**, *157*, A487 – A492; c) A. Dobley, C. Morein, K. M. Abraham, *ECS Meeting Abstracts* **2006**, *502*, 823.

[147] a) F. Bardé, P. G. Bruce, S. A. Freunberger, Y. Chen, L. J. Hardwick, Toyota Motor Europe, University of St. Andrews Japan, **2011**; b) F. Bardé, P. G. Bruce, S. A. Freunberger, L. J. Hardwick *Vol. PCT/JP2010/059494*, Toyota Motor Europe, University of St. Andrews Japan, **2010**; c) Y.-C. Lu, Z. Xu, H. A. Gasteiger, S. Chen, K. Hamad-Schifferli, Y. Shao-Horn, *J. Am. Chem. Soc.* **2010**, *132*, 12170 – 12171.

[148] a) Y.-C. Lu, H. A. Gasteiger, M. C. Parent, V. Chiloyan, Y. Shao-Horn, *Electrochem. Solid-State Lett.* **2010**, *13*, A69 – A72; b) Y.-C. Lu, H. A. Gasteiger, E. Crumlin, J. R. McGuire, Y. Shao-Horn, *J. Electrochem. Soc.* **2010**, *157*, A1016 – A1025; c) A. Débart, J. Bao, G. Armstrong, P. G. Bruce, *J. Power Sources* **2007**, *174*, 1177 – 1182; d) A. Débart, A. Paterson, J. Bao, P. Bruce, *Angew. Chem.* **2008**, *120*, 4597 – 4600; *Angew. Chem. Int. Ed.* **2008**, *47*, 4521 – 4524; e) Ref. [86a]; f) V. Giordani, S. A. Freunberger, P. G. Bruce, J.-M. Tarascon, D. Larcher, *Electrochem. Solid-State Lett.* **2010**, *13*, A180 – A183; g) Y.-C. Lu, H. A. Gasteiger, Y. Shao-Horn, *J. Am. Chem. Soc.* **2011**, *133*, 19048 – 19051.

[149] S. A. Freunberger, Y. Chen, Z. Peng, J. M. Griffin, L. J. Hardwick, F. Bardé, P. Novák, P. G. Bruce, *J. Am. Chem. Soc.* **2011**, *133*, 8040 – 8047.

[150] C. O. Laoire, S. Mukerjee, E. J. Plichta, M. A. Hendrickson, K. M. Abraham, *J. Electrochem. Soc.* **2011**, *158*, A302 – A308.

[151] M. Winter, J. O. Besenhard, *Electrochim. Acta* **1999**, *45*, 31 – 50.

[152] B. D. McCloskey, R. Scheffler, A. Speidel, D. S. Bethune, R. M. Shelby, A. C. Luntz, *J. Am. Chem. Soc.* **2011**, *133*, 18038.

[153] a) D. Aurbach, M. Daroux, P. Faguy, E. Yeager, *J. Electroanal. Chem.* **1991**, *297*, 225 – 244; b) F. Mizuno, S. Nakanishi, Y. Kotani, S. Yokoishi, H. Iba, *Electrochemistry* **2010**, *78*, 403 – 405; c) S. A. Freunberger, L. J. Hardwick, Z. Peng, V. Giordani, Y. Chen, P. Maire, P. Novák, J.-M. Tarascon, P. G. Bruce in *IMLB 2010—The 15th International Meeting on Lithium Batteries*, Montreal, Canada, June 27 – July 2, **2010**; d) W. Xu, V. V. Viswanathan, D. Wang, S. A. Towne, J. Xiao, Z. Nie, D. Hu, J.-G. Zhang, *J. Power Sources* **2011**, *196*, 3894 – 3899; e) B. D. McCloskey, D. S. Bethune, R. M. Shelby, G. Girishkumar, A. C. Luntz, *J. Phys. Chem. Lett.* **2011**, *2*, 1161 – 1166; f) V. S. Bryantsev, M. Blanco, *J. Phys. Chem. Lett.* **2011**, *2*, 379 – 383.

[154] Z. Zhang, J. Lu, R. S. Assary, P. Du, H.-H. Wang, Y.-K. Sun, Y. Qin, K. C. Lau, J. Greeley, P. C. Redfern, H. Iddir, L. A. Curtiss, K. Amine, *J. Phys. Chem. C* **2011**, *115*, 25535 – 25542.

[155] S. A. Freunberger, Y. Chen, N. E. Drewett, L. J. Hardwick, F. Bardé, P. G. Bruce, *Angew. Chem.* **2011**, *123*, 8768 – 8772; *Angew. Chem. Int. Ed.* **2011**, *50*, 8609 – 8613.

[156] Y. Chen, S. A. Freunberger, Z. Peng, F. Bardé, P. G. Bruce, *J. Am. Chem. Soc.* **2012**, *134*, 7952 – 7957.

[157] a) V. S. Bryantsev, M. Blanco, *J. Phys. Chem. Lett.* **2011**, *2*, 379 – 383; b) V. S. Bryantsev, V. Giordani, W. Walker, M. Blanco, S. Zecevic, K. Sasaki, J. Uddin, D. Addison, G. V. Chase, *J. Phys. Chem. A* **2011**, *115*, 12399 – 12409; c) R. S. Assary, L. A. Curtiss, P. C. Redfern, Z. Zhang, K. Amine, *J. Phys. Chem. C* **2011**, *115*, 12216 – 12223.

[158] C. J. Allen, S. Mukerjee, E. J. Plichta, M. A. Hendrickson, K. M. Abraham, *J. Phys. Chem. Lett.* **2011**, *2*, 2420 – 2424.

[159] J. Hassoun, F. Croce, M. Armand, B. Scrosati, *Angew. Chem.* **2011**, *123*, 3055 – 3058; *Angew. Chem. Int. Ed.* **2011**, *50*, 2999 – 3002.

[160] B. Kumar, J. Kumar, R. Leese, J. P. Fellner, S. J. Rodrigues, K. M. Abraham, *J. Electrochem. Soc.* **2010**, *157*, A50 – A54.

[161] S. S. Zhang, D. Foster, J. Read, *J. Power Sources* **2010**, *195*, 3684 – 3688.

[162] a) S. Hasegawa, N. Imanishi, T. Zhang, J. Xie, A. Hirano, Y. Takeda, O. Yamamoto, *J. Power Sources* **2009**, *189*, 371 – 377; b) N. Imanishi, S. Hasegawa, T. Zhang, A. Hirano, Y. Takeda, O. Yamamoto, *J. Power Sources* **2008**, *185*, 1392 – 1397.

[163] J. Hassoun, B. Scrosati, *Angew. Chem.* **2010**, *122*, 2421 – 2424; *Angew. Chem. Int. Ed.* **2010**, *49*, 2371 – 2374.

[164] P. He, Y. Wang, H. Zhou, *Electrochem. Commun.* **2010**, *12*, 1686 – 1689.

[165] Y. Mao, Q. Kong, B. Guo, X. Fang, X. Guo, L. Shen, M. Armand, Z. Wang, L. Chen, *Energy Environ. Sci.* **2011**, *4*, 3442 – 3447.

[166] a) E. Yoo, H. Zhou, *ACS Nano* **2011**, *5*, 3020 – 3026; b) E. Yoo, J. Nakamura, H. Zhou, *Energy Environ. Sci.* **2012**, *5*, 6928 – 6932.

[167] a) http://www.ohara-inc.co.jp; b) N. Kamaya, K. Homma, Y. Yamakawa, M. Hirayama, R. Kanno, M. Yonemura, T. Kamiyama, Y. Kato, S. Hama, K. Kawamoto, A. Mitsui, *Nat. Mater.* **2011**, *10*, 682 – 686.
[168] B. E. Conway, *Electrochemical Supercapacitors*, *Vol. 1*, Kluwer Academic/Plenum Publishers, New York, **1999**.
[169] a) A. Frumkin, S. Reichstein, R. Kulvarskaja, *Kolloid-Z.* **1926**, *40*, 9 – 11; b) A. Frumkin, *Z. Phys.* **1926**, *35*, 792 – 802; c) B. E. Conway, E. Gileadi, M. Dzieciuch, *J. Electrochem. Soc.* **1963**, *110*, C68 – C68.
[170] B. E. Conway, *J. Electrochem. Soc.* **1991**, *138*, 1539 – 1548.
[171] J. P. Zheng, *Electrochem. Solid-State Lett.* **1999**, *2*, 359 – 361.
[172] H. Shi, *Electrochim. Acta* **1996**, *41*, 1633.
[173] G. Salitra, A. Soffer, L. Eliad, Y. Cohen, D. Aurbach, *J. Electrochem. Soc.* **2000**, *147*, 2486 – 2493.
[174] a) J. Chmiola, G. Yushin, Y. Gogotsi, C. Portet, P. Simon, *Science* **2006**, *313*, 1760 – 1763; b) E. Raymundo-Piñero, K. Kierzek, J. Machnikowski, F. Béguin, *Carbon* **2006**, *44*, 2498 – 2507.
[175] a) G. Feng, R. Qiao, J. S. Huang, B. G. Sumpter, V. Meunier, *Acs Nano* **2010**, *4*, 2382 – 2390; b) J. S. Huang, B. G. Sumpter, V. Meunier, *Angew. Chem.* **2008**, *120*, 530 – 534; *Angew. Chem. Int. Ed.* **2008**, *47*, 520 – 524.
[176] J. Chmiola, G. Yushin, R. Dash, Y. Gogotsi, *J. Power Sources* **2006**, *158*, 765 – 772.
[177] A. Kajdos, A. Kvit, F. Jones, J. Jagiello, G. Yushin, *J. Am. Chem. Soc.* **2010**, *132*, 3252.
[178] a) A. G. Pandolfo, A. F. Hollenkamp, *J. Power Sources* **2006**, *157*, 11 – 27; b) S. J. Kim, S. W. Hwang, S. H. Hyun, *J. Mater. Sci.* **2005**, *40*, 725 – 731; c) S. W. Hwang, S. H. Hyun, *J. Non-Cryst. Solids* **2004**, *347*, 238 – 245; d) I. Bispo-Fonseca, J. Aggar, C. Sarrazin, P. Simon, J. F. Fauvarque, *J. Power Sources* **1999**, *79*, 238 – 241.
[179] a) K. G. Gallagher, G. Yushin, T. F. Fuller, *J. Electrochem. Soc.* **2010**, *157*, B820 – B830; b) C. Portet, G. Yushin, Y. Gogotsi, *Carbon* **2007**, *45*, 2511 – 2518.
[180] R. Xue, J. W. Yan, X. X. Liu, Y. Tian, B. L. Yi, *J. Appl. Electrochem.* **2011**, *41*, 1357 – 1366.
[181] M. Rose, Y. Korenblit, E. Kockrick, L. Borchardt, M. Oschatz, S. Kaskel, G. Yushin, *Small* **2011**, *7*, 1108 – 1117.
[182] C. Portet, G. Yushin, Y. Gogotsi, *J. Electrochem. Soc.* **2008**, *155*, A531 – A536.
[183] K. Evanoff, J. Khan, A. A. Balandin, A. Magasinski, W. J. Ready, T. F. Fuller, G. Yushin, *Adv. Mater.* **2012**, *24*, 533 – 537.
[184] K. Evanoff, A. Magasinski, J. Yang, G. Yushin, *Adv. Energy Mater.* **2011**, *1*, 495 – 498.
[185] C. Moreno-Castilla, M. B. Dawidziuk, F. Carrasco-Marin, Z. Zapata-Benabithe, *Carbon* **2011**, *49*, 3808 – 3819.
[186] Y. Korenblit, M. Rose, E. Kockrick, L. Borchardt, A. Kvit, S. Kaskel, G. Yushin, *Acs Nano* **2010**, *4*, 1337 – 1344.
[187] H. Nishihara, Q. H. Yang, P. X. Hou, M. Unno, S. Yamauchi, R. Saito, J. I. Paredes, A. Martinez-Alonso, J. M. D. Tascon, Y. Sato, M. Terauchi, T. Kyotani, *Carbon* **2009**, *47*, 1220 – 1230.
[188] C. M. Niu, E. K. Sichel, R. Hoch, D. Moy, H. Tennent, *Appl. Phys. Lett.* **1997**, *70*, 1480 – 1482.
[189] J. N. Barisci, G. G. Wallace, R. H. Baughman, *J. Electroanal. Chem.* **2000**, *488*, 92 – 98.
[190] J. N. Barisci, G. G. Wallace, R. H. Baughman, *J. Electrochem. Soc.* **2000**, *147*, 4580 – 4583.
[191] J. N. Barisci, G. G. Wallace, D. R. MacFarlane, R. H. Baughman, *Electrochem. Commun.* **2004**, *6*, 22 – 27.
[192] J. H. Chen, W. Z. Li, D. Z. Wang, S. X. Yang, J. G. Wen, Z. F. Ren, *Carbon* **2002**, *40*, 1193 – 1197.
[193] S. Talapatra, S. Kar, S. K. Pal, R. Vajtai, L. Ci, P. Victor, M. M. Shaijumon, S. Kaur, O. Nalamasu, P. M. Ajayan, *Nat. Nanotechnol.* **2006**, *1*, 112 – 116.
[194] L. J. Gao, A. P. Peng, Z. Y. Wang, H. Zhang, Z. J. Shi, Z. N. Gu, G. P. Cao, B. Z. Ding, *Solid State Commun.* **2008**, *146*, 380 – 383.
[195] C. Emmenegger, P. Mauron, P. Sudan, P. Wenger, V. Hermann, R. Gallay, A. Zuttel, *J. Power Sources* **2003**, *124*, 321 – 329.
[196] D. N. Futaba, K. Hata, T. Yamada, T. Hiraoka, Y. Hayamizu, Y. Kakudate, O. Tanaike, H. Hatori, M. Yumura, S. Iijima, *Nat. Mater.* **2006**, *5*, 987 – 994.
[197] B. J. Yoon, S. H. Jeong, K. H. Lee, H. S. Kim, C. G. Park, J. H. Han, *Chem. Phys. Lett.* **2004**, *388*, 170 – 174.
[198] W. Lu, L. T. Qu, K. Henry, L. M. Dai, *J. Power Sources* **2009**, *189*, 1270 – 1277.
[199] H. Zhang, G. P. Cao, Y. S. Yang, Z. N. Gu, *Carbon* **2008**, *46*, 30 – 34.
[200] R. Shah, X. F. Zhang, S. Talapatra, *Nanotechnology* **2009**, *20*, 395202.
[201] a) S. W. Lee, N. Yabuuchi, B. M. Gallant, S. Chen, B.-S. Kim, P. T. Hammond, Y. Shao-Horn, *Nat. Nano* **2010**, *5*, 531 – 537; b) S. W. Lee, B. S. Kim, S. Chen, Y. Shao-Horn, P. T. Hammond, *J. Am. Chem. Soc.* **2009**, *131*, 671 – 679.
[202] a) C. S. Du, N. Pan, *Nanotechnology* **2006**, *17*, 5314 – 5318; b) C. S. Du, N. Pan, *J. Power Sources* **2006**, *160*, 1487 – 1494.
[203] C. S. Du, J. Yeh, N. Pan, *Nanotechnology* **2005**, *16*, 350 – 353.
[204] S. R. C. Vivekchand, C. S. Rout, K. S. Subrahmanyam, A. Govindaraj, C. N. R. Rao, *J. Chem. Sci.* **2008**, *120*, 9 – 13.
[205] M. D. Stoller, S. J. Park, Y. W. Zhu, J. H. An, R. S. Ruoff, *Nano Lett.* **2008**, *8*, 3498 – 3502.
[206] Y. Wang, Z. Q. Shi, Y. Huang, Y. F. Ma, C. Y. Wang, M. M. Chen, Y. S. Chen, *J. Phys. Chem. C* **2009**, *113*, 13103 – 13107.
[207] Y. Chen, X. Zhang, P. Yu, Y. W. Ma, *J. Power Sources* **2010**, *195*, 3031 – 3035.
[208] T. Thomberg, A. Janes, E. Lust, *Electrochim. Acta* **2010**, *55*, 3138 – 3143.
[209] J. Sato, Y. Takasu, K. Fukuda, W. Sugimoto, *Chem. Lett.* **2011**, *40*, 44 – 45.
[210] Y. Y. Shao, J. Wang, M. Engelhard, C. M. Wang, Y. H. Lin, *J. Mater. Chem.* **2010**, *20*, 743 – 748.
[211] Q. L. Du, M. B. Zheng, L. F. Zhang, Y. W. Wang, J. H. Chen, L. P. Xue, W. J. Dai, G. B. Ji, J. M. Cao, *Electrochim. Acta* **2010**, *55*, 3897 – 3903.
[212] Ref. [136a].
[213] Z. Y. Lin, Y. Liu, Y. G. Yao, O. J. Hildreth, Z. Li, K. Moon, C. P. Wong, *J. Phys. Chem. C* **2011**, *115*, 7120 – 7125.
[214] J. R. Miller, R. A. Outlaw, B. C. Holloway, *Science* **2010**, *329*, 1637 – 1639.
[215] M. M. Hantel, T. Kaspar, R. Nesper, A. Wokaun, R. Kotz, *Electrochem. Commun.* **2011**, *13*, 90 – 92.
[216] H. S. Kim, T. S. Arthur, G. D. Allred, J. Zajicek, J. G. Newman, A. E. Rodnyansky, A. G. Oliver, W. C. Boggess, J. Muldoon, *Nature Commun.* **2011**, *2*, 427.